CHARACTERIZATION OF A_2: THE LYSIS PROTEIN OF SSRNA PHAGE Qβ

A Dissertation

by

CATRINA ANNE REED

Submitted to the Office of Graduate Studies of
Texas A&M University
in partial fulfillment of the requirements for the degree of

DOCTOR OF PHILOSOPHY

August 2012

Major Subject: Biochemistry

Characterization of A_2: The Lysis Protein of ssRNA Phage Qβ

CHARACTERIZATION OF A_2: THE LYSIS PROTEIN OF SSRNA PHAGE Q*B*

A Dissertation

by

CATRINA ANNE REED

Submitted to the Office of Graduate Studies of
Texas A&M University
in partial fulfillment of the requirements for the degree of

DOCTOR OF PHILOSOPHY

Approved by:

Chair of Committee,	Ryland F. Young
Committee Members,	Gregory D. Reinhart
	James M. Scholtz
	Deborah A. Siegele
Head of Department,	Gregory D. Reinhart

August 2012

Major Subject: Biochemistry

ABSTRACT

Characterization of A_2: The Lysis Protein of ssRNA Phage Qβ. (August 2012)

Catrina Anne Reed, A.S., Cisco Junior College;

B.S., McMurry University

Chair of Advisory Committee: Dr. Ryland F. Young

Lysis in cells infected with the ssRNA phage Qβ is effected by the A_2 protein. It was previously shown that a single copy of A_2 assembled on the surface of the Qβ virion inhibited the activity of MurA, which catalyzes the first committed step of murein biosynthesis. This led to a model for lysis timing in which A_2 is not active as a MurA inhibitor until assembled into virion particles. Here we report that MurA inactivates purified Qβ particles. Moreover, over-expression of MurA does not inactivate particles during the Qβ infection cycle; thus, casting doubt on the notion that completed virions could be the lytic agent *in vivo* and also that the MurA-virion interaction does not occur in the infected cell. Furthermore, RNA released from particles was found to protect virions from inactivation by MurA *in vitro*, suggesting that Qβ RNA might serve as the protective element during the infection cycle. Comparison of A_2 accumulation between Qβ and Qβ^{por} mutants, which are Qβ A_2 mutants with a shorter infection cycle and reduced burst size, reveals that a delicate balance between assembled and unassembled A_2 levels regulates lysis timing. A new model is proposed in which "free", unassembled

A_2 inhibits MurA. From *in vitro* binding studies and genetic analyses it was determined that A_2 binds MurA in a closed conformation with UDP-*N*-acetylglucosamine bound.

DEDICATION

This dissertation is dedicated to my family. To my husband first and foremost, who is my biggest supporter. Thank you for bringing joy into my life and not allowing me to give up on my dreams. For my children, who are my inspirations to strive for a better life. Finally, to my parents, especially my Dad, who have allowed me to follow my own path in life without ever giving up on me.

ACKNOWLEDGEMENTS

I would like to thank my P.I., Dr. Ry Young, for all of your support. You truly are an uncommon mentor who strives to bring the best out of scientists. I would also like to thank my committee members, Dr. Greg Reinhart, Dr. Marty Scholtz, and Dr. Debby Siegele for their guidance and support throughout the course of this research.

I also want to extend my gratitude to the Young Lab members, past and present, for their support and insightful discussions. Thanks also go to my friends and colleagues in the Biochemistry/Biophysics department for making my time at Texas A&M University a great experience. A special thanks to Daisy Wilbert for your unwavering support to all of us in the department.

I would like to thank my church family for holding me accountable and helping to bring balance to my life. Finally, thanks to my family for all their patience and love.

TABLE OF CONTENTS

Page

ABSTRACT iii

DEDICATION v

ACKNOWLEDGEMENTS vi

TABLE OF CONTENTS vii

LIST OF FIGURES xi

LIST OF TABLES xvii

CHAPTER

I INTRODUCTION AND LITERATURE REVIEW 1

Mode of Phage Virion Release 1
dsDNA phage lysis 1
ssDNA/ssRNA phage lysis 7
The Qβ Life Cycle 9
Adsorption of ssRNA phage and injection of viral RNA 10
Replication 15
Virion morphogenesis 20
Lysis 22
MurA 29
Project Aims 34

II THE REGULATION OF LYSIS IN Qβ INFECTIONS 36

Introduction 36
Materials and Methods 39
Bacterial strains and growth conditions 39
Plasmid construction 39
MurA expression and purification 41
Phage inactivation assay 42
RNA release assay 42
MurA quantification 43
A_2 induction and quantification 43

CHAPTER Page

Released/intracellular titer 44
MurA titration assay 45
Results and Discussion 47
MurA inactivates Qβ particles 47
Quantification of MurA and A_2 *in vivo* 50
Quantification of A_2 accumulation during infection 50
Por mutants produce A_2 more rapidly and cause early lysis 52
MurA over-production blocks lysis but does not inactivate intracellular virions 57
Particles are protected by a soluble viral component 60
Virion particles are protected from in vitro inactivation by Qβ RNA 63
Lysis inhibition of Qβ 64
Discussion 67
A_2 inhibition of MurA and MurA-inactivation of Qβ: Models for regulation 67
Protection of intracellular virions 69

III STRUCTURE AND FUNCTION ANALYSES OF A_2 71

Introduction 71
Materials and Methods 71
Bacterial strains and growth conditions 71
Plasmid construction 73
Protein expression and purification 74
Fusion cleavage assay 76
MurA activity assay 76
Circular dichroism analysis 76
Results and Discussion 77
Function and structure analyses of A_2 fusion proteins 77
Functional analysis of A_2 fusion proteins *in vivo* 80
Purification of soluble fusions of A_2 80
Functional analysis of A_2 fusion protein *in vitro* 96
Characterization of the A_2 fusion structure 101
Probing the A_2 lytic domain 102

IV INHIBITORY MECHANISM OF THE Qβ LYSIS PROTEIN A_2 106

Introduction 106

CHAPTER Page

Materials and Methods 107
Bacterial strains and growth conditions 107
Plasmid construction 108
Protein expression and purification 108
MurA activity assay 108
Batch affinity fractionation experiments 110
Fusion cleavage assay 110
MurA bioassay 111
Results and Discussion 111
Inhibition of purified MurA by Qβ 111
The A_2 interaction with MurA is conformation-dependent 114
Identification of a MurA binding surface for A_2 122
Discussion 127
A_2-MurA interaction: Model for inhibition 127
Proteins as inhibitors of enzymes 131

V *Bacillus subtilis* MURAA STRUCTURE AND FUNCTION 133

Introduction 133
Material and Methods 134
Bacterial strains and growth conditions 134
Plasmid construction 136
Protein expression and characterization 136
Phage purification and plating 137
Results and Discussion 137
$MurAA^{D306A}$ mutation does not protect in bioassay 137
MurAA is sensitive to Qβ A_2^{por} but not Qβ 143
MurAA binding by A_2 cannot be detected *in vitro* 144
A_2 truncation effects on MurAA inhibition 147
Analysis of the MurAA surface 150
Discussion 153

VI SUMMARY AND FUTURE DIRECTIONS 156

Overview 156
Model for A_2 Regulation During a Qβ Infection 156
Characterization of A_2^{por} Mutants 160
Mechanism of MurA Inhibition 161
Characterization of A_2 binding to a dormant complex of MurA 162
Probing the A_2 Lytic Domain 162

CHAPTER Page

Characterization of the A_2 lytic domain 163
Lysis Inhibition of Qβ (LIN) 164

REFERENCES 166

VITA 181

LIST OF FIGURES

FIGURE		Page
1	The λ lysis paradigm	2
2	Holin topologies	4
3	Genomic maps of phages with single lysis gene products	8
4	Cell wall synthesis pathway	24
5	*Alloleviviridae* A_2 and *Leviviridae* A alignment	28
6	MurA catalysis	30
7	Structural view of MurA catalysis	31
8	Qβ RNA	37
9	Qβ particles are inactivated by incubation with MurA *in vitro*	45
10	K_i determination for Qβ inactivation by MurA	46
11	Sucrose gradient analysis of Qβ particles incubated with MurA	48
12	MurA quantification	49
13	Plasmid-borne A_2 induces cellular lysis	51

FIGURE Page

14 Qβ and Qβ^{por} phenotype of infected cells 53

15 Qβ^{por} plating phenotype 54

16 Cloned A_2^{por} does not lyse a $MurA^{rat}$ strain 56

17 Expression of MurA protects during a Qβ infection 58

18 Qβ lysate is not inactivated by MurA 60

19 Bacterial lysate does not protect Qβ from inactivation by MurA 61

20 A_2 lysis is not regulated by Coat or A_1 62

21 Qβ is protected from MurA inactivation by RNA 64

22 Qβ lysis inhibition 66

23 A_2 fusion constructs 78

24 A_2 fusion lysis phenotype 79

25 SUMO-A_2 solubility at 37°C and 16°C expression 81

26 GST-A_2 NusA-A_2 solubility at 37°C expression 82

27 GST-A_2 NusA-A_2 solubility at 16°C expression 83

28 GST-A_2 Talon resin purification 84

FIGURE Page

29 GST-A_2 absorbance spectrum 85

30 NusA-A_2 Talon resin purification 86

31 NusA-A_2 absorbance spectrum 87

32 MBP-A_2 purification with Talon resin 88

33 MBP-A_2 purification with amylose resin 89

34 Western blot of MBP-A_2 purification with amylose resin 90

35 MBP-A_2 purification with protease inhibitor cocktail 91

36 MBP-A_2 absorbance spectrum 91

37 MBP purification with amylose resin 92

37 MBP absorbance spectrum 93

39 MBP-A_2 osmolyte expression test 94

40 MBP-A_2 and MBP-A_2^{1-189} fusion cleavage 95

41 GST-A_2 and NusA-A_2 inhibition of MurA 97

42 MBP-A_2 inhibition of MurA 99

43 Circular dichroism analysis of MBP-A_2 and MBP-A_2^{1-189} 100

FIGURE Page

44 Secondary structure prediction of A_2 101

45 A_2 Fragment analysis 103

46 A_2-A hybrid lysis phenotype 104

47 MurA protection assay induction series 112

48 Purified Qβ inhibits MurA *in vitro* 113

49 A_2 binds MurA in a substrate-dependent manner 115

50 Active site analyses of MurA substrate-dependent conformations 117

51 A_2 binds $MurA^{L138Q}$ 119

52 Yeast-two-hybrid analysis of the A_2-MurA interaction 120

53 $MurA^{rat}$ alleles protect against A_2 at lower inducer concentrations 121

54 MurA* variant expression test 123

55 Rat residues define a Qβ A_2 interaction surface important for inhibition of MurA 124

56 MurA mutant surface maps 126

FIGURE Page

57 The surface of MurA has negatively charged and hydrophobic characteristic 130

58 The A_2^{1-189} protein inhibits *Bs* MurAA 135

59 *Bs* $MurAA^{D306A}$ does not protect during a Qβ infection 138

60 *Bs* $MurAA^{D306A}$ is expressed 139

61 *Bs* $MurAA^{D306A}$ mutant is nonfunctional 140

62 *Bs* $MurAA^{D306A}$ has reduced solubility 141

63 MurAA protects during a Qβ infection 142

64 Purification of MurAA 144

65 Batch affinity fractionation of MBP-A_2 and MurAA 145

66 Fusion cleavage analysis of MBP-A_2 with MurAA 146

67 Active site comparison of *E. coli* MurA and *Bs* MurAA 148

68 *E. coli* MurA and *Bs* MurAA alignment 149

69 Comparison of A_2 interaction surface between *E. coli* MurA and *Bs* MurAA 151

FIGURE Page

70 Electrostatic density map comparison of *Bs* MurAA and *E. coli* MurA 154

71 Model for Qβ lysis 157

72 Model for Qβ^{por} lysis 159

LIST OF TABLES

TABLE		Page
1	f2 plating on a nonpermissive host	19
2	Cellular pools of MurA ligands	33
3	Plasmids used in this study	40
4	Primers for A_1 cloning	41
5	Sucrose gradient fraction analysis of Qβ RNA release	48
6	Critical concentration of A_2 to induce host lysis	49
7	Qβ A_2 quantification	52
8	Qβ^{por} sequence	55
9	Quantification of MurA protection during a Qβ infection	59
10	Primers used in construction of A_2 fusion proteins	72
11	Primers for construction of *murA** alleles	109
12	MurA*^{D305A} Qβ protection assay	128

CHAPTER I

INTRODUCTION AND LITERATURE REVIEW

Mode of Phage Virion Release

Studies of the bacteriophage (phage) infection cycle have been important for our understanding of gene replication, expression, and regulation. One fundamental question of this infection cycle that has received less attention is: How do newly formed virion particles escape their host cell? Two basic strategies have evolved for this purpose: (i) a nonlethal form of secretion is employed by filamentous phages in which a secretion apparatus is encoded for continuous extrusion of progeny phage from the host cell and (ii) a lytic method that results in host cell rupture (lysis) due to physical degradation of the bacterial cell wall (murein) or alternatively, inhibition of cell wall biosynthesis/turnover (15).

dsDNA phage lysis

Interestingly, the means by which lytic phages lyse a host cell correlates with the size of their genome. Phages with large genomes encode a muralytic enzyme that degrades the cell wall, along with other proteins to regulate its function and, in the case of Gram-negative bacteria, to disrupt the outer membrane (174) (FIG. 1). Lysis and the

---

This dissertation follows the style of Journal of Bacteriology.

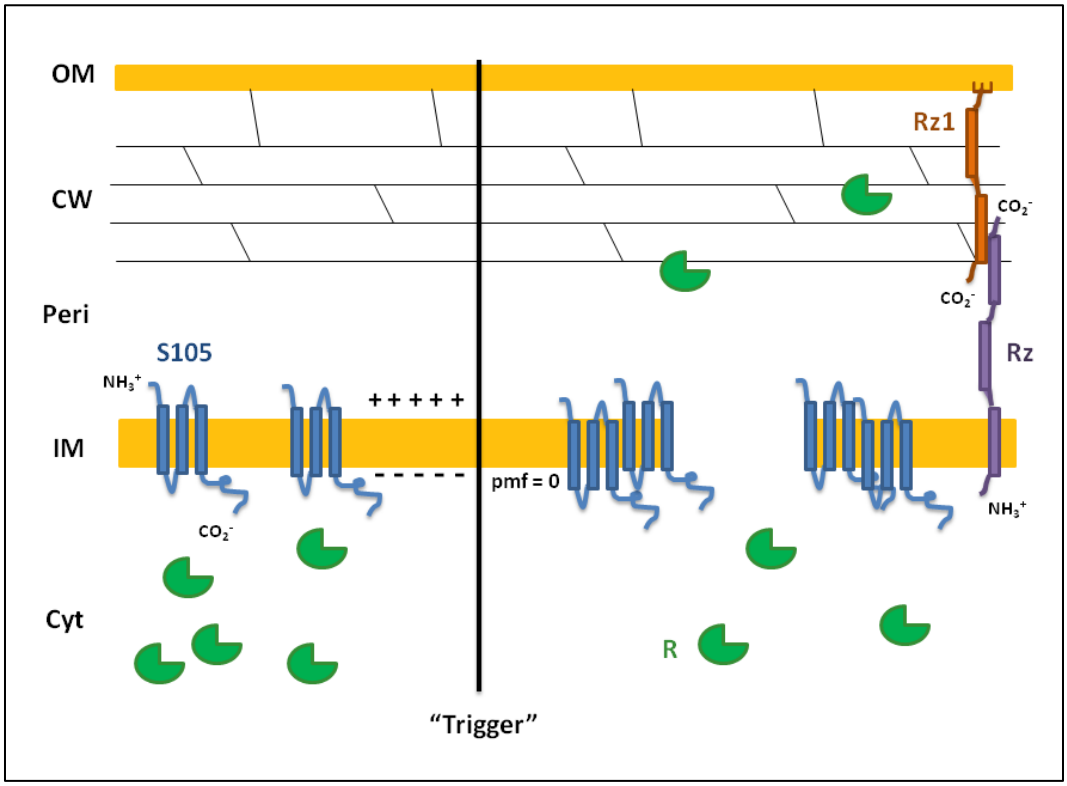

FIG. 1. The λ lysis paradigm. Lysis proteins accumulate in the membranes and cytoplasm of the cellular envelope of a Gram-negative host: S105 (blue, IM), R (green, Cyt), Rz (purple, IM), and Rz1 (orange, OM). S105 accumulates and oligomerizes in the inner membrane (IM) until an allele specific triggering time when the proton motive force collapses and triggers a large hole formation. This triggering event releases R molecules that were accumulating in the cytoplasm (Cyt) into the periplasmic space (Peri) to degrade the cell wall (CW). The last event in lysis is disruption of the outer membrane (OM) by the spanin-complex (Rz-Rz1).

termination of the infection cycle is an explicitly programmed event for complex phages with double-stranded nucleic acids. For Caudovirales, at least two and as many as five proteins are required for efficient, temporally-regulated lysis (174). The minimal set is comprised of a holin and an endolysin. The former is a small integral membrane protein that controls the timing of lysis by permeabilizing the cytoplasmic membrane in a temporally-regulated manner. This allows release of the endolysin into the periplasmic space to attack the peptidoglycan. Holins are genetically malleable, allowing rapid mutational adjustment of the length of the infection cycle to fit changing environmental scenarios.

In terms of membrane topology, there are three classes of holins that have been experimentally characterized (FIG. 2) (174): (i) Class I, proteins with three transmembrane domains (TMD) and an N-out, C-in topology. Representatives of this class include λ S and P2 Y. (ii) Class II proteins have two TMDs, with both N and C termini disposed in the cytoplasm. The prototypical protein from this class is S^{21} from phage 21. (iii) Finally, class III contains protein with a single TMD and a large periplasmic domain that adopts an N-in and C-out topology. This class is represented by the 216 amino acid (aa) T protein of phage T4. Class I and II holins are extremely diverse, with many unrelated gene families. Class III is uniquely populated by T and its homologs, mostly in T4-like phages.

All three holin classes are regulated by different mechanisms. The prototypical class I holin gene, λ *S*, is a reading frame of 107 codons encoding two gene products,

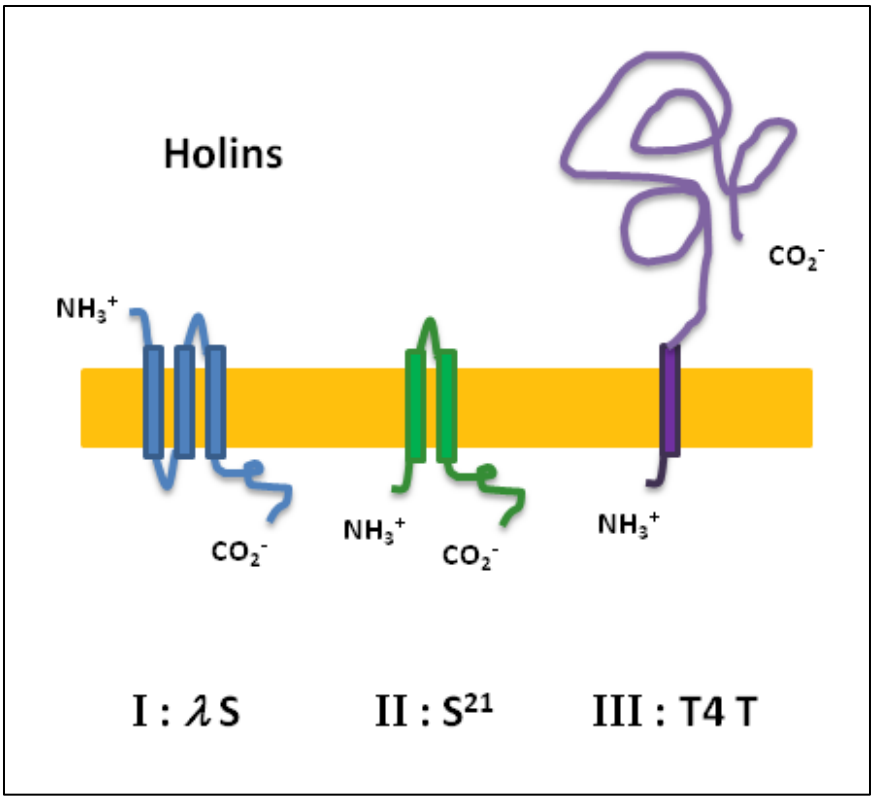

FIG. 2. Holin topologies. Three general classes of holins have been experimentally determined. Class I holins, such as λ S, have 3 transmembrane domains (TMD) with N-out, C-in topology. Class II holins like S^{21} from phage 21, have 2 TMDs with N-in, C-in topology. The third class of holins have a single TMD with the N-terminus inside and a large C-terminal domain in the periplasm.

S107 and S105, based on translational initiations at either codon 1 or codon 3 (123). The holin, S105, accumulates harmlessly in the membrane until suddenly "triggering" to form large holes of a 100 nm-1 μm scale (34). The precise molecular basis of holin triggering is unknown, but it involves massive oligomerization, a collapse of the proton motive force (PMF), and a reorganization of the holin into a large hole of micron scale diameter (34, 174, 175). The massive hole allows non-specific escape of the phage endolysin from the cytoplasm, leading to immediate degradation of the peptidoglycan (159). The S107 product is designated as an antiholin, in that it binds to S105 and inhibits its oligomerization (19). The operational difference between S107 and S105 is that there is a lysine residue at position 2; the additional positive charge prevents S107 from assuming the N-out, C-in topology.

The S^{21} protein from phage 21 is the only class II holin that has been characterized experimentally (174). Unlike S105, when S^{21} triggers, it forms small heptameric holes, with channels estimated at < 2 nm diameter (114). For this reason, S^{21} has been designated as a "pinholin". Because these holes, designated as "pinholes" are so small, endolysins cannot pass through them to attack the cell wall (120). Thus pinholins require that the endolysin be secreted by the host *sec* system. These special endolysins, designated as SAR endolysins, accumulate in the periplasm in an inactive, membrane-tethered form (172, 174). Upon depolarization of the membrane by holin triggering, the SAR endolysins release from the bilayer, refold into an active conformation, and attack the peptidoglycan. Like λ *S*, the S^{21} gene produces both a holin and antiholin form based on alternate translational starts (5).

Some phages, like the classical phage T7, encode class II holins but also make canonical endolysins, lacking signal sequences. These class II holins must thus make large holes like λ and other class I holins, but this has not been experimentally addressed (174).

Both class I holins and the class II pinholins do not appear to be regulated in a real time sense; that is, a particular allele of either type of holin will trigger lysis at an allele-specific time. Class III holins, such as T4 T, share the ability to make large holes like those made by the λ holin (34, 174). However, T and its homologs have the ability to be actively regulated by environmental information. This process, known as lysis inhibition (LIN), is regulated by the antiholin, RI in T4 infections, which is secreted into the periplasmic space (107, 153). RI complexes with the holin, T, and prevents holin oligomerization (107, 153). RI is susceptible to proteolytic cleavage with a half-life of ~ 2 minutes (152); therefore, continuous secretion of RI is needed to maintain the LIN state. An unknown signal from superinfecting phages assists in stabilizing RI and extending the half-life nearly tenfold.

The final step in virion release is disruption of the OM of the Gram-negative host cell. This is accomplished in λ infections by production of a spanin complex, Rz and Rz1, which spans the width of the periplasmic space (17). It has been proposed that upon removal of the murein, by the endolysin, a conformational change of the spanin complex induces inner and outer membrane fusion and release of progeny virions.

ssDNA/ssRNA phage lysis

There are three types of small phages with single-strand nucleic acids and genome sizes of ~5 kb or less, all of which infect Gram-negative bacteria: the *Alloleviviridae* (ssRNA; prototype Qβ), *Leviviridae* (ssRNA; prototype MS2), and *Microviridae* (ssDNA; prototype ϕX174) (FIG. 3). In contrast to phages with large genomes, these three types of simple phages effect lysis by expression of a single gene without muralytic activity (15). Of these "single gene" lysis systems, two are known to cause lysis by inhibition of an essential enzyme in the murein precursor pathway: Qβ A_2 inhibits MurA (16) and ϕX174 E inhibits MraY (13). In both cases, lysis primarily occurs when the host cell attempts to septate in the absence of murein synthesis. The third, MS2 L, effects lysis by an unknown mechanism that does not affect murein synthesis nor require cell division.

The ssRNA phages are similar in their virion structure and mechanism of infection but are distinguished based on their 5' and 3'-end RNA secondary and tertiary structures, serological properties, and lysis proteins (156). MS2 and Qβ have a similar core genomic structure, with three genes: 5'-*assembly-coat-replicase*-3' (56, 67) (FIG. 3). The assembly protein in Qβ (A_2) serves as the lysis protein for this system; however, MS2 has a fourth gene, *L*, dedicated to lysis, which lies in an alternative reading frame that overlaps the 3'-end of the *coat* gene and the 5'-end of the *replicase* gene.

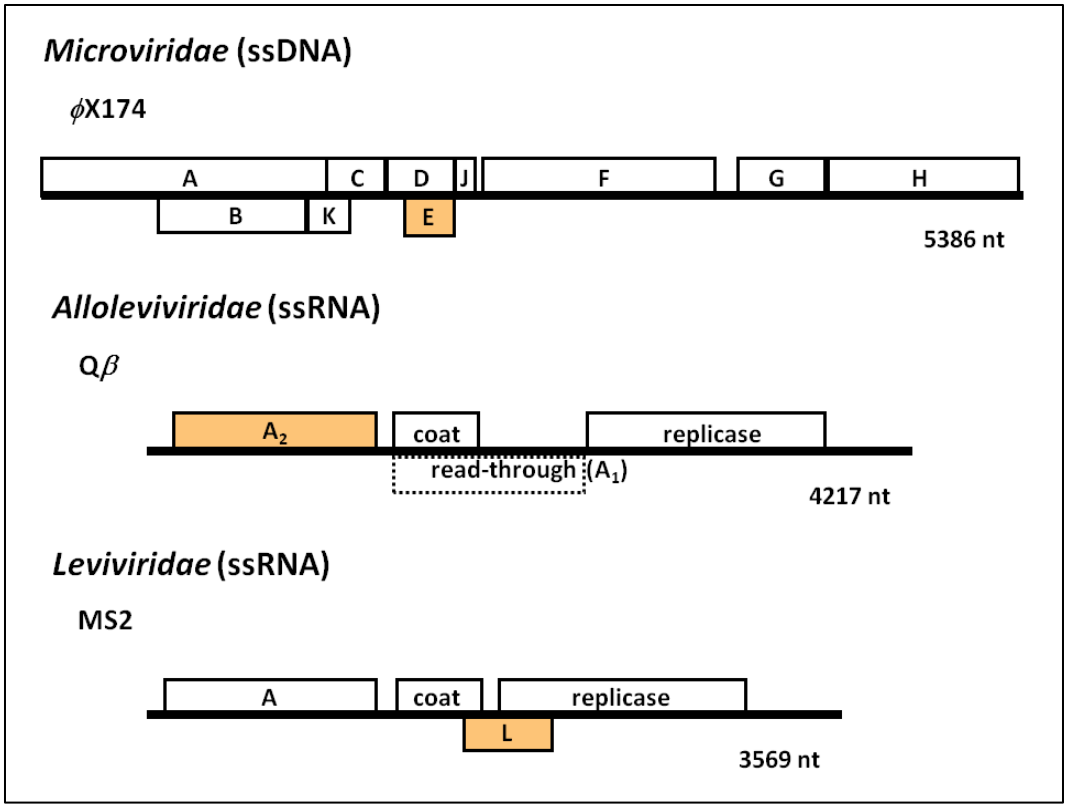

FIG. 3. Genomic maps of phages with single lysis gene products. *Microviridae* phages have a circular genome of ssDNA (depicted as linear). *Alloleviridae* and *Leviviridae* phages have genomes comprised of ssRNA. Qβ-like phages produce A_1 protein from read-through of the *coat* gene. Lysis proteins are highlighted.

Little is known in these systems about lysis regulation at the post-translational level. In ϕX174 infections, E appears to be made in sufficient quantities to inhibit all the MraY in the cell soon after infection (14). Production of sufficient virions is achieved only because there is a significant lag time between the halt in cell wall biosynthesis and the average time before the host cell attempts to septate. A host cis-trans peptidylprolyl isomerase, SlyD, is required for stabilization of the E protein and may be key to lytic regulation (12). The Qβ lysis system is unique in that the lysis protein, A_2, has other roles essential to maturation protein functions, such as morphogenesis, adsorption to the host, and penetration of the genomic RNA to the cytoplasm. At the very least, the other functions assigned to A_2 require binding to Qβ RNA, the phage particle, and the host F-pilus, thus providing an assortment of potential regulatory modes in the infected cell.

The Qβ Life Cycle

Qβ was isolated by Watanabe in 1964 (71, 162) three years after the first RNA phage was discovered (95). Much of what is known about the Qβ system comes from the studies of the related Levivirus phages. Qβ is a ssRNA bacteriophage whose 4.2kb genome contains three cistrons that encode four proteins: *maturation* or A_2, *coat*, read-through coat or A_1 and *replicase* (FIG. 3). The 5'gene is called *A* in MS2 and A_2 in Qβ. It encodes a ~ 48 kDa protein that is present in a single copy on the virion, has multiple functions and is required for infectivity. In both Qβ and MS2, it is also referred to as "maturation protein" or "assembly protein" depending on the context. The maturation

protein binds a single RNA genome and is assembled with approximately 165 copies of the coat protein, ~ 15 copies of the read-through coat protein and a single copy of A_2 (156) mounted on the surface of the virion particle. A_1 is the result of low level read-through of the UGA termination codon of *coat*, resulting in insertion of a tryptophan residue and extension of the reading frame by 196 residues (84). Despite the low level of expression, estimated at < 15 copies per progeny virion, A_1 is required for infectivity (42, 57, 84, 165). The *replicase* gene product is an RNA-dependent, RNA polymerase, necessary for synthesis of new viral RNA. Replicase associates with several host proteins: EF-Ts, EF-Tu, S1 to form the replicase holoenzyme (71), and in the case of Qβ an additional host protein, Hfq (HF-I), is required for synthesis from the positive strand (25, 45, 103).

Adsorption of ssRNA phage and injection of viral RNA

RNA phages require a conjugative pilus for infection. The best-studied RNA phages are those that bind to the F sex factor pilus, the MS2-like *Leviviridae* and the Qβ-like *Allolevivirida*e. Adsorption of virion particles to filtered F-pili was observed with the MS2-like f2 phage but not an f2 mutant that lacked the A protein (93), which suggests that the maturation protein is located on the surface of the particle and serves a role as recognition protein for the F-pilus. Association of the particle to purified pili was also shown to be dependent on the presence of a divalent cation (155), and this dependence has also been reported for infection of bacteria by phage (115).

Visualization of phage and pili complexes showed that RNA phage adsorb along the side of the pilus unlike filamentous phage that adsorb to the tip (26). Moreover, mutant forms of the major F-pilus subunit, TraA, with increased overall positive charge were shown to reduce the ability of RNA phage to adsorb (46).

Adsorption of R17 virion particles, a MS2-like phage, to the F-pilus is heterogeneous (86, 118) due to a mixture of infectious and noninfectious particles. About 10% of a population, thought to be deficient in the maturation protein, does not adsorb to the pilus. Another 10% of the phage efficiently bind the pilus and are highly infective. The remaining 80% of phage particles weakly adsorb to the F-pilus and are not infective. A possible explanation for the difference between the infectious and noninfectious particles that adsorb to the pilus could be from an improper orientation of the maturation protein on the surface of the particle such that particles are able to weakly bind the F-pilus but not elicit ejection of the viral RNA.

It was discovered that an f2 phage titer, defined as the plaque-forming-units (PFU) per ml, decreases in the presence of cell-free F-pili. This particle association with purified F-pili was thought to "inactivate" particles (155). However, subjecting the pili-phage mixture to shearing in a blender released viable particles. Also, addition of RNase to the reaction did not cause dissociation from the purified pili as in the case with cell-associated pili suggesting that ejection of the RNA from the capsid is not occurring. Therefore, the authors proposed that particles are able to reversibly bind to cell-free pilin, and that an additional step beyond physical association of the maturation protein to

the F-pilus is needed for RNA ejection from the capsid. The ejection step is believed to be energy dependent since cell-associated pili are required for ejection of the RNA from the capsid and a drop in cellular nucleotide triphosphates is also observed with infection (116).

Upon ejection from the capsid, the viral RNA is piloted into the host cell with the assistance of the maturation protein (83, 85). Wong and Paranchych proposed that the ejection is polar with ejection of the 3'-end first. The authors chemically treated R17 phage particles with ascorbate and Cu^{2+}, which fragmented the RNA, and added the treated phage particles to a bacterial culture. Analysis of the particles after infection revealed a simultaneous loss of the A protein and the 3'-end fragment (170) suggesting that the A protein and the 3'-end of the viral RNA are ejected from the capsid first.

Injection of the viral RNA proceeds rapidly in the first 5 minutes of an infection after which the penetration slows down for the rest of the infection cycle. This initial injection stage or eclipse period correlates with a reduction in the amount of cellular nucleoside triphosphates (32, 119). Krahn and colleagues had found that only 30-35 phage RNA equivalents can penetrate a single cell (85, 116); however, Paranchych and colleagues determined that as much as 250 viral RNA molecules can be transferred to a bacterial host during a single eclipse period with high inputs of infective phage particles (116). The authors observed that with an input multiplicity of infectious (MOI) phage particles $\leq$ 10 per cell, nearly all the RNA is able to penetrate, but if input MOI was higher than 10 phage per cell, large increases in infectious phage particles are required to

achieve small increases in RNA penetration. This suggests that the bacterium has developed a mechanism to limit the amount of RNA that penetrates the cell.

The maturation protein pilots the viral RNA into the host cell and in the process is thought to be cleaved, based on experiments with radiolabelled particles (83, 85). Krahn and colleagues found that labeled A protein from the MS2-like phage, R17, is injected into the bacteria at a 1:1 molar ratio of A protein to viral RNA (85). Analysis of the protein from the infected cells revealed three distinct peaks which correspond to 39, 24 and 15 kDa; the sum of the latter two protein masses matches that of the full length A protein (39 kDa), so the authors proposed that the maturation protein was cleaved upon injection into the host cell. Kozak and Nathans also reported two peaks that appear to be of similar size to the protein cleavage products seen by Krahn and colleagues, with the smaller of the two running at about the same molecular weight as coat (83, 85); however, the authors proposed that the peaks could be degradation products from experimental manipulation prior to sample analysis. The cleavage of the maturation protein was thought to be an attractive possibility for signaling of RNA ejection from the particles (119). A different conclusion was reached by Zinder and Cooper. The authors infected a nonsuppressor strain with an f2 mutant containing a nonsense mutation in the *A* gene (83, 180). From the infection they claimed to obtain on average one viable phage per cell; thus the authors proposed that a physical transfer of viral RNA, along with the maturation protein, from the parent to the progeny must occur. Another lab had also reported a low level of recycling of infecting phage RNA. They observed a 3% transfer of infecting viral RNA to progeny virions, which they concluded was from re-utilization

of superinfecting phage RNA (33). The physical transfer of the maturation protein was not studied in detail in any of these studies. Additionally, the fate of the Qβ maturation protein has not been studied in detail.

There is controversy over whether the nucleic acid is injected into the central lumen of the pilus upon ejection from the capsid or simply slides down the outside of the pilus (22, 119, 171). Wong and Paranchych provided the strongest evidence that argues against RNA injection through the central core of the pilus. The authors chemically treated R17 phage particles with ascorbate and Cu^{2+}, which fragments the viral RNA. Electrophoretic analysis of the injected RNA (^{3}H-labeled) under non-denaturing and denaturing conditions revealed that the RNA contained breaks that must have been held together by base pairing as the RNA was injected into the host cell (171). This data suggests that the overall secondary structure of the viral RNA is maintained during infection. The complex secondary of the viral RNA would be too large to traverse the 3 nm central core of the F-pilus (161) and supports the notion of an alternative means of viral RNA delivery to the host cell.

It was proposed that the F-pilus retracts to bring phage particles close to the vicinity of the bacterial membrane for viral RNA injection (31, 98); however, several lines of evidence argue against the pilus retraction model: (i) destruction of the pilus occurs upon phage adsorption since the loss of F-pili correlates with an observed increase in pili fragments in the medium (116), (ii) visualization of bacterial mating pairs showed that exchange of genetic material occurs between cells that are not visibly in

close contact (111), and (iii) adsorption of chemically modified R17 phage resulted in both pili retraction and extension (28). Taken together, this would argue against injection through the central lumen of the F-pilus but more likely support the notion that the pilus is just an appendage on which the RNA travels for delivery to the outer membrane. Interestingly, a couple of groups have shown that purified viral RNA void of maturation protein produce plaques when spheroplasts are infected (62, 112). However, another group reported that viral RNA is only infectious with non-spheroplasted cells if the maturation protein is also present (135). This suggests that the maturation protein plays an active role in the injection process rather than just delivery of the viral RNA to the cellular membrane. Moreover, Shiba and Suzuki (1981) found that fragments of viral RNA act as competitive inhibitors of maturation-bound RNA infection by physically occluding the pili binding domain of the maturation protein. This suggests that other than adsorption to the pilus and ejection of the viral RNA from the capsid, binding of the F-pilus by the maturation protein is required for injection into cells.

Replication

Qβ RNA does not replicate through a DNA intermediate (30, 35, 55) but encodes a RNA-dependent RNA polymerase termed "replicase" (53, 142, 168) that is synthesized immediately from the viral RNA upon entry into the host cytoplasm (156). After translation the replicase associates with host proteins: EF-Ts, EF-Tu, and ribosomal protein S1 to form the replicase holoenzyme (71). EF-Ts and EF-Tu are protein

synthesis elongation factors that are required for minus strand initiation (21, 88, 166). EF-Tu has a high affinity for guanosine nucleotides and is thought to assist in priming the pppG 5'-end of the minus strand for replication initiation (71, 166). EF-Ts was hypothesized to assist in release the 5'-end of the nascent RNA product (71), but more recently, it was determined that it assists in stabilizing EF-Tu in the holoenzyme (73). Binding of the Replicase to the positive strand of the Qβ RNA is achieved by S1, which is a dissociable r-protein that acts as a bacterial translation factor (70, 71). The Replicase holoenzyme, with the assistance of S1, also acts as a translational repressor by binding to a sequence in the central region of the viral RNA that overlaps the coat ribosome binding site (RBS) (81, 82, 103, 163). This process prevents re-initiation of ribosomes at the coat start codon and clears the positive strand RNA. This is important for minus strand replication, because c RNA synthesis cannot precede with ribosomes bound to the template (80, 82). The minus strand serves as the template for new positive strand synthesis (128, 143), which does not require additional host factors besides the Replicase and EF-Ts/EF-Tu during *in vitro* synthesis (126). Qβ requires an additional host protein, Hfq (HF-I), for synthesis from the positive strand (25, 45, 103). HF-I is a bacterial protein that associates with Qβ RNA and remodels the secondary structure of the 3'-end of the plus strand to permit replication (90, 103, 134). MS2-like phages do not require Hfq.

Folding of the RNA into complex secondary structures during replication is thought to prevent annealing between the positive and minus strands (4, 139). The Replicase holoenzyme holds the minus and positive strands in a configuration that

permits transient hydrogen bonding as chain elongation occurs. It was determined that this bond formation is specific to the holoenzyme since treatment of the replicative complex with protein denaturants converts the intermediates into double-stranded RNA yet the same treatment of just positive and minus strands devoid of protein does not yield the same result (71, 167). Replicase expression is repressed by Coat binding to a region distal to the *coat* cistron and overlapping the start of the *replicase* reading frame (10, 148). This regulation is phage-type-specific since f2 Coat has no effect on Qβ RNA replication (126). Without repression, Replicase expression is upregulated and the amount of dsRNA is increased.

Replicating RNA was determined to undergo coupled transcription and translation since replicating complexes were found in polysomes at the start of the infection cycle (48, 60, 61). *In vitro* translation experiments supported this hypothesis when Staples and colleagues showed that the maturation protein can only be synthesized from replicating nascent strands that are shorter than 500 nucleotides in length (145). This suggests that ribosome initiation and elongation of the maturation protein precedes RNA folding into complex secondary and tertiary structures. The idea that the maturation protein gene is negatively regulated by RNA folding is supported by secondary structure analyses of the 5'-end of Qβ RNA, which revealed that long-distance interactions sequester the RBS of A_2 (7). Groeneveld and colleagues had also shown that by decreasing or increasing hairpin loop length in the 5'end RNA secondary structures, the levels of maturation protein translation were modified, perhaps due to transient RNA folding kinetics (50). Increasing the long-distance nucleotide base

pairing with the RBS, however, did not affect maturation protein translation levels, which suggests that the rate of the RNA folding is the primary determinant for ribosome accessibility to the maturation protein RBS, which supports the hypothesis that translation occurs from nascent RNA molecules. Recently, Jayant and colleagues determined that A_2 expression is also regulated by ribosomal competition for binding since ribosomes had a higher affinity for the Coat RBS than that of the Maturation protein (66). Both RNA folding kinetics and ribosomal competition for initiation could explain why maturation protein synthesis is only 2-5% that of Coat in *in vitro* translation experiments (92).

Replication of viral RNA is dependent on the delicate balance between the coupled transcription and translation. By isolating several amber mutants of phage f2, Zinder and Cooper had shown that phage with a nonsense mutation in the *coat* gene were unable to lyse cells of a nonsuppressor strain (see TABLE 1). However, when this infected strain was subjected to a secondary infection i.e., "superinfected", WT f2 phage lysed the cells (180). This *coat* mutant produces little RNA early in infection (94); therefore, the simplest interpretation is that in the absence of active replication, superinfection is not inhibited. Alternatively, a mutation in the *maturation* cistron of phage f2 had prevented superinfection of WT f2 phage from taking place (180). This mutant undergoes normal infection and replication, but is unable to produce maturation protein to make infectious particles. This suggests that Coat could bind to the RNA of superinfecting phage and prevent replication. On the other hand, the su-11 allele of *coat* does not support superinfection (TABLE 1) (180). Su-11 is a mutation in *coat* that

produces excess amount of Replicase, which in turn, yields excessive dsRNA (94). Excessive Replicase produced from this mutant appears to have detrimental effects on superinfecting phage. Whatever the factor is it has to be produced within a few minutes and be diffusible to inhibit replication of the superinfecting phage. Interestingly, superinfection of MS2-infected cells by Qβ is permitted (91) and suggests that the mechanism of exclusion is phage-specific and not a host cell factor.

TABLE 1. f2 plating on a nonpermissive host.[a]

Phage #	**Lysis**	**Coat antigen (μg/ml)**	**RNA (P/ml)**	**Viable yield**	**Gene mutation[b]**	**Superinfection**
Su-1	+	10-20	$3x10^{12}$	1	Maturation	-
Su-3	-	<1	$<3x10^{10}$	$<10^{-2}$	Coat[c]	+
Su-11	-	<1	-	$<10^{-2}$	Coat[c,d]	-
f2	+	10-20	$3x10^{12}$	8,000	None (WT)	n.d.

n.d. not determined

[a]Data from Zinder and Cooper (1964).

[b]Assignment based on mutation data.

[c]Polar mutant that affects L (lysis protein) expression.

[d]Polar affects on replicase expression (Lodish and Zinder 1966)

Virion morphogenesis

The capsid of dsDNA phages is constructed by assembling the major capsid protein around an internal scaffold built over a dodecameric portal ring. Once the prohead, consisting of the full complement of capsid proteins and cleared of the scaffold, an ATP-driven motor, the Terminase, catalyzes the packaging of the viral DNA, resulting in near crystalline-like states in the filled head (18). In contrast, Leviviruses initiate virion morphogenesis with cooperative coat binding and nucleation of the viral RNA to form the capsid. The viral RNA secondary structure has evolved not only to regulate RNA and protein synthesis but also to signal and support virion particle morphogenesis (106).

Once viral RNA is synthesized the maturation protein binds to the 5' and 3'-ends, circularizing the RNA prior to nucleation of the capsid (40, 136). It was shown through *in vitro* reconstitution of virion particles that the A protein must be bound to the RNA prior to coat nucleation to obtain infectious particles (78, 125). Several lines of evidence indicate that the A protein, bound to the RNA, is located on the surface of the assembled virion particle. The most direct evidence is that treatment of particles with various chemicals can cause dissociation of the maturation protein from the capsid (78). Moreover, the maturation protein is responsible for virion particle adsorption to the F-pilus (93) so it must be accessible on the surface of the capsid.

After a sufficient concentration of Coat has accumulated, the protein binds to the viral RNA not only to suppress Replicase synthesis but also to initiate capsid nucleation

(63). Cooperative capsid assembly with the RNA then proceeds through a series of intermediate steps that were identified through *in vitro* assembly experiments (147, 164). The initial Coat-RNA complex, termed "complex I", represses translation of the replicase protein. The RNA at this stage is only partially protected from RNase activity, and addition of maturation protein to this complex prior to complete particle assembly yields infectious assembled virion particles. The second complex, "complex II", are fully assembled particles which were characterized by their sedimentation profile. These particles are partially sensitive to RNase activity and do not produce infectious virions when A protein is added. Intermediate stages between these two complexes were characterized in studies of MS2 assembly (106). First, coat protein forms two different dimeric states for nucleation of the capsid, an asymmetric dimer (A/B) and a symmetric dimer (C/C), that differ with respect to the fold of the FG-loop (40). The FG-loop connects two beta stands, F and G, and provide important contacts in the five-fold and six-fold axes of symmetry of the assembled particles (110). These A/B and C/C complexes form hexamers and decamers of dimers that assemble with the RNA to build the virion capsid (40). Initiation of the capsid begins when the Coat dimers bind the TR loop, a high affinity Coat nucleation initiation RNA stem-loop. The authors determined that there are two possible assembly pathways in which the initial Coat-TR loop complex form: one that follows formation of the hexameric dimer complex to build a face of the icosahedron or alternatively, the formation of the decameric dimer complex which builds a vertex of the icosahedrons; flux through either of these pathways is dependent on the relative RNA:Coat protein ratio.

For *Leviviridae*, the final assembled virion capsid is an icosahedron with T = 3, quasi-equivalence symmetry (27) comprised of 20 faces and 12 vertices, made up of 180 copies of coat. In Alloleviviruses, the minor capsid protein A_1 accounts for ~15 copies of the 180 subunits of the capsid (96). The amount of A_1 incorporated into the capsid is close to the amount of vertices in the T = 3 symmetrical particle and could suggest a preference for A_1 to assemble into Coat dimers that are precursors for the decameric vertices. Support for this notion comes from the fact that the maturation protein is localized to a vertex for the MS2 phage (151). Moreover, A_1 is also a necessary capsid component that is required for infectivity (57) suggesting a direct involvement of A_1 in proper assembly of A_2 onto the virion. Additionally, Toropova and colleagues (2011) reported an increase in density above vertices in particles imaged with cryo-EM. This density could reflect A1 localization since it was also observed on the 3 fold axis of symmetry to a lesser degree.

Lysis

Attempts to identify the lysis proteins of Leviviruses began over 50 years ago when the ssRNA phages were first isolated. Characterization of these phages was performed by genetic analysis of nonsense mutations. Zinder and Cooper (1964) had isolated mutants of a Levivirus phage f2, an MS2-like phage, that were deficient in lysis. Analysis of the mutants revealed that Coat was not produced although RNA was still synthesized (TABLE 1). A suppressor mutation was obtained that reinstated Coat

production; however, the phages were still deficient in lysis. In 1968 another group proposed that the Coat protein perhaps indirectly initiates lysis by activating an unidentified lysozyme (181). It was not until three years after the genome of MS2 was sequenced that the lysis protein, L, was identified as a gene product from an alternate reading frame that overlaps the *coat* and *replicase* genes (3, 8, 105) (FIG. 3). The host target of L is still unknown; however, it likely targets a step in cell wall maintenance/turnover since peptidoglycan precursor molecules are still incorporated into the cell wall (11, 58).

Horiuchi and Matsuhashi (1970), performing genetic analyses of the Allolevivirus Qβ, isolated an amber nonsense mutant of A_2, the maturation protein, that formed defective particles yet did not lyse cells (59). This is in contrast to Leviviruses, where maturation protein nonsense mutants produce defective particles but support normal lysis in non-suppressing conditions (180). Three years later, Ozaki and Valentine had linked lysis to cell wall synthesis inhibition when they determined that infection with Qβ prevented incorporation of peptidoglycan precursor molecules into the cell wall (112). A_2 was not identified as the lysis protein for Qβ until 10 years later (72, 169). The host target of A_2 was discovered when Bernhardt and colleagues employed a genetic approach to identify which step of the cell wall synthesis pathway was blocked in Qβ infections (16) (FIG. 4). The authors isolated survivors of induction of a cloned A_2 gene and screened them for Qβ resistance. Two mutants survived these series of screens and were termed *rat1* and *rat2* (***r***esistant to $\boldsymbol{A_2}$). Both isolates contained

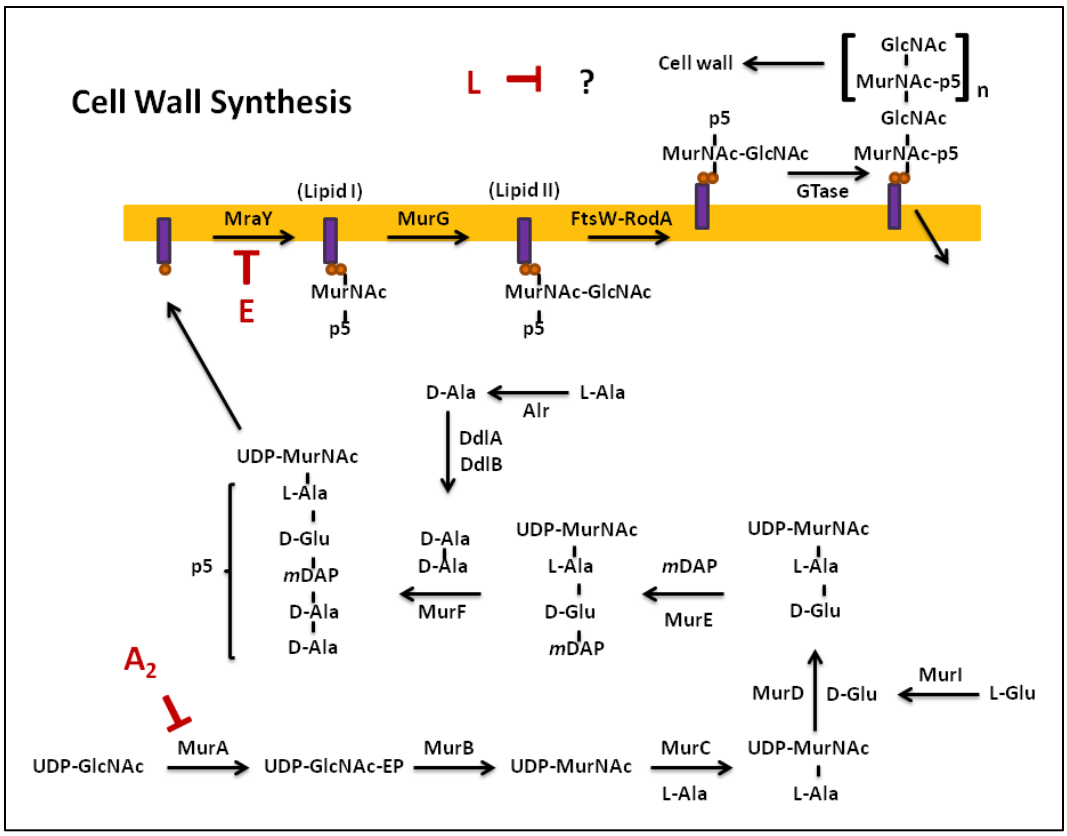

FIG. 4. Cell wall synthesis pathway. MurA is the first committed step of the peptidoglycan synthesis pathway. The enolpyruvate moiety is transferred from PEP to UDP-GlcNAc. The product of this reaction is converted to UDP-MurNAc by MurB. UDP-MurNAc-pentapeptide (p5) is formed by addition of amino acid or derivatives by additional enzymes in the pathway. The UDP-MurNAc-p5 precursor is attached to undecaprenyl phosphate by MraY, thereby forming the Lipid I precursor molecule. MurG generates the Lipid II precursor molecule by catalyzing the addition of GlcNAc to Lipid I. Lipid II is then flipped across the membrane, and a glycosyltransferase (GTase) catalyzes polymerization of the nascent peptidoglycan chain. The undecaprenyl phosphate is then flipped back across the membrane for further precursor subunit synthesis. Lysis proteins are shown inhibiting a given step in the pathway: Qβ A_2 inhibits MurA and ϕX174 E inhibits MraY. The target of L is not known; however, the protein does not inhibit precursor subunit incorporation.

mutations that mapped to *murA* as a single amino acid substitution, L138Q. Further evidence for MurA as the target of A_2 was presented when uridine 5'-diphosphate-N-acetylglucosamine (UNAG), the substrate of MurA, was found to accumulate upon A_2 induction from a plasmid. The authors also determined that the time required from the point at which A_2 inhibits cell wall synthesis to cellular lysis was approximately 20 minutes. Finally, MurA activity in a crude lysate was shown to be inhibited by intact Qβ particles, containing a single A_2 protein on the surface of each virion. Further support for an A_2-MurA interaction was obtained when compensatory mutants were isolated from rare plaques of Qβ plated on the $murA^{rat}$ strain. The mutants were termed *por* (***p***late ***o***n ***r***at), and were found to contain one of three amino acid substitutions: L28P, D52N and E125G (89). Preliminary studies on the *por* mutants revealed an increase in the amount of A_2 expression (89). Thus, the mutations may not provide residual effects that compensate for the L138Q mutation but rather affect the reaction equilibrium by increasing A_2 expression.

A model for lysis timing has been proposed, suggesting that lysis only occurs after the level of virion-associated A_2 reaches that of MurA, allowing time for morphogenesis (54). Previous work by C. Langlais implies that "free" A_2 is the inhibitory molecule in an infection (89). Quantification of MurA, total amount of A_2 produced and number of virion particles will shed light into how lysis timing is controlled during a Qβ infection.

Lysis gene regulation

In all three cases of single gene lysis, total expression of the lysis protein is severely limited compared to the morphogenesis proteins (156, 173). For phage ϕX174, the lysis gene *E* is transcribed constitutively from all promoters; however, the protein's overall translation level is severely limited by the fact that the E gene is embedded in the +1 reading frame of a highly expressed morphogenesis gene (6).

In contrast, strict negative translational control mechanisms based on dynamic RNA structures have been invoked to down-regulate the production of both Qβ A_2 and MS2 L (7, 50, 156). For MS2, the translation of L is linked to Coat protein translation since the L gene does not have a Shine-Dalgarno sequence (74). Two models were proposed for translation of L: (i) a frameshifting model in which L is translated after early termination of Coat translation (74) and (ii) a lateral diffusion model that proposes after completion of Coat translation, the ribosomes diffusion along the RNA until a the L start codon is recognized (1, 9, 77). Berkhout and colleagues found that destabilization of the hairpin loop that sequesters the RBS of *L* by translation of the *coat* gene precedes L translation (9). Thus, position of the coat termination site is important in regulation of L translation levels (9, 156). Klovins and colleagues (1997) also found that mutation of hairpin loops that do not alter the primary structure of the Coat protein greatly affect the fitness of the phage. Selection of suppressor mutants revealed restoration of the RNA secondary structure which further supports the role of RNA secondary structure in lysis protein expression.

In vitro experiments indicated Qβ A_2, as a maturation protein, is only translated from newly synthesized, nascent RNA strands (145). It was shown that once the RNA exceeds 500 nt, the viral RNA adopts a very complex secondary structure that forms several long distance interactions that sequester the ribosomal binding site. Increasing the amount of base pairing surrounding the RBS had no effect on the translation rate of A_2 (50). It was only when the length of the folding RNA stem-loop structures was modified that an effect on A_2 expression was observed (122). Thus, it was concluded that the rate of the RNA folding regulates the amount of maturation protein translation from the nascent transcribed viral RNA (127, 145).

Mapping the lytic domain of A_2

Attempts at mapping the lytic domain of A_2 have been reported by two groups (72, 89). Karnik and Billeter (1983) were unsuccessful in identifying a functional truncation of A_2. In contrast, C. Langlais was able to identify a C-terminal truncation that consists of the first 179 residues of A_2 still retains lytic activity. An alignment of the maturation proteins from Allolevivirus with that of Leviviruses, which have an alternative lysis protein, (FIG. 5) revealed that the region with the least amount of primary structure similarity lies in the first half of the protein. This was also the region in which the 'compensatory' *por* mutations, discussed previously, were also mapped (16, 89).

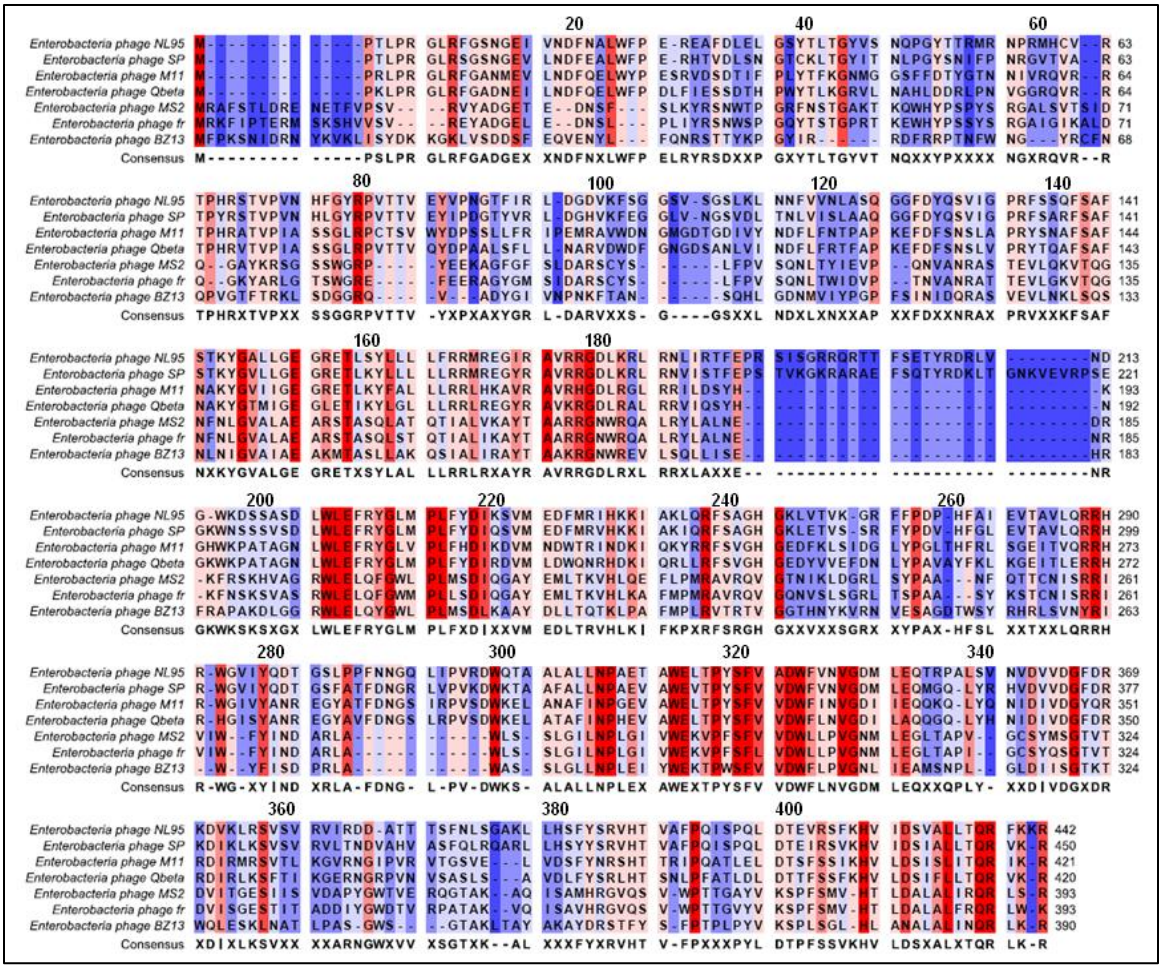

FIG. 5. *Alloleviviridae* A_2 and *Leviviridae* A alignment. *Alloleviviridae* A_2 proteins (phages: NL95, SP, M11, and Q*β*) and *Leviviridae* A proteins (phages: MS2, fr, and BZ13) were aligned. Alignment of the maturation proteins was performed with CLC Sequence Viewer (ref). Conserved residues are shown in red and non-conserved residues are depicted with blue.

Interestingly the C-terminal domain of the maturation proteins had two regions of highly conserved residues from around residues 204-218 and 307-334. These regions are more likely pili binding domains since the residues are highly conserved and dispensable for lytic function. A third region that spans residues 140-187 is not as highly conserved but is present in the truncated A_2 protein identified as retaining lytic function. A truncation that consists of the first 171 residues does not retain lytic activity. Loss of activity can be explained by two possibilities: (i) loss of a secondary structural element required for folding this N-terminal domain of A_2 or (ii) deletion of part of the lytic domain. Further experiments are needed to distinguish between these two possibilities.

MurA

MurA catalyzes the transfer of the enolpyruvyl moiety (EP) from phosphoenolpyruvate (PEP) to UNAG yielding two products, EP-UNAG and inorganic phosphate (Pi) (52) (FIG. 6). Several catalytic states of MurA have been crystallized for *E. coli* and *Enterobacter cloacae* (93% identity, 97% similarity to *E. coli*): (i) unliganded, open conformation (pre-catalysis state; PDB entries: 1DLG and 3SPB) (131, 179), (ii) UNAG-bound state (PDB entry: 3KQJ, H. Han, unpublished; and PDB entry: 3UPK) (179), (iii) UNAG-bound state with a covalent adduct formed between the catalytic Cys and PEP (PDB entry: 3SWA), (iv) fosfomycin-inhibited state with UNAG bound (PDB entry: 1UAE) (138), (v) a tetrahedral intermediate state with both UNAG

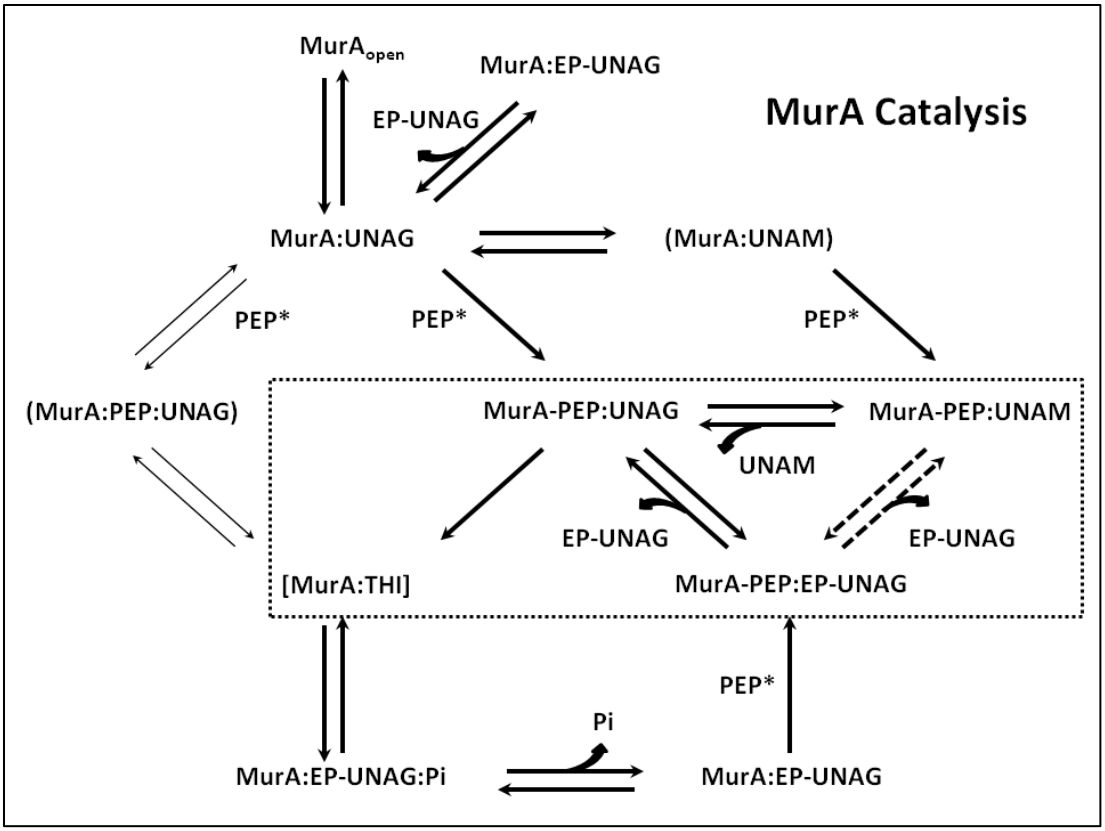

FIG. 6. MurA catalysis. Pathway modified from results reported previously (179). Unliganded MurA (open conformation) binds UDP-*N*-acetylglucosamine (UNAG) prior to binding phosphoenolpyruvate (PEP). Upon PEP binding a covalent adduct is generated with the catalytic Cys115 prior to formation of the tetrahedral ketal intermediate (THI). The enolpyruvate moiety (EP) is transferred to UNAG forming EP-UNAG and releasing inorganic phosphate (Pi) in the elimination reaction. After release, PEP binds and forms another covalent adduct with Cys115. MurA remains bound to EP-UNAG until displaced by either UNAG or UDP-*N*-acetylmuramic acid (UNAM), if the cellular [UNAG] is low. MurA-PEP:UNAM is a dormant complex, and UNAM remains bound until cellular the [UNAG] increases. The covalent catalytic pathway of MurA is highlighted with the dashed box. An alternative, non-covalent catalytic pathway with PEP bound is depicted with arrows that are weighted less. Changes in the previously reported pathway are shown with dashed arrows. PEP is designated with an asterisk to note points of catalysis that fosfomycin inhibits. Points in the pathway without available crystal structures are indicated with parentheses.

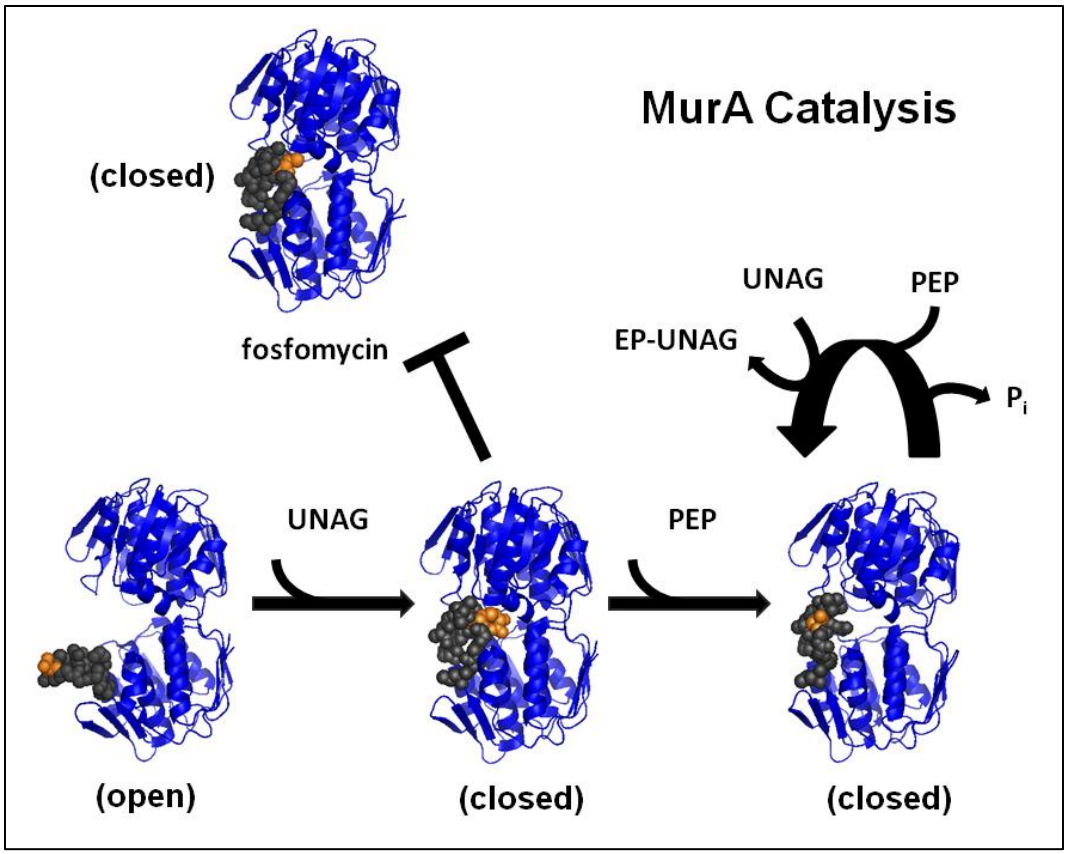

FIG. 7. Structural view of MurA catalysis. MurA is an induced fit enzyme with an open conformation (PDB entry: 1DLG) until UDP-*N*-acetylglucosamine (UNAG) binding (PDB entry: 3KQJ), which induces a conformational change of the catalytic loop (shown as spheres) and converts the enzyme into a closed conformation. Additional binding of phosphoenolpyruvate (PEP) (PDB entry: 1A2N) causes a slight conformational change in the catalytic loop as seen by the position of the catalytic Cys (highlighted in orange). Fosfomycin is a dead-end inhibitor of MurA. The structure of MurA-fosfomycin-UNAG (PDB entry: 1UAE) adopts a conformation similar to the UNAG-liganded MurA structure. MurA catalysis proceeds through the primary pathway shown in FIG. 6. Several steps were omitted here for simplification, which are depicted with a large bent arrow. PyMOL was used to generate figures (133).

and PEP liganded (PDB entries: 1A2N and 1Q3G) (43, 137), (vi) the EP-UNAG/Pi bound state (PDB entry: 1RYW) (44), and (vii) an EP-UNAGal-liganded conformation (containing the UNAG analog UDP-*N*-acetylgalactosamine) covalently bound to PEP (3SWI) (179). These structures provide insight into the MurA catalytic cycle, which is summarized in FIG. 6. Based on these structures, a major feature of the conformational changes associated with catalysis appears to be the dynamic behavior of the loop (FIG. 7) containing the catalytic Cys residue at position 115. Binding of UNAG is responsible for the major conformational change of the loop and UNAG binding is required before PEP can bind (132) (179). An additional structure showed that PEP is excluded from the active site by a covalent bond formation of fosfomycin with residue C115 of MurA and the C-3 hydroxyl of UNAG (138); this structure adopts a conformation similar to the UNAG-bound state. Mutation of the C115 residue is the basis for fosfomycin resistance of *Mycobacterium tuberculosis* MurA (76) and suggests that MurA has an alternative pathway for catalysis that does not involve the covalent adduct to PEP (179) (FIG. 6), but no crystal structure is available for this intermediate.

A dormant state of MurA has recently been identified in which the enzyme co-purifies with uridine 5'-diphosphate-N-muramic acid (UNAM) and a covalent adduct formed with PEP (104, 179) implying an important regulatory role *in vivo*. UNAM is the product of MurB the enzyme that acts immediately after MurA in the cell wall synthesis pathway (FIG. 6). Both UNAM and EP-UNAG have an approximately 100-fold lower K_d than that of UNAG (TABLE 2). This higher affinity of substrates for MurA could be important in the regulation of MurA catalysis and should be factored in

TABLE 2. Cellular pools of MurA ligands.

Substrate	[L] (μM)	K_d (μM)	θ[a]	Reference
UNAG	100	50	0.67	(100, 179)
PEP	150	0.17[b]	0.99	(100, 179)
EP-UNAG	2	0.17	0.92	(100, 179)
UNAM	5-37	0.94	0.84-0.98	(99, 104)

[a]See text for equation (1).

[b]Value is for UNAG bound MurA since the K_d for unliganded MurA (240 μM) (132) is greater than the cellular pool of PEP suggesting an ordered addition of UNAM then PEP.

vitro experimentation and may not reflect the state of catalysis *in vivo*. Insight into the pathways *in vivo* can be obtained from calculating the percentage of ligand bound to MurA (θ) based on previously determined K_ds and the cellular concentrations for the ligands with equation (1) (109):

$$\theta = \frac{[L]}{[L] + K_d}$$ where [L] is the concentration of ligand

Data for the binding equilibria for various ligands of MurA are listed in TABLE 2. The data support that MurA is predominantly found in a covalent adduct with PEP since the calculated θ = 0.99. This was the basis for drawing the catalytic cycle with PEP covalently attached as the primary pathway of MurA (FIG. 6). The calculated θ value for UNAG (0.67) was lower than that of EP-UNAG (0.92) and UNAM (0.84-0.98). This

is surprising since it would seem that the percentage bound should be higher but these numbers reflect the percent bound without any other ligand considered in the calculation. The cellular pools of EP-NAG and UNAM are 10-fold higher than the prospective MurA K_d values for the ligands (TABLE 2), which suggests that these ligands are actively competing with UNAG binding. This is supported by Mizyed and colleagues findings in which the authors performed competition experiments with UNAM that measured MurA activity in the presence of 100 μM UNAG, the concentration of the cellular pool of UNAG (TABLE 2). These analyses revealed that at ~ 6 μM of UNAM MurA activity was reduced by ~ 25% and at ~ 12 μM of UNAM approximately 95% reduction in activity was observed (based on Fig. 5b) (104). The concentrations of UNAM used in these studies are between 7 and 10-fold the amount of the K_d value but within the range of the cellular pool of UNAM (TABLE 2) suggesting that UNAG is in direct competition with UNAM as a ligand for MurA. Taking this data into consideration the MurA catalytic cycle shows an equilibrium between the MurA-PEP adduct and the 3 ligands (UNAG, UNAM, and EP-UNAG) (FIG. 6).

Project Aims

This work will address several gaps in our understanding of the Qβ infection cycle: (i) How is A_2 function regulated *in vivo*: a) what form of A_2 is inhibitory and b) at what point of an infection is cell wall synthesis blocked? (ii) How does A_2 inhibit

MurA: a) is inhibition the result of an A_2-MurA complex formation and b) can it be demonstrated with purified protein?

CHAPTER II

THE REGULATION OF LYSIS IN Qβ INFECTIONS

Introduction

The three known types of simple phages with single-strand nucleic acid genomes: Alloleviviridae (ssRNA; Qβ), *Leviviridae* (ssRNA; MS2) and *Microviridae* (ssDNA; ϕX174), effect lysis by expression of a single gene without muralytic activity (15). Of these, two are known to cause lysis by inhibiting an essential enzyme in the murein precursor pathway: Qβ A_2 inhibits MurA (16) and ϕX174 E inhibits MraY (13). In both cases, lysis occurs when the host cell attempts to septate in the absence of murein synthesis. The third, MS2 L, effects lysis by an unknown mechanism.

Qβ has long been one of the paradigm experimental systems for studying viral RNA-dependent RNA polymerase and RNA evolution, in part because of its simplicity (20, 37-39). The Qβ genome consists of only three genes, encoding four proteins: Maturation or A_2, Coat, Read-through coat or A_1, and Replicase (FIG. 8A). A single copy of A_2 is mounted on the Qβ virion, comprised of a T=3 capsid containing ~ 165 copies of coat, ~15 copies of A_1, and the 4.2 kb ssRNA (156). Among the three simple phage systems, the Qβ lysis system is unique in that the lysis protein, A_2, has other functions: it protects the genomic RNA from RNase degradation (164), mediates specific adsorption to the F-pilus, and chaperones the genome into the host cytoplasm (83). Since the other functions of A_2 require binding to Qβ RNA, the phage particle, and the host F-pilus, an assortment of potential regulatory modes are possible in the infected

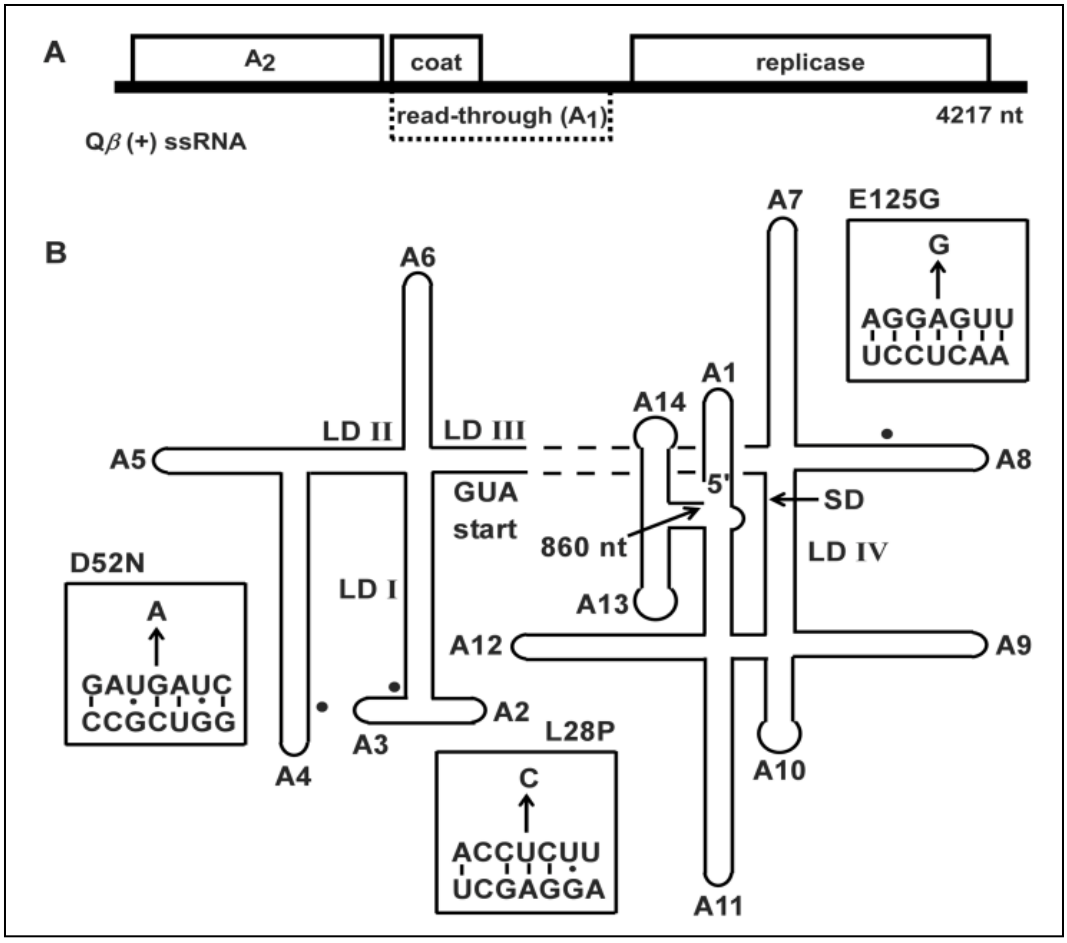

FIG. 8. Qβ RNA. (A) Qβ is a (+) ssRNA phage with a 4.2 kb genome. Replication of the chromosome is dependent on encoded replicase and four additional host proteins. Qβ RNA is encased by three gene products: Coat, the major virion structural protein, A_1 a minor component translated from read-through of the leaky coat UGA stop codon, and a single copy of A_2. (B) RNA secondary structure of Qβ 5'-end (nt 1-860). Stem-loops and long-distance interactions (LD) drawn and labeled according to Beekwilder and colleagues (7). Single nucleotide substitutions of Qβ*por* mutants depicted with black dots with specific sequence substitutions shown in boxes (arrow). Shine-Dalgarno (SD)

cell. A_2 expression is tightly regulated by extensive secondary structure surrounding its translational initiation region (7, 50) (FIG. 8B), and *in vitro* translation experiments indicate that A_2 is produced only from nascent transcripts (127, 145).

In 1983, Winter and Gold (169) revealed another function for this protein by showing that induction of *A_2* cloned on a medium copy plasmid was necessary and sufficient to induce host lysis. Nearly 20 years later, Bernhardt and colleagues (2001) discovered that induction of a plasmid-borne cDNA copy of *A_2* caused cell wall synthesis to cease at ~20 minutes prior to lysis, indicating that A_2 was acting as a "protein antibiotic" targeting murein biosynthesis. To address the mechanism of Qβ lysis, survivors of *A_2* induction were screened for insensitivity to viral infection. Two independent *rat* (*resistance to A_2*) mutants were mapped to *murA*, which encodes UDP-N-acetylglucosamine enolpyruvyl transferase, the enzyme catalyzing the committed step for the biosynthetic pathway of murein precursors. Both *rat* alleles proved to have a single missense change, L138Q. Biochemical studies of A_2 were impeded due to insolubility of the protein apart from the capsid (15, 16). However, MurA activity in a crude lysate was shown to be inhibited by intact Qβ particles. This led to a model for regulation of lysis in Qβ infections in which A_2 does not become inhibitory until fully assembled into the capsid (54).

Here, we have examined the inhibition of virion-assembled A_2 with purified MurA and quantified both MurA and A_2 during the Qβ infection cycle. The results are discussed in terms of a new model for regulation of lysis in Qβ infections.

Materials and Methods

Bacterial strains and growth conditions

The following *Escherichia coli* strains were used in this study: XL1-Blue (140) was used for all plasmid constructions. XL1-Blue^{rat} cells (16) were used for phage infections. HfrH *λ- relA1 spoT1 thi-1 lacI^{q} fhuA::*Tn*10* (HfrH) and HfrH *λ^{-} relA1 spoT1 thi-1 lacI^{q1} lacZ::*Tn*5* (HfrH *lacZ::*Tn*5*) served as lawns for bacteriophage plaque assays and cells for gradient induction, respectively. HfrH^{rat} construction was previously described (89). ER2738 (F′*proA*$^{+}$*B*$^{+}$ *lacI*^{q} *Δ*(*lacZ*)$_{M15}$ *zzf*::Tn*10*) *fhuA2 glnV Δ*(*lac-proAB*) *thi-1 Δ*(*hsdS-mcrB*)$_{5}$ (New England Biolabs) was used for phage propagation and protein expression. *E. coli* strains were grown with aeration at 37°C in standard LB medium supplemented with 100 μg ml^{-1} ampicillin, 40 μg ml^{-1} kanamycin, or 10 μg ml^{-1} tetracycline when appropriate. For Qβ infections, medium was supplemented with 2 mM $CaCl_2$.

Plasmid construction

Standard molecular biology techniques were performed as previously described (129). Plasmids used in this study that were constructed previously are listed in TABLE 3. The plasmid pZA32-*coat/A$_1$* was generated by amplification of the *coat* and *read-through* (*A$_1$*) gene from pQβ m100 (102) with the primers: A1-For and A1-Rev. The PCR product was digested with KpnI and XbaI and ligated into pZA32 (96), similarly

digested. To generate pZA32-*A1*, the coat stop was converted to the TGG Trp codon by site-directed mutagenesis (Stratagene) with primers: A1-stop-W-For and A1-stop-W-Rev. Primers used in this study are listed in TABLE 4.

TABLE 3. Plasmids used in this study.

Plasmid	**Reference**
pZE12-*murA*	(16)
pZE12-murAHis	(89)
pZE12-*murABs*	(89)
pZE12-A_2	(89)
pZE12-A_2*L28P*	(89)
pZE12-A_2*D52N*	(89)
pZE12-A_2E125G	(89)

TABLE 4. Primers for A_1 cloning.

Primer	Sequence
A1-For	GGGGTACCATGGCAAAATTAGAG
A1-Rev	GCTCTAGACTAAGCACGAGGAAC
A1-stop-W-For	GAACCCAGCGTATTGGACACTGCTCATTGCC
A1-stop-W-Rev	GGCAATGAGCAGTGTCCAATACGCTGGGTTC

MurA expression and purification

ER2738 cells harboring pZE12-*murAHis* were grown at 37°C with aeration and induced with 1 mM IPTG for 3 hours. Cells were collected by centrifugation at 4,000 xg for 15 minutes at 4°C, resuspended in buffer (0.1 M Tris-HCl [pH 8], 20 μg ml^{-1} DNase and 10 μg ml^{-1} RNase), and lysed by passage through a SLM-Aminco French pressure cell (Spectronic Instruments) at 16,000 psi. The lysate was clarified by centrifugation at 5,800 xg for 15 minutes at 4°C. Protein was precipitated with 70% ammonium sulfate, collected by centrifugation at 5,800 xg for 10 minutes at 4°C, and resuspended with equivalent volume of buffer (0.1 M Tris-HCl, pH 8). The crude protein sample was then applied to a Talon metal affinity resin (Clontech) and eluted with a 0 to 0.5 M imidazole gradient in the same buffer. One-hundred drop fractions were collected with a micro-fractionator (Gilson). Fractions were assessed for protein concentration (A_{280}) and activity as previously described (97). Fractions with the highest protein concentration

and activity were pooled and stored as an ammonium sulfate precipitant at 4°C until further use. All *in vitro* analyses use the oligo-histidine-tagged protein.

Phage inactivation assay

Qβ particles were purified as previously described (146). $4x10^{11}$ PFU of Qβ were mixed with 1 μg of MurA. A Qβ-only control as well as a sample including 1 μg of bovine serum albumin (BSA) (Sigma) was prepared in parallel. Samples were brought to 20 μl with buffer and incubated at 37°C for 1 hour. Samples were then brought to 1 ml with SM medium (129) supplemented with 5 mM $CaCl_2$. Ten-fold serial dilutions were prepared and 100 μl of various dilutions were included in the bacterial overlay for plating comparison. Plates were incubated at 37ºC for 6-8 hours and efficiency of plating was assessed. RNaseA (Sigma, 1.25 ng μl^{-1}) was also included in the inactivation assay with purified particles and MurA.

RNA release assay

RNA release from virion particles was determined by addition of an inactivation sample containing MurA (7 μg) and Qβ ($6x10^{13}$ particles) in 100 μl, incubated at 37°C for 1 hour, on top of a 5 and 50 percent sucrose step gradient (100 μl). The sample was run at 200,000 xg for 1 hour at 5ºC. 150 μl was removed from the top of the gradient.

The remaining sample was removed and 50 μl of buffer (0.1M Tris-HCl [pH 8.0]) was added to the tube to resuspend the pellet fraction. All three fractions were assessed for nucleic acid (A_{260}) and protein content (8% Tris-Tricine SDS-PAGE). MurA and Qβ only controls were performed in parallel.

MurA quantification

Quantification of MurA was performed by standard SDS-PAGE and immune-blotting procedures (51). HfrH cellular samples were precipitated with 10% TCA and washed with acetone prior to resuspending with sample loading buffer and running on an 8% Tris-Tricine gel. Blots were probed with α-MurA raised against the synthetic peptide: CHGKRPKAVNVRTAP (GenScript) at 1:3,000 dilution and goat-anti-rabbit 2° antibody (Pierce) at a 1:3,000 dilution. The SuperSignal West Femto developer kit (Pierce) was used for chemiluminescent detection. For a blotting control a *murA* knockout in which the chromosomal *murA* was replaced with a kanamycin cassette (23) was prepared via P1 transduction (101), with pZE12-*murA*^{Bs} provided *in trans*, to generate HfrH *murA::kan* pZE12-*murA*^{Bs}.

A_2 induction and quantification

The critical concentration for A_2-mediated lysis was determined by gradient induction of HfrH *lacZ::*Tn*5* pZE12-*A_2* with IPTG at final concentrations: 0, 12.5, 25,

50, 100 and 1000 μM. Cell growth was monitored as A_{550} and samples were taken for TCA precipitation. SDS-PAGE and immune-blotting was performed, as described above, with a 1:10,000 dilution of α-A_2 raised against a synthetic peptide: PKLPRGLRFGA (Bethyl Laboratories, Inc.) and 1:3,000 dilution of goat-anti-rabbit 2° antibody (Pierce). An A_2 standard was obtained by purifying inclusion bodies from cells expressing A_2 protein. The inclusion bodies were processed as previously described (113) and dissolved in 10 % SDS. An amino acid analysis of the purified protein was performed by the Protein Chemistry Laboratory (Texas A&M University) to determine the concentration of the A_2 in solution.

Quantification of A_2 during an infection was performed as described above, with samples of XL1-Blue cells infected with an input multiplicity of infection of 1 Qβ PFU per cell. The amount of A_2 per cell was determined by measuring the total amount of A_2 per ml, dividing by the total number of cells per ml, and multiplying by 1.6 to correct for the number of expected number of uninfected cells based on Poisson statistics.

Released/intracellular titer

To measure released PFU accumulation, 1 ml of culture was pelleted, and the supernatant was titered. For intracellular PFU accumulation, pellets were resuspended in 3 ml of LB and subjected to disruption by passage through a French pressure cell as described above. Serial dilutions of samples were prepared and an aliquot was added to an HfrH overlay.

MurA titration assay

Protection was determined by infecting HfrH *lacZ::*Tn*5* cells containing either pZE12-*luc* or pZE12-*murAHis* with a cell to PFU ratio of 1. Gradient induction of cells was performed, as described above, to determine the concentration at which MurA expression protects against a Qβ infection. Samples were taken at 60 minutes post infection for MurA quantification. At the end of a single round of infection (140 minutes), a sample was removed, centrifuged and the supernatant was titered for unadsorbed particles.

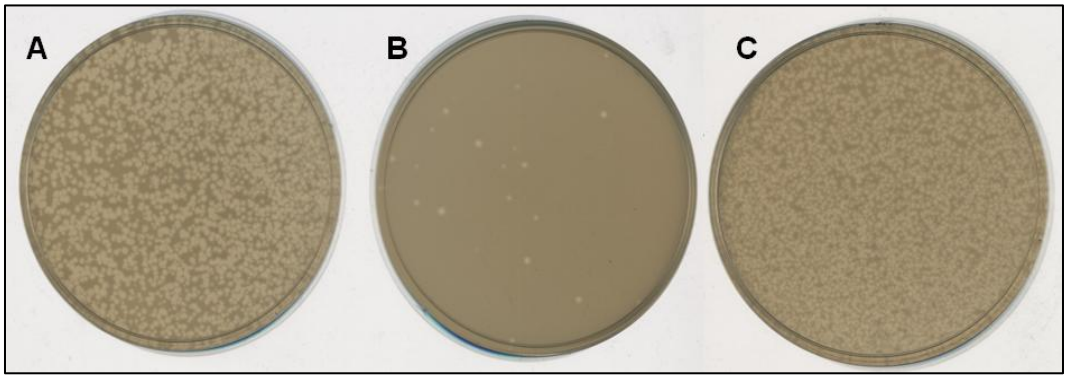

FIG. 9. Qβ particles are inactivated by incubation with MurA *in vitro*. Plating of purified Qβ particles (panel A) in an HfrH overlay. Incubation of Qβ with MurA (panel B) or BSA (panel C) was performed prior to plating.

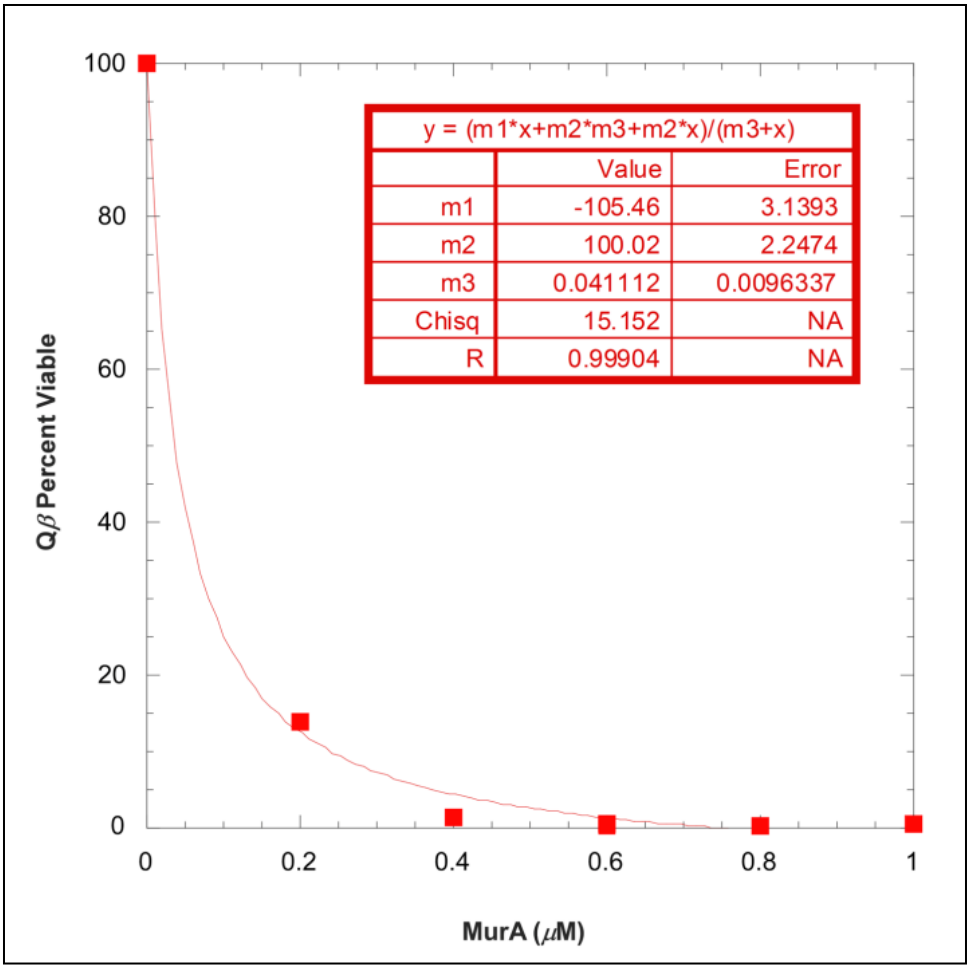

FIG. 10. K_i determination for Qβ inactivation by MurA. Percent viability of Qβ was measured after 30 minutes incubation with increasing amounts of MurA. K_i was determined by plotting viability vs. MurA concentration by plotting with KaleidaGraph and fit to the equation (2) (124):

$$V = \frac{Vmax[A] + V_o K_m + V_o[A]}{K_m + [A]}$$

Where [A] is [MurA] and V_o is the percent viable when [A] = 0. Vmax is m1, V_o is m2, and the K_i (K_m) is m3 with μM units.

Results and Discussion

MurA inactivates Qβ particles

Qβ inhibition of MurA activity has previously been addressed (16), but the effect of MurA association on Qβ plating has not. Incubation of purified Qβ with a three-fold excess of purified MurA prior to titering resulted in a reduction in plating efficiency of two orders of magnitude (FIG. 9A-B). In contrast, BSA did not reduce the plating efficiency (FIG. 9C), indicating that the inactivation is specific to MurA. Simple occlusion of virion particles to the F-pilus by MurA can be ruled out since the virion-MurA complex is diluted by $5x10^5$-fold before inclusion in the overlay. Based on this inactivation reaction, the apparent affinity of MurA for the virions was found to be ~ 40 nM *in vitro* (FIG. 10). The inactivation reaction was further examined by fractionation on a sucrose step gradient. Analysis of the fractions showed RNA release from a Qβ sample that was incubated with MurA; release was not observed with a virion only control (FIG. 11 and TABLE 5). The simplest interpretation is that MurA binding causes a conformational change of the maturation protein, allowing RNA release thus inactivating the particle. This result raises the question of how the two roles of A_2, as maturation protein and sole lysis protein, are balanced such that Qβ progeny are not inactivated during the latent period.

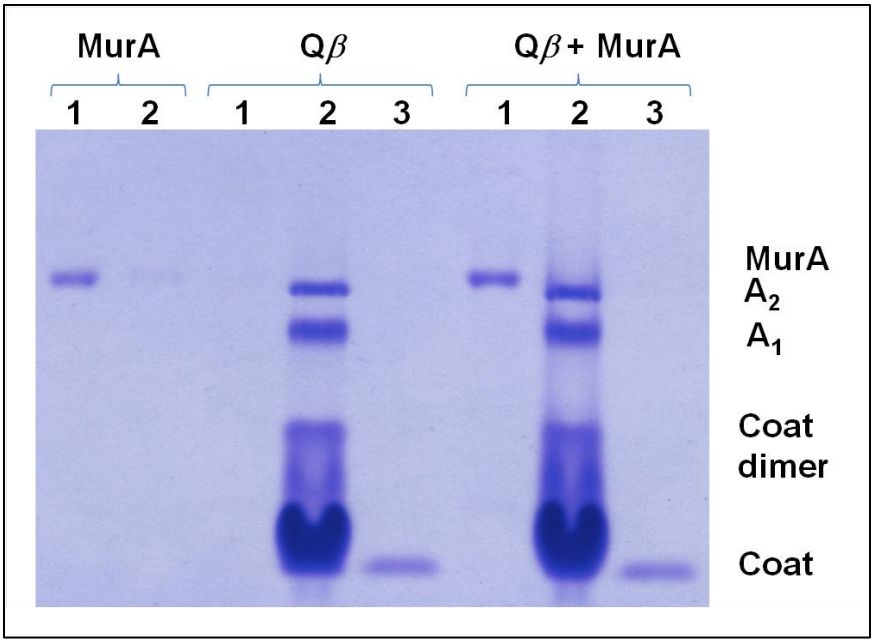

FIG. 11. Sucrose gradient analysis of Qβ particles incubated with MurA. MurA and Qβ incubation reactions were applied to a sucrose step gradient and centrifuged. All fractions were resolved on SDS-PAGE and assessed for nucleic acid content (TABLE 5).

TABLE 5. Sucrose gradient fraction analysis of Qβ RNA release.

MurA (A_{280})		**Qβ (A_{260})**			**Qβ + MurA (A_{260})**		
Fraction 1	Fraction 2	Fraction 1	Fraction 2	Fraction 3	Fraction 1	Fraction 2	Fraction 3
0.061	0.023	0.008	31.4	1.10	0.255	43.3	1.49

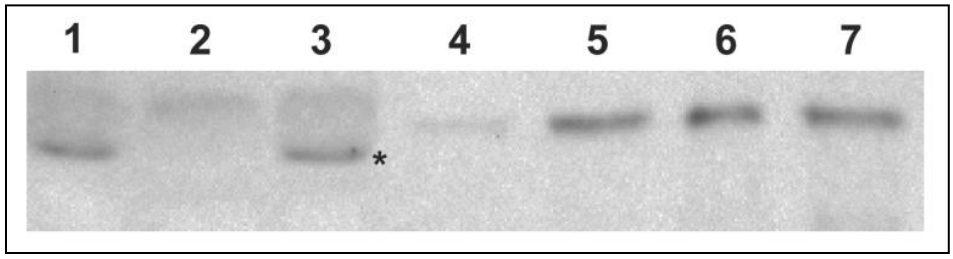

FIG. 12. MurA quantification. 5 x 10^8 HfrH cells (lane 3) were blotted with HfrH pZE12-*murA*^{Bs} (lane 1) and HfrH *murA::kan* pZE12-*murA*^{Bs} (lane 2) for determination of MurA band (asterisks). MurA standards were included: 7.5, 15, 22.5, and 30 ng in lanes 4-7 respectively.

TABLE 6. Critical concentration of A_2 to induce host lysis.

Level of induction (μM IPTG)[a]	**Lysis (+/-)**	**A_2 molecules/ cell**	**Time of analysis (min)**
0	-	n.d.	n.d.
12.5	-	n.d.	n.d.
25	-	2.2 x10^2	60
50	-	2.3 x10^2	60
100	+	3.6 x10^2	15
100	+	4.9 x10^2	30
1000	+	1.4 x10^3	15

n.d. not determined

[a]pZE12-*A2*

Quantification of MurA and A_2 in vivo

To address this question, it was necessary to quantify both MurA and A_2. The endogenous level of MurA was determined by quantitative Western blotting, using purified MurA as a standard. The result, 390 ± 30 molecules per cell (FIG. 12), is in agreement with another determination of 410 MurA molecules per cell by MS profiling (65). Similarly, the level of A_2 necessary for lysis was estimated by gradient induction of an IPTG-inducible plasmid clone. Lysis onset is observed at 40 minutes at 100 μM IPTG (FIG. 13). At this level of induction, ~350 and ~500 A_2 molecules accumulate, per cell, at 15 minutes and 30 minutes (TABLE 6). Lysis occurs even earlier at higher levels of inducer (FIG. 13). These results indicate that the cell is committed to lysis when free A_2 titrates out the available MurA.

Quantification of A_2 accumulation during infection

The context of the viral infection cycle might change the stoichiometry of A_2 and MurA, especially considering that in this framework, A_2 has multiple roles. To address this issue, A_2 was quantified during a Qβ infection of the male strain XL1-Blue. The total A_2 concentration was found to exceed that of MurA by 30 minutes after infection

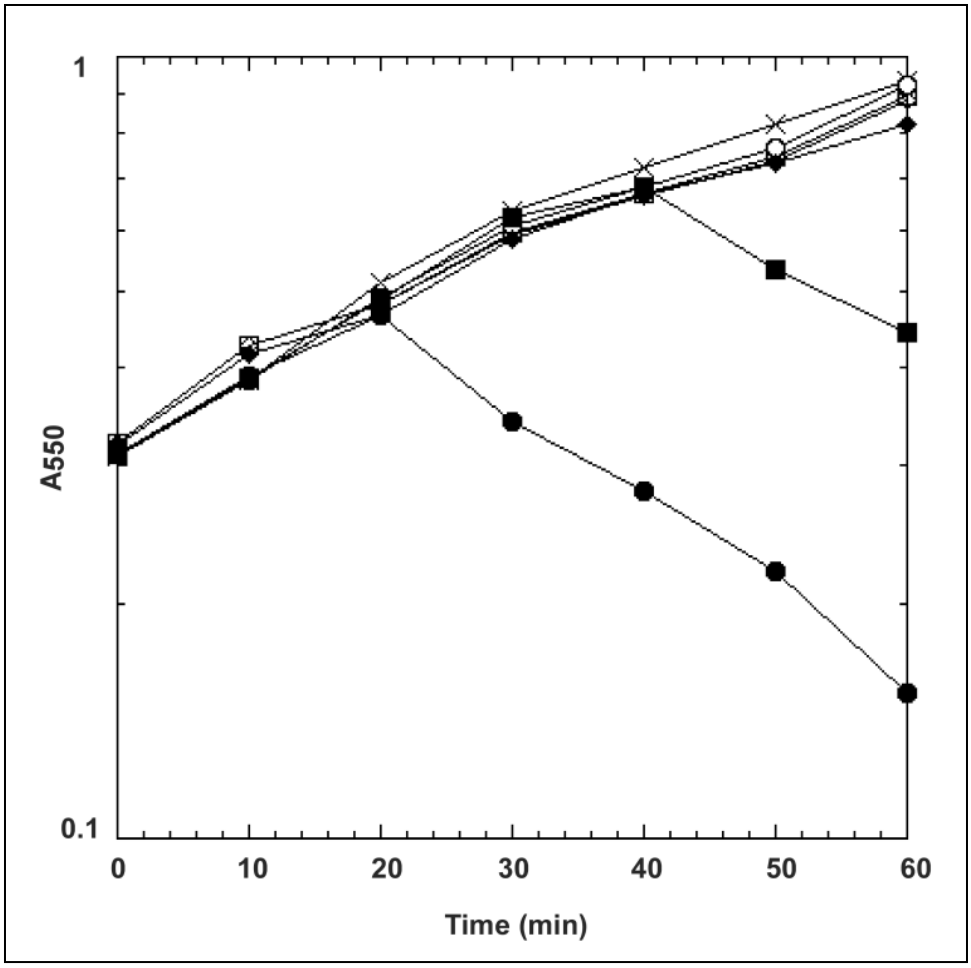

FIG. 13. Plasmid-borne A_2 induces cellular lysis. A_2 lysis and accumulation was measured at various concentrations of inducer: pZE12-*luc* control (1 mM: X); pZE12-A_2 (uninduced: white diamonds, 12.5 μM: white squares, 25 μM: white circles, 50 μM: black diamonds, 100 μM: black squares, and 1 mM: black circles).

TABLE 7. Qβ A_2 quantification.

Time (min)	**XL1-Blue**			
	Qβ A_2WT	**Qβ A_2L28P**	**Qβ A_2D52N**	**Qβ A_2E125G**
15	n.d.	n.d.	n.d.	n.d.
30	5.1×10^2	1.0×10^3	1.7×10^3	1.3×10^3
45	7.5×10^2	n.d.	n.d.	n.d.
60	1.2×10^3	n.d.	n.d.	n.d.
75	2.9×10^3	n.d.	n.d.	n.d.

n.d. not determined

(TABLE 7). Lysis was monitored both by culture turbidity and the release of Qβ virions (FIG. 14A-B). Lysis onset was not observed until 80 minutes, suggesting that a component of the Qβ infection cycle is sequestering A_2 from binding to MurA.

Por *mutants produce A_2 more rapidly and cause early lysis*

Further evidence addressing the relationship between the rate of A_2 production and lysis timing was obtained from analysis of Qβ^{por} (*p*lates *o*n *r*at) mutants (16). These

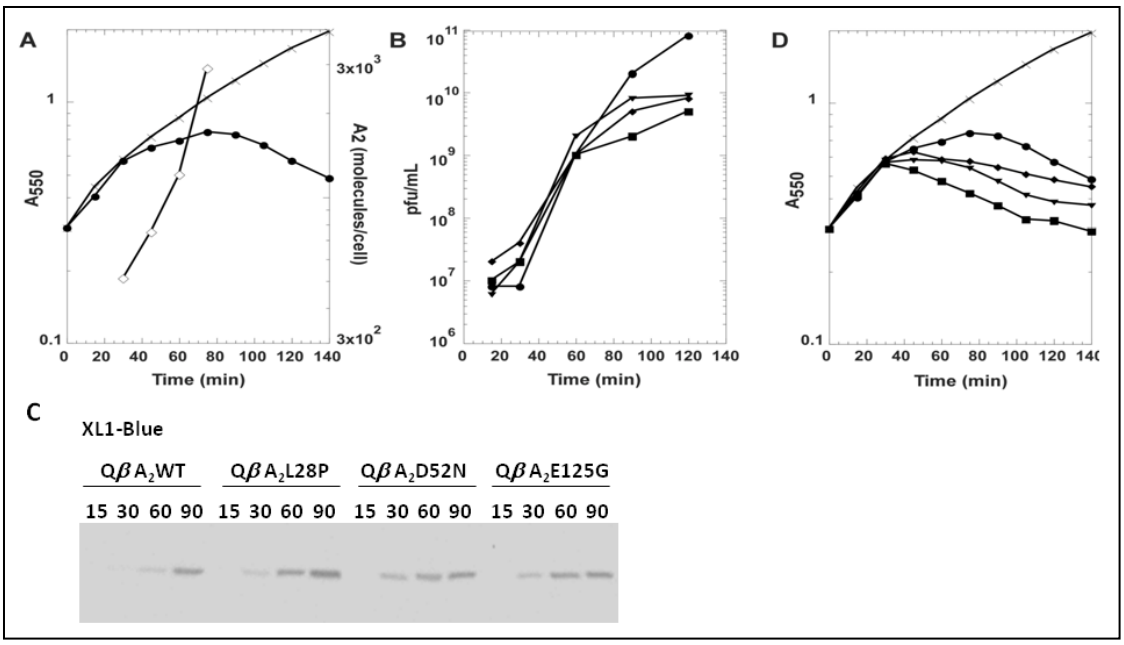

FIG. 14. Qβ and Qβ^{por} phenotype of infected cells. (A) Infection of XL1-Blue cells with Qβ. Reduction in cellular mass accumulation is observed starting at 30 minutes with a maximum at 80 minutes with phage input MOI of 1. A_2 accumulation (white diamonds) was quantified at intervals during infection. (B) Qβ has a higher released PFU titer after a single infection cycle than Qβ^{por}. (C) A_2 accumulation during infection of XL1-Blue. Loading was normalized to total volume. Samples were taken at time points listed (min). (D) Qβ^{por} mutants have an earlier lysis phenotype in XL1-Blue infected cells. Qβ infection reproduced (panel A) with Qβ^{por} infections. Symbols: (X) cells only control, Qβ A_2WT (black circles), Qβ A_2L28P (black diamonds), Qβ A_2D52N (black squares), and Qβ A_2E125G (black triangles)

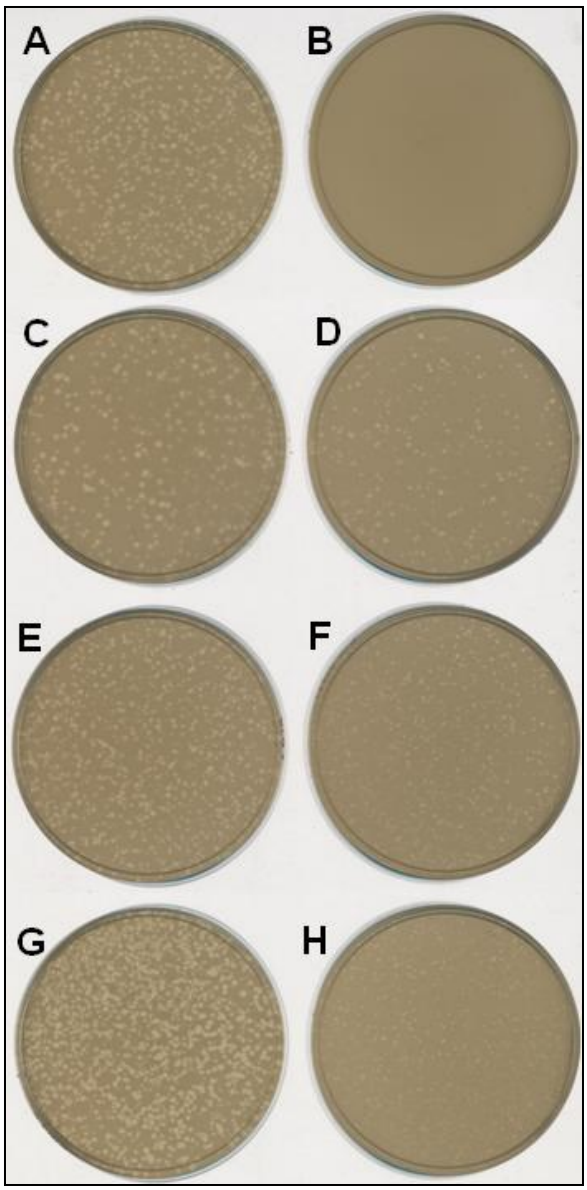

FIG. 15. Qβ ^{por} plating phenotype. Phage were plated on HfrH (left) and HfrH^{rat} (right): Qβ (panels A-B), Qβ A_2L28P (panels C-D), Qβ A_2D52N (panels E-F), Qβ A_2E125G (panels G-H).

TABLE 8. Qβ ^{por} sequence.

Qβ A_2^{por} Mutations[a]								
Substitution	D52N gat>aat	E125G gag>ggg F412S ttt>tct	D52N gat>aat P66P cca>ccg H67R cat>cgt	L28P ctc>ccc	D52N gat>aat	D52G gat>ggt	D52G gat>ggt	L28P ctc>ccc

[a](I. Wang, unpublished)

mutants were isolated as rare plaque-formers on the *murA*^{rat} host (FIG. 15). Eight independent mutants were obtained (TABLE 8); sequence analysis revealed that each had mutations in the N-terminal domain of the A_2 gene. The simplest interpretation was that missense changes in A_2 could suppress the defect in the inhibition of the MurA^{L138Q} mutant and implied that the N-terminal domain of A_2 carried the lytic determinant. This would be consistent with the observation that the principle differences between the lytic maturation proteins of Qβ and other *Alloleviviridae* and the non-lytic maturation proteins of the *Leviviridae* are in the N-terminal region. However, clones of the A_2^{por} alleles, although fully lytic in the parental host, failed to support inducible lysis in the *murA*^{rat} background (FIG. 16). Moreover, Western blot analysis of samples taken from

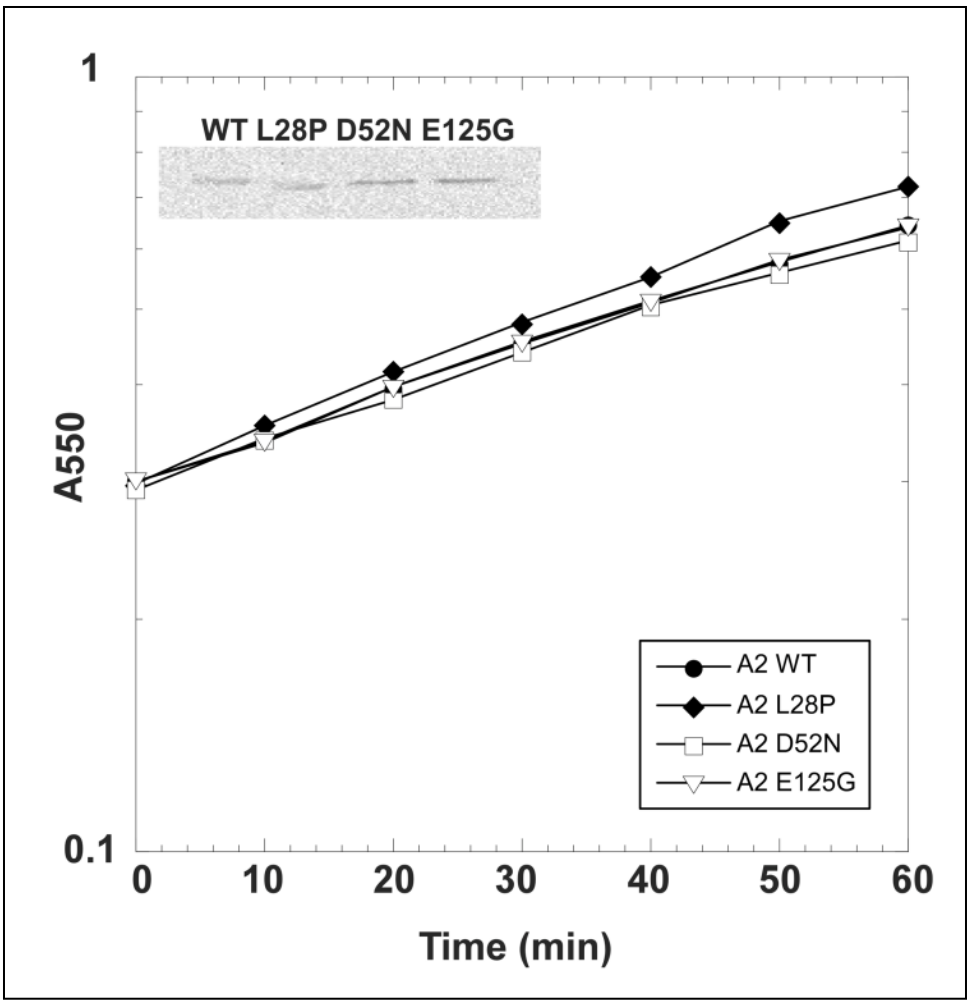

FIG. 16. Cloned A_2^{por} does not lyse a MurA^{rat} strain. XL1-Blue ^{rat} cells harboring plasmids: pZE12-A_2 (black circles), pZE12-A_2L28P (black diamonds), pZE12-A_2D52N (white squares), and pZE12-A_2E125G (white triangles) were induced with 1 mM IPTG. A_2 and A_2^{por} accumulation at 20 minutes is shown in inset.

infections with the *por* mutants clearly showed that A_2 was accumulating more rapidly than in WT infections (FIG. 14C). These results indicated that the ability of *por* mutants to support plaque-formation on the *murA*^{rat} background is due to a higher rate of synthesis of A_2 *in vivo*, rather than an altered ability to inhibit MurA^{L138Q}. Inspection of the secondary structure map of the A_2 mRNA shows that each of the mutations alters a base-pairing element that is predicted to be involved in repressing translational initiation (FIG. 8B). Thus, the *por* mutations derange the normal translational control of A_2.

Based on the previous results with the inducible cDNA clones of A_2 (FIG. 13), we expected that the *por* mutants would show earlier lysis in infections of WT cells. FIG. 14D shows that this is indeed the case, with lysis onset occurring 30-45 minutes earlier than with WT Qβ. The early lysis also reduces the yield of progeny (FIG. 14B), demonstrating that the normal regulation of lysis is important for the fitness of Qβ. With all three *por* alleles, the level of total A_2 production by 30 minutes is equal to or greater than that achieved by the WT phage at 60 minutes, accounting for the earlier lysis (TABLE 7 and FIG. 14C).

MurA over-production blocks lysis but does not inactivate intracellular virions

The low concentration of cytoplasmic MurA suggests that it should be possible to block Qβ lysis by expressing MurA in excess from a plasmid clone. To determine the amount of MurA needed for protection during an infection, gradient induction of HfrH

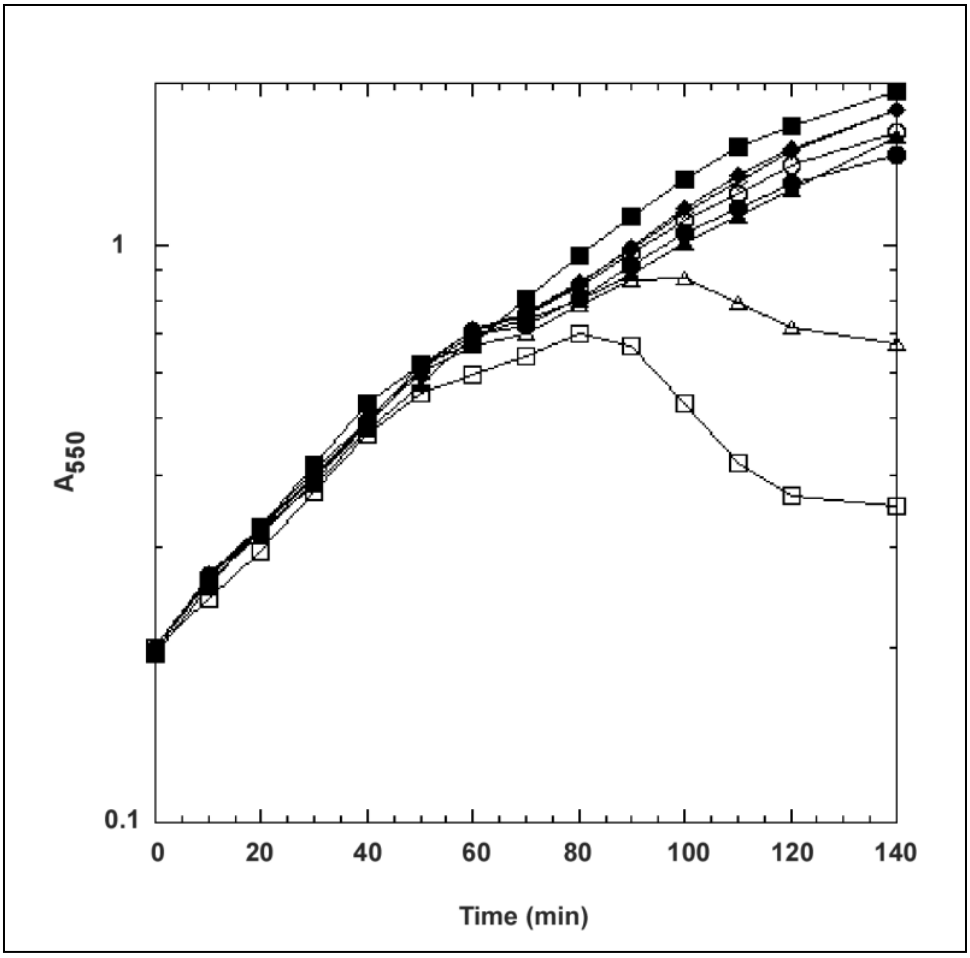

FIG. 17. Expression of MurA protects during a Qβ infection. HfrH *lacZ::*Tn5 cells were infected with Qβ containing various plasmid constructs: pZE12-*luc* (induced 1 mM: white squares), pZE12-*murA* (uninduced: white triangles; induced 12.5 μM: black circles, 25 μM: white circles, 50 μM: black diamonds, 100 μM: white diamonds, 1 mM: white triangles). Black squares: uninfected pZE12-*luc* strain (induced 1mM). IPTG was added simultaneously with virion particles.

TABLE 9. Quantification of MurA protection during a Qβ infection.

Plasmid	Level of induction (μM IPTG)	MurA molecules/ cell	Released PFU/ml (140')	Lysis (+/-)	PFU/cell (90')[a]
pZE12-*luc*	1000	3.9×10^2	4×10^{10}	+	880 ± 110
pZE12-*murAHis*	0	4×10^2	3×10^{10}	+	n.d.
	12.5	1×10^3	2×10^9	-	n.d.
	25	4×10^3	3×10^8	-	n.d.
	50	5×10^3	4×10^7	-	n.d.
	100	1×10^4	2×10^7	-	n.d.
	1000	3×10^4	5×10^6	-	760 ± 90

n.d. not determined

[a]determined in XL1-Blue^{rat} strain

*lacZ::*Tn*5* pZE12-*murAHis* infected cells was performed, and MurA accumulation was quantified. As predicted, a delay in lysis was observed with basal expression of MurA from the plasmid as compared to the vector control (pZE12-*luc*), and lysis was completely abolished in cells induced at IPTG concentrations ≥ 12.5 μM (FIG. 17). This confirms that the amount of A_2 normally deployed for inhibiting MurA is less than 1×10^3 molecules (TABLE 9). We next asked whether MurA levels in vast excess over the level sufficient to block lysis completely would lead to inactivation of intracellular Qβ particles and thus a reduced yield of progeny. Whether the experiments were done in a WT or a *murA*^{rat} background, intracellular virion production was unaffected, compared

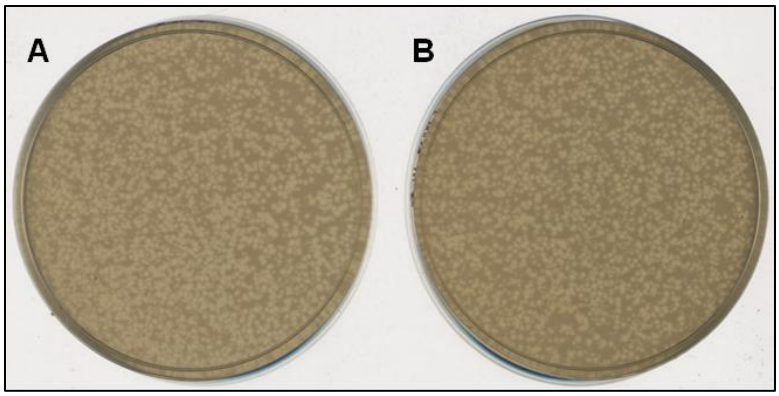

FIG. 18. Qβ lysate is not inactivated by MurA. (A) Qβ lysate only and (B) Qβ lysate incubated with MurA

with a control in which Luciferase was produced (TABLE 9), despite MurA reaching levels ~100 fold higher than the normal endogenous level. This suggests that, during the latent period, the progeny virions are protected from inactivation by MurA and consequently, virion-mounted A_2 is not the molecule that binds and inhibits MurA but rather free, unassembled A_2.

Particles are protected by a soluble viral component

The simplest explanation for intracellular virion particle protection from MurA inactivation is that the particles are simply sequestered from MurA during morphogenesis; however, this does not seem to be the case since i*n vitro* particle inactivation in a cell-free phage lysate, as opposed to purified phage particles, does not occur (FIG. 18) suggesting that a soluble, intracellular factor protects the particles.

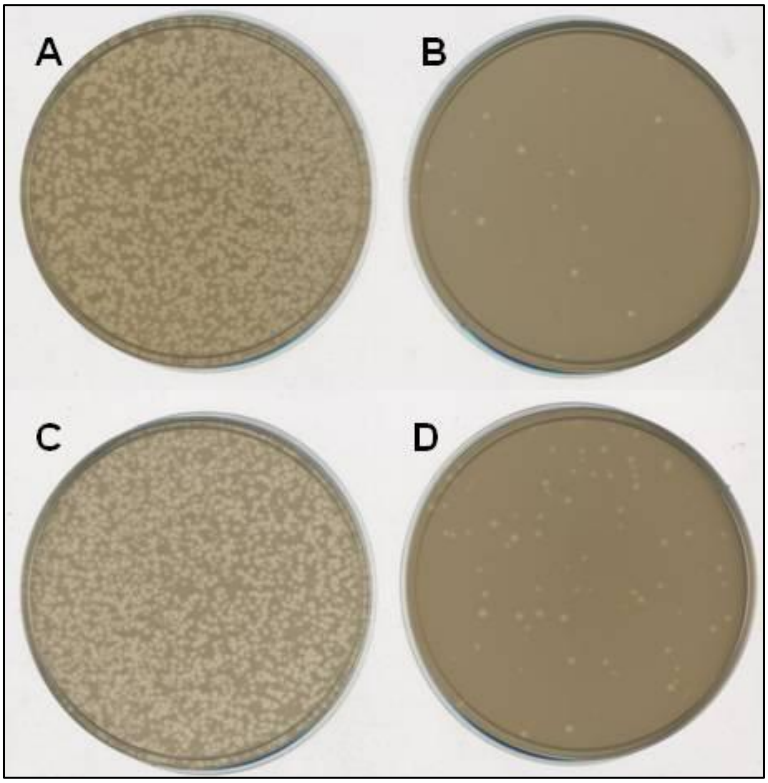

FIG. 19. Bacterial lysate does not protect Qβ from inactivation by MurA. (A) Purified Qβ only, (B) Purified Qβ incubated with MurA, (C) Purified Qβ with bacterial lysate, and (D) Purified Qβ with bacterial lysate incubated with MurA

Addition of bacterial lysate to the *in vitro* inactivation experiment with purified Qβ and MurA did not provide the particles from protection against MurA inactivation (FIG. 19), which implies that a viral component protects the particles from inactivation. Viral Coat and A_1, which interact with A_2 in the assembled particle, can be excluded as the soluble factor since expression of these proteins had no effect on the A_2 lysis phenotype (FIG. 20), and leave the two other viral factors that are produced during an infection:

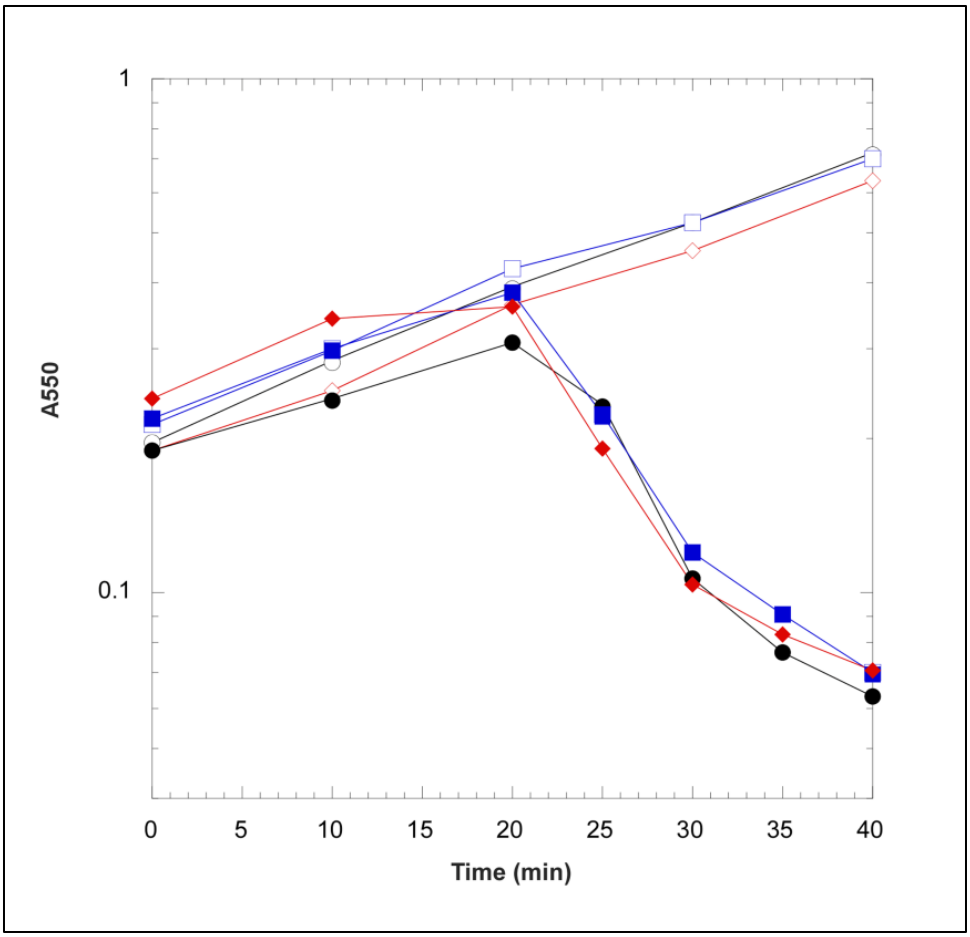

FIG. 20. A_2 lysis is not regulated by Coat or A_1. A_2 was expressed from pZE12-*A_2* in the presence of pZA32-*luc* (circles: uninduced, white; induced black), pZA32-*coat/A_1* (diamonds: uninduced, white; induced, red), and pZA32-*A_1* (squares: uninduced, white; induced, blue). Plasmids induced with 1 mM IPTG at Time = 0'.

(i) Replicase and (ii) Qβ RNA as potential candidates. The Replicase is an unlikely candidate since it is present only at ~ 500 copies during an infection (154) and associated with replicating viral RNA at polysomes (48).

Virion particles are protected from in vitro inactivation by Qβ RNA

When the *in vitro* particle inactivation experiment was repeated with another purified Qβ preparation, no inactivation was observed (FIG. 21A). This was unexpected, especially since the phage preparation had a protein composition indistinguishable from the inactivation-competent preparation (FIG. 21B). Moreover, we noticed that variability in the sensitivity to MurA-mediated inactivation could be correlated with losses in PFU titer and the concomitant increase in released Qβ RNA. To ask whether released virion RNA could be exerting a protective effect, the insensitive preparation was treated with RNase and then re-tested for MurA inactivation. The results were unambiguous; RNase treatment restored sensitivity to MurA (FIG. 21C) suggesting released RNA protects particles from MurA inactivation. However, attempts to reconstitute MurA protection by supplementing with purified Qβ RNA were unsuccessful (not shown). These results suggest that Qβ RNA, in a conformation obtained from spontaneous release from the virion, can protect Qβ virions from MurA inactivation *in vitro*, and raises the possibility that Qβ RNA may play a protective role for progeny virions during the latent period.

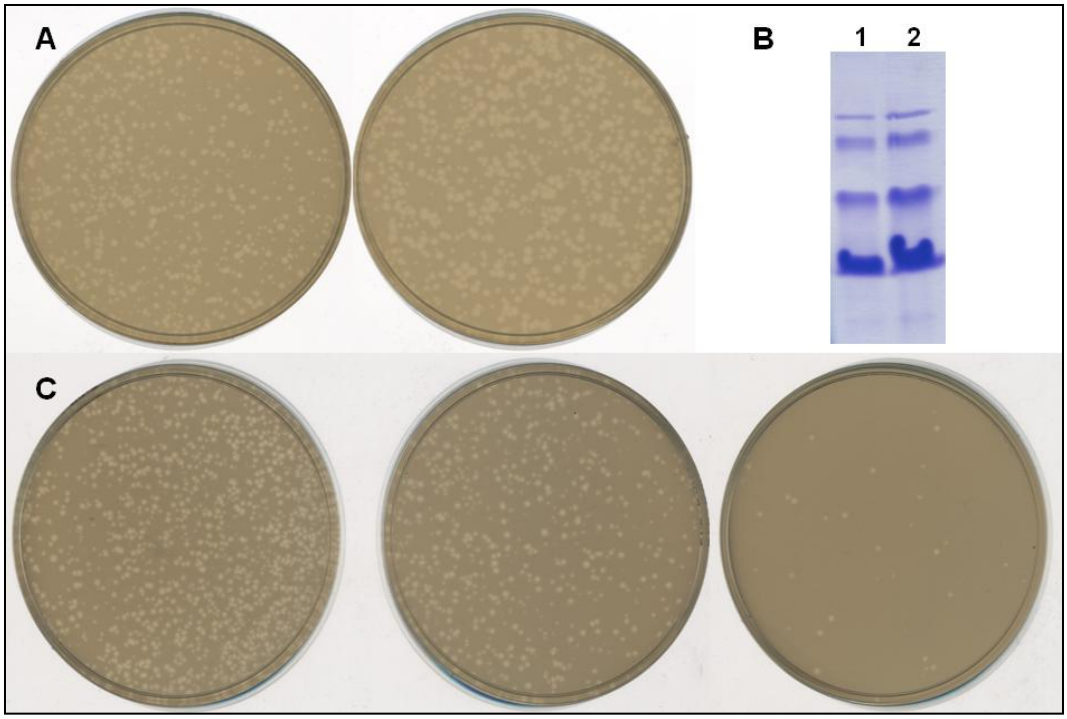

FIG. 21. Qβ is protected from MurA inactivation by RNA. (A) A non-inactivating virion preparation was incubated prior to plating: phage only (left), plus MurA (right). (B) Protein content was assessed by resolving the inactivating (lane 1) and non-inactivating Qβ preparations (lane 2) with SDS-PAGE. (C) RNase degradation restores particle inactivation. The non-inactivating phage only control (left) was incubated with RNase (middle) and with RNase including MurA (right).

Lysis inhibition of Qβ

Characterization of a lysis inhibited (LIN) state for lytic phage infections has been limited to T4 and homologs. However, a review of the ssRNA phage literature revealed a reference to a LIN state for an MS2-like phage, R17 (41). The authors had

found that with an input MOI of 10 that < 0.1% of cells had lysed after a 90 minute infection cycle. Another group had found with another MS2-like phage, f2, that if phage were incubated for 10 minutes and then washed to remove the phages, lysis is observed at 90 minutes (117). It is interesting that presumably continuous infection by the phage in the sample that was not washed is enough to delay lysis. Ellis and colleague also reported viral replication in the LIN state of the R17 phage with particle accumulation suggesting that the LIN state does not perturb viral replication.

Here, in the process of studying the timing of lysis in Qβ infections, a state of LIN was observed with Qβ when the input MOI of phage was ≥ 10 (FIG. 22). This LIN state is not due to reduction in the level of A_2 since the infected cells under all conditions had comparable amounts of the lysis protein. This unexpected observation makes a case for LIN being a general capability of ssRNA phages, since the *Alloleviviridae* and the *Leviviridae* effect lysis by fundamentally different pathways. LIN cultures continue to accumulate cellular density as judged by the absorbance profile over time (FIG. 22), which suggests the mode of the LIN state is not due to the cessation of division. Given that the two lysis proteins accumulate in different compartments, with L localized to the cellular envelope and A_2 remaining free or particle-bound in the cytoplasm, it is unclear how cell division can be affected.

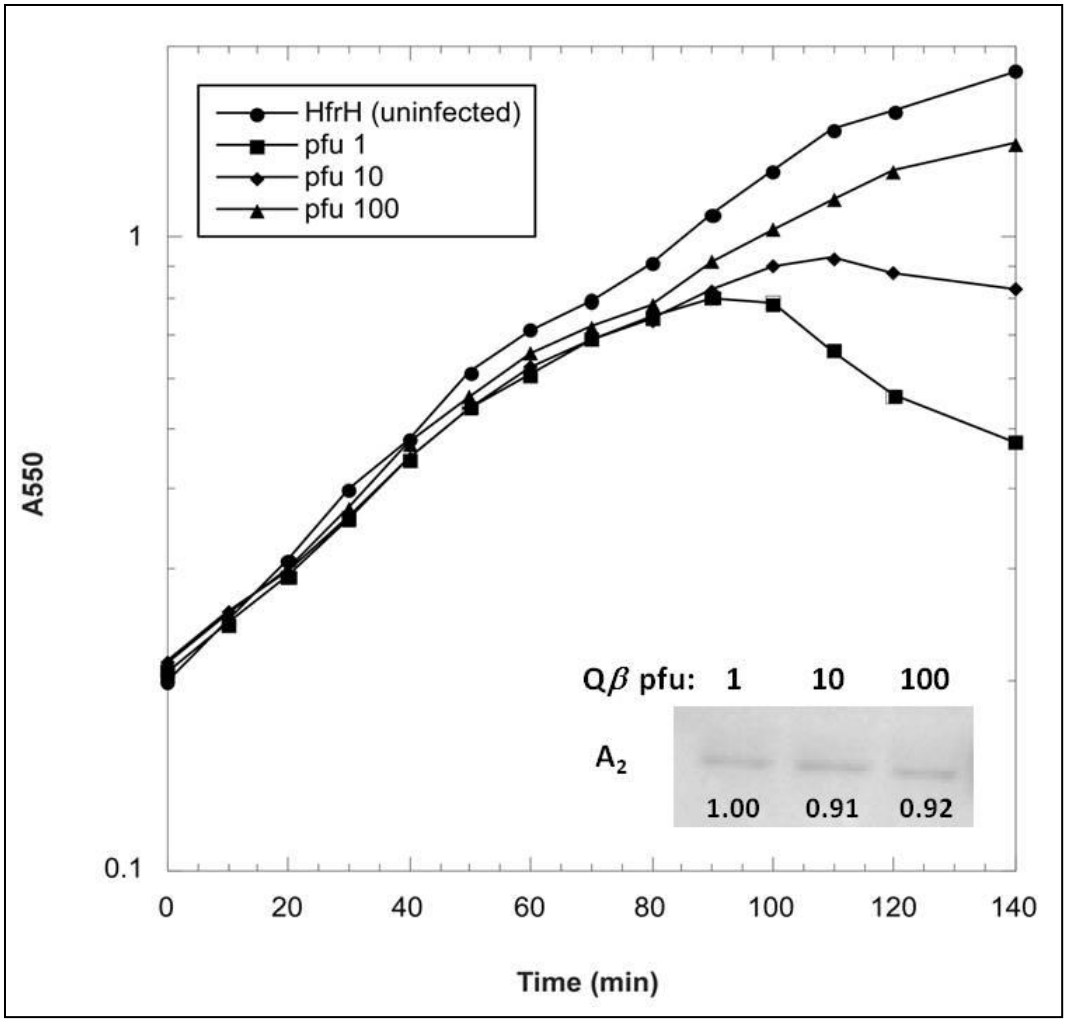

FIG. 22. Qβ lysis inhibition. HfrH cells were infected with variable input MOI: 1 (squares), 10 (diamonds) and 100 (triangles) at Time = 0'. A_2 accumulation at 60' was measured (inset). Infected cultures were pelleted to remove contaminating phage in the medium prior to sample analysis.

Discussion

A_2 inhibition of MurA and MurA-inactivation of Qβ: Models for regulation

Biochemical studies on A_2 have been retarded because of the insolubility of the protein. The only soluble form of A_2 known is the single molecule on the surface of the infectious Qβ particle (16, 156). While using this form of A_2, we were surprised to find that Qβ virions are rapidly and efficiently inactivated by contact with purified MurA (FIG. 9). This immediately cast doubt on the simplest idea proposed for the regulation of lysis in Qβ infections, in which infectious virions simply accumulated until they titrated out the MurA complement of the cell. The next simplest model would be that A_2 was produced in a large excess over MurA, so that attrition of infectious virions by contact with MurA would be negligible. However, our measurements of both MurA and A_2 revealed that (i) MurA is present at ~400 molecules per cell and (ii) Qβ-infected cells produce A_2 at levels roughly comparable to the total number of MurA molecules and assembled virions. Moreover, the two to three-fold increase in the accumulation rate of A_2 exhibited by the Qβ^{por} mutants leads to a much shorter and less productive infection cycle (FIG. 14B and D). Based on previous work indicating that A_2 is translated only off of nascent RNAs (127, 145) and also recent findings that Qβ assembly initiates with a single molecule of A_2 binding both 5' and 3'-ends of the genomic RNA (40), we suggest a third model where A_2 is synthesized off of nascent RNAs in slight stoichiometric excess. The vast majority of A_2 molecules are thus committed to assembly and only a small fraction is free and able to form the inhibitory complex with

MurA. Accordingly, the early lysis phenotype of the *por* mutants simply reflects a derangement of this stoichiometric balance, such that free A_2 is available in quantity from much earlier in the infection cycle.

Several studies have indicated that the ability to adapt to conditions that require altered lysis timing is an important fitness factor for a bacteriophage (24, 158, 177). The simple model proposed above can accommodate this requirement by mutational changes that alter the level of excess A_2 production over the unit stoichiometry, presumably by changes analogous to the *por* mutations but less drastic. ssRNA phage have complex RNA secondary structures that not only protect the RNA from RNase activity but also assist in regulation of protein expression (9, 50, 156). Analysis of the RNA's 5'-end hairpin structures revealed that the rate of folding and not the stability of base pairing surrounding the ribosome binding site was the regulatory factor in the level of maturation protein expression (50). Therefore, mutations that change the kinetics of RNA folding provide plenty of opportunities for adjusting the amount of protein expression which could also remain silent in terms of A_2 function. Alternatively, in the MS2 system, translation of the L protein is regulated by a hairpin structure that contains the ribosomal binding site (9, 156). Destabilization of this hairpin by ribosomal translation of coat precedes L translation; however, the position of coat termination relative to the L initiation site is important. Insertions or deletions between these two sites greatly affect the level of L translation (9) and could be a means to adjustment of lysis protein expression levels to evade selective pressures from the host during an infection.

Protection of intracellular virions

The A_2-MurA lysis system would seem to have clear advantages: (i) MurA is a highly conserved enzyme essential for the supply of murein precursors, and its inhibition leads inescapably to lysis (69, 76, 150). (ii) Moreover, as noted above the nature of the complex Qβ RNA structure confers facile adjustability to lysis timing. However, this system also confers MurA sensitivity to purified Qβ virions. Although this was unexpected, in retrospect the sensitivity of virions to a protein ligand is consistent with A_2 roles in recognition of pilin and release of the genomic RNA during infection (119, 155, 156). This raises the issue of whether or not there is substantial attrition of viable virions during a normal infection. This seems unlikely considering that the number of MurA molecules available *in vivo* to inactivate Qβ virions would be comparable to the average yields of viable virions per cell (59, 154). Moreover, massive over-production of MurA, although completely blocking lysis, has no effect on the viability of the intracellular virions (TABLE 9). These data indicate that there is an intracellular factor that protects the A_2 molecule mounted on the virion from MurA, a conclusion supported by the finding that purified MurA does not inactivate Qβ particles present in a crude lysate (FIG. 18).

The identity of the protecting factor(s) is unknown. Candidates might include protein chaperones that bind the virion in such a way to sterically protect A_2 from MurA. Phages frequently make use of cellular chaperones during morphogenesis (121); however, we favor a phage-specific factor, based on the inability of bacterial lysate to

protect particles from MurA inactivation (FIG. 19) and differences in MurA sensitivity of purified Qβ preparations. Most preparations are fully sensitive to MurA (FIG. 9A-B) whereas other preparations are insensitive (FIG. 21A-B); this insensitivity is often associated with increased age of the preparation (data not shown). Importantly, the insensitivity is associated with significant levels of released RNA and can be fully reversed by RNase treatment (FIG. 21C) and suggests a simple model for protection based on the RNA-protein intermediates in the Qβ assembly pathway. Qβ viral morphogenesis begins with a single A_2 molecule binding both ends of the genomic RNA, after which coat progressively nucleates capsid formation (40, 156). We suggest that the exposed RNA of one or more of these intermediates can bind a completed virion *in trans* in such a way as to protect the A_2 molecule from MurA interaction. We were not able to recapitulate MurA protection by the addition of purified Qβ RNA, suggesting that RNA-protein interactions and consequent RNA secondary or tertiary structures might be required for the protective effect. Efforts to localize the interaction surfaces on the MurA and A_2 molecules may clarify these issues and are currently underway.

CHAPTER III

STRUCTURE AND FUNCTION ANALYSES OF A_2*

Introduction

In vitro characterization of proteins is dependent on the use of soluble protein; A_2 characterization is limited in this respect since the protein is insoluble apart from assembly on the virion capsid. Identification of A_2 as the lysis protein was achieved by the fact that purified Qβ particles, with a single copy of A_2 on the surface, efficiently inhibited MurA (16). However, the use of virion particles to further characterize the A_2-MurA interaction is impractical in the sense that the particle themselves are too large for many techniques. Moreover, from previous results (Chapter II), it was determined that an interaction between MurA and A_2 on the surface of the particles releases viral RNA.

Materials and Methods

Bacterial strains and growth conditions

The *Escherichia coli* strains used in this study: XL1-Blue, ER2738, HfrH *lacZ::*Tn*5*, and BL21(DE3) are previously described (Chapter II)(153). Standard

*Part of the data reported in this chapter is reprinted with permission from Understanding the lytic function of A_2: The maturation protein of ssRNA bacteriophage Qβ, C. Langlais, 2007, Texas A&M, College Station, TX. [2007]

molecular biology techniques were performed as described elsewhere (129). Bacterial growth conditions were described previously (Chapter II).

TABLE 10. Primers used in construction of A_2 fusion proteins.

Primer	Sequence
A2SalI-For	CGCGTCGACATGCCTAAATTACCGCGTGG
A2BamHI-Rev	CGCGGATCCTCAACGCTTTACGGGTTGGG
GST-For	GATATACATATGTCCCCTATACTAGGTTAT
EK1-A2-For	GGCTCCGGTGATGACGACGACAAGATGCCTAAA TTACCGCGTGG
EK1-A2-Rev	CCACGCGGTAATTTAGGCATCTTGTCGTCGTCAT CACCGGAGCC
RV-Xba-Bam-A2-Rev	TGGTAAGGATCCTCTAGAGATATCTTATCAACG CTTTACGCGTTGGG
SeqPET	TAATACGACTCACTATAGGG
KpnI-NdeI-A2-For	GTATAAGAGGTACCACATATGCCTAAATTACC
A2-Rev-BamHI	GCAGCCGGATCCAGTTTCA
A2-A hybrid-For	AAGGCGTACACTGCTGTTAAGCGTGGCGATTTA CGTGC
A2-A hybrid-Rev	CACGAGCGCAATCAGTAAAAGCCCGAGATATTT TATAGTCTC

Plasmid construction

Construction of pZE12-*murAHis* and pZA31-*murA*^{Bs} (*murAA*) was previously described (89). The pZA31-*murA*^{Bs} plasmid has a $P_{Ltet0-1}$ promoter which is constitutively on in a *tetR*$^{-}$ background. Amplification of A_2 for sub-cloning into vectors was performed as previously described (89). A_2 fusion constructs were generated previously (89) but were not published. Primers used in construction of A_2 fusions are listed in TABLE 10. To generate pET*SUMO*-A_2 the A_2 gene was amplified using primers: A2SalI-For and A2BamHI-Rev digested and ligated into pTB146 (kindly provided by Tom Bernhardt, Harvard) cut with SalI and BamHI. pET*GST*-A_2 was constructed via SOE PCR (153) with three separate PCR reactions: (i) the GST-tag was amplified with GST-For and EK1-A2-Rev using pET41 (Novagen) as the template, (ii) A_2 gene amplification was achieved with primers EK1-A2-For and RV-Xba-Bam-A2-Rev, (iii) SOE PCR was performed with the purified gene products above and primers: GST-For and RV-Xba-Bam-A2-Rev. Digestion of SOE PCR product and ligation into pET41 vector was achieved with NdeI and BamHI. pET*NusA*-A_2 was prepared similarly to GST-A_2 with primers: (i) SeqPET and EK1-A2-Rev for NusA-tag amplification from pET44 (Novagen), (ii) EK1-A2-For and RV-Xba-Bam-A2-Rev for A_2 amplification, and (iii) T7 promoter and RV-Xba-Bam-A2-Rev with purified gene products for SOE PCR. Purified SOE PCR product was digested with NdeI and BamHI for ligation into pET44. To generate pET*MBP*-A_2, the A_2 gene was amplified using KpnI-NdeI-A2-For and A2-Rev-BamHI primers. The PCR product was digested with NdeI and BamHI and ligated into p202 (pET28b-*MBP* vector with a TEV protease cleavage site, kindly provided by

Dr. Sacchettini, Texas A&M University), similarly digested. pET*MBP-$A_2$1-189* was generated by insertion of amber codon at position 190 via site-directed mutagenesis with the following primers: A2Δ190-420For and A2Δ190-420Rev, described previously (89). An A_2 (166-173)-A (158-165) hybrid was constructed by ExSite PCR (ref) with the following primers: A2-A hybrid-For and A2-A hybrid-Rev with pZE12A_2 for the template, previously described (89).

Protein expression and purification

To test fusion protein functionality, cellular mass accumulation of induced BL21(DE3) pLysS (Novagen) cells harboring a plasmid borne copy of A_2 truncations and/or fusions were monitored over time as described in the previously (Chapter II). Induction of proteins was performed with 1 mM final of IPTG unless otherwise indicated. Protein accumulation was assayed by TCA precipitation, SDS-PAGE, and immune-blotting analyses as previously described (Chapter II).

To assist in toxic protein accumulation for expression analyses, A_2 fusion proteins were co-expressed with *Bs* MurAA. Expression of A_2 fusion proteins were performed at 37°C for 3-4 hours and/or at 16°C for 18 hours. Solubility of the A_2 fusion proteins were determined by analysis of distribution between the supernatant and pellet fractions of disrupted cells post centrifugation, 12,000 xg for 15 min at 4°C; 25 ml of culture, harvested by centrifugation at 16,000 xg for 15 min at 4°C, was resuspended in 3 ml of buffer and disrupted as previously described (Chapter II). Buffers used for

solubility included 20 μg ml^{-1} DNase, 5 mM $MgCl_2$, and protease inhibitor cocktail (Sigma): SUMO-A_2 (10 mM sodium phosphate [pH 7.4] and 100 mM NaCl), GST-A_2 (0.1 M Tris [pH 8.45] and 100 mM NaCl), NusA-A_2 (0.1 M Tris [pH 8.45] and 100 mM NaCl), and MBP-A_2 (20 mM Tris-HCl [pH 8], 150 mM NaCl, 10% glycerol). All protein induction was performed with 1 mM IPTG, final, but for expression at 16°C cells were chilled in an ice water bath for 1 hour prior to induction.

For protein purification analyses, 250 ml of culture was pelleted as above and resuspended in 6.25 ml of buffer for lysis (listed above). The clarified lysate, centrifuged as above, was filtered with 0.45 μm filter prior to loading onto a column. Talon resin (Clontech) was used for purification of proteins with a His-tag. Elution was performed with the above buffers including 200 mM imidazole. Low imidazole (20 mM) washes were performed prior to elution. For amylose resin (Amylose High Flow resin, NEB) purification of MBP-A_2, the cellular pellet was resuspended in lysis buffer (20 mM Tris-HCl [pH 8], 150 mM NaCl, 1% glycerol, 1 mM EDTA, 20 μg ml^{-1} DNase, 10 μg ml^{-1} RNaseA, and protease inhibitor cocktail (Sigma)) and eluted with buffer (20 mM Tris-HCl [pH 8], 150 mM NaCl, 1% glycerol, and 10 mM maltose); 0.2 % glucose was included in medium for protein expression that is purified with amylose resin. Expression and purification of MurA was described previously (Chapter II).

Fusion cleavage assay

Proteins containing the MBP fusion (2 μM) were incubated with10 μg of MBP-TEV-protease (kindly provided by V. Kuznetsov, Texas A&M University) in protease in PBS buffer (10 mM sodium phosphate [pH 7.4], 100 mM NaCl, and 1 mM DTT) overnight at 4°C. Solubility of proteins was assessed by centrifugation of cleaved protein. An aliquot of samples was removed prior to centrifugation at 18,000 xg, 15 minutes at 4°C. Supernatant was removed and the pellet was resuspended in equivalent volume of buffer. Fractions were analyzed with SDS-PAGE and immune-blotting, probed with the α-A_2 antibody.

MurA activity assay

MurA activity was performed as previously described (16, 97) with the following modifications: MurA was assayed in the presence of various fusion proteins.

Circular dichroism analysis

To assess the secondary structure content of A_2, circular dichroism (CD) was performed on equal molar concentrations (4 μM) of MBP, MBP-A_2 and MBP-$A_2^{1\text{-}189}$ dialyzed in PBS without DTT. Data were collected with a 1 mm cuvette using an Aviv (model 62DS) instrument. A buffer spectrum was obtained and subtracted from the raw

data. Mean residue ellipticity (MRE) was calculated for each protein (49). Deconvolution of the data was performed with K2d (2), and the global alpha-helical content of A_2 was determined with the equation (3):

(MBP % of construct)(% alpha helix of MBP) + (A_2 % of construct)X = % alpha helix of fusion

where X is the percent of A_2 alpha helical content.

Results and Discussion

Function and structure analyses of A_2 fusion proteins

Characterization of A_2 has been limited due to the insolubility of the protein, apart from the assembled virion particles. One way of obtaining soluble protein for *in vitro* analyses is to purify the protein as a hybrid fusion protein. There are several proteins that have been well characterized as fusion proteins including: small ubiquitin-related modifier (SUMO), glutathione *S*-transferase (GST), MalE or maltose-binding protein (MBP), and N-utilization substance A (NusA). Each fusion protein varies in the ability to perform as a fusion tag to increase solubility and potential to assist in protein folding. Also, each construct contains a site for specialized protease cleavage to remove the fusion tag. The SUMO-specific protease, Ulp1, recognizes a Gly-Gly motif at the C-terminus of the tag, and cleavage of the protein from the tag leaves only the native protein without unwanted residues. GST tags have been shown to provide some

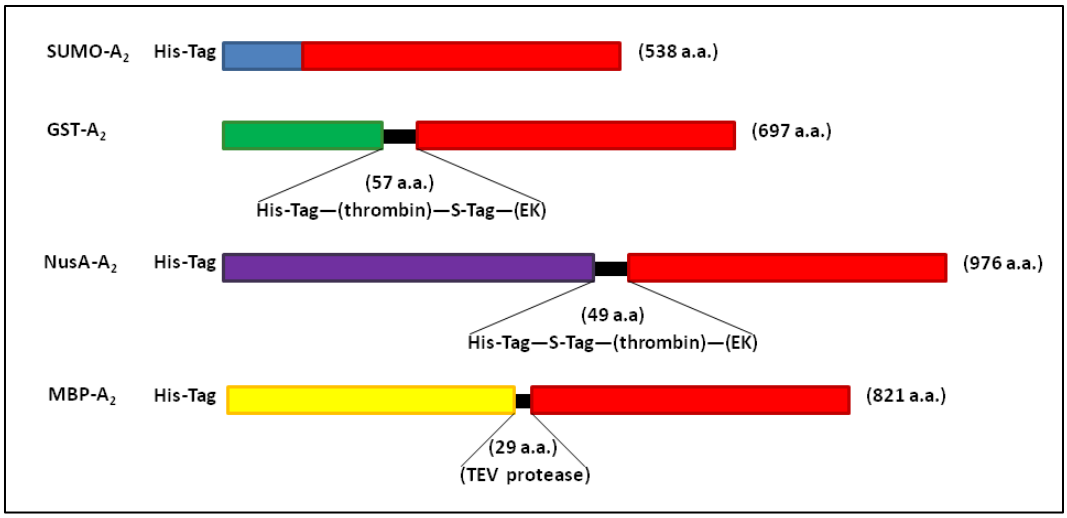

FIG. 23. A_2 fusion constructs. Primary structure organization of A_2 fusions: SUMO (blue), GST (green), NusA (purple), and MBP (yellow). All constructs are N-terminal fusions to A_2 (red). Linkers are depicted with tags and (protease cleavage sites): Enterokinase (EK). Length of linkers and fusion proteins are listed in parentheses.

protection against intracellular protease degradation (157). MBP and NusA have similar ability to solubilize proteins and assist to some degree in folding of the fusion partner (108).

All fusion constructs are N-terminal tags (FIG. 23). SUMO-A_2 (62 kDa) is the smallest fusion construct with an N-terminal His-Tag; the construct does not contain a linker between the two proteins. GST-A_2 (80 kDa) is the second largest construct; the chimera has a 57 aa linker that contains both a His-tag and S-tag with Thrombin and Enterokinase (EK) cleavage sites. NusA-A_2 (110 kDa) is the largest fusion construct with an N-terminal His-tag; the 49 aa linker of this construct also contains both the His-

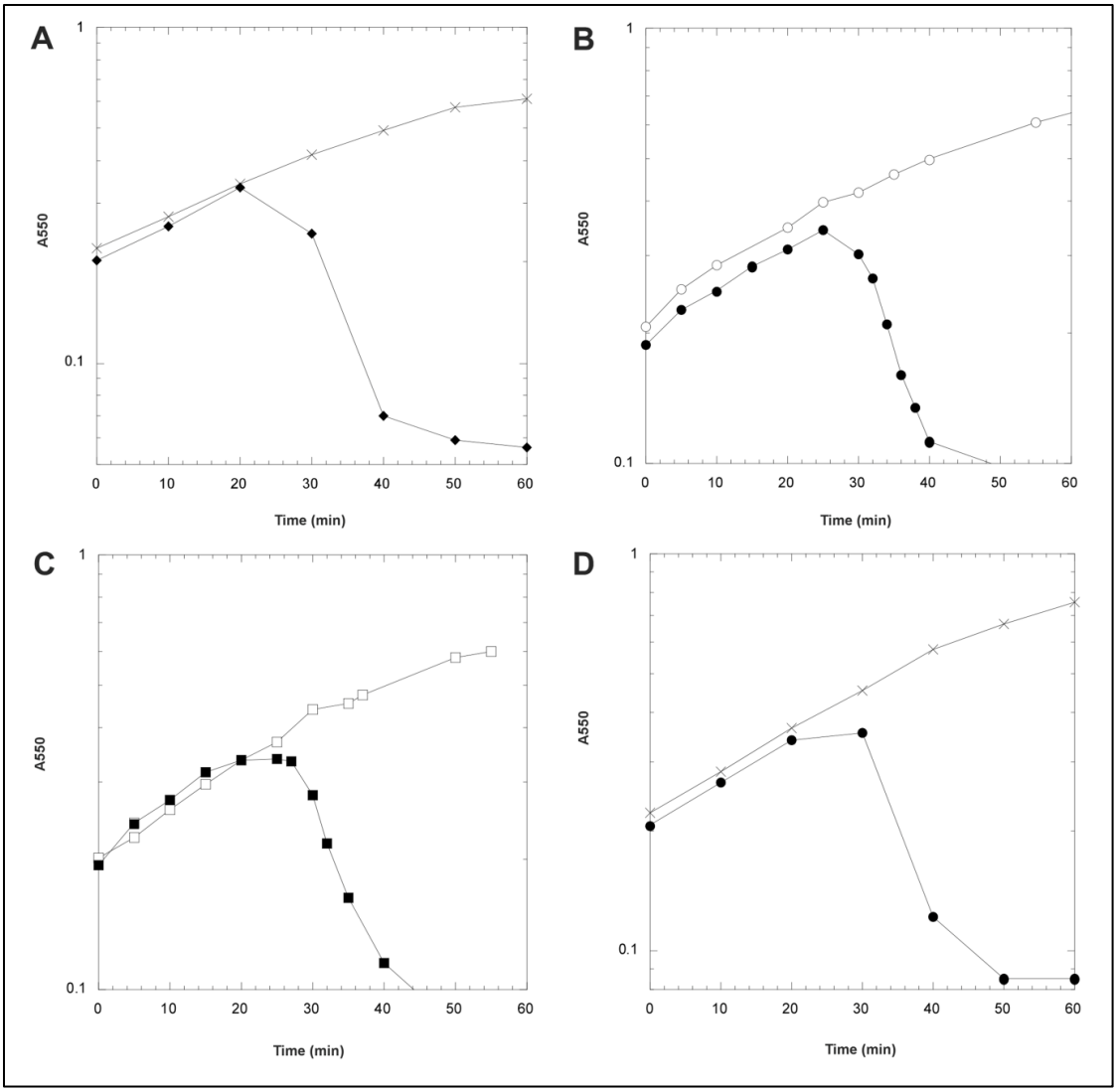

FIG. 24. A_2 fusion protein lysis phenotype. BL21(DE3) pLysS containing A_2 fusion constructs for expression were induced at Time = 0 minutes with 1 mM IPTG, final. (A) SUMO-A_2 (B) GST-A_2 (C) NusA-A_2 (D) MBP-A_2

tag and S-tag with Thrombin and EK cleavage sites. The MBP-A_2 (93 kDa) construct is smaller than the NusA-A_2 with a 29 aa linker that contains a TEV protease cleavage site.

Functional analysis of A_2 fusion proteins in vivo

To determine whether A_2 fusion proteins were functional *in vivo*, cultures carrying chimeric constructs SUMO-A_2, GST-A_2, MBP-A_2, and NusA-A_2 were induced and monitored for optical density over time (FIG. 24). All four fusion proteins lysed at ~ 25 minutes, which was the same lysis timing of A_2 expressed with a T7 promoter (89); thus, A_2 lytic activity is not affected by having a large fusion tag tethered at the N-terminus of the protein.

Purification of soluble fusions of A_2

SUMO-A_2

At 37°C, the SUMO-A_2 construct exhibited poor expression (FIG. 25), with soluble material representing no more than 50% of the total. Expression at 16°C increased the amount of SUMO-A_2 (FIG. 25); however, ~ 90% of the protein was insoluble. SUMO-A_2 was thus abandoned as a construct for A_2 purification.

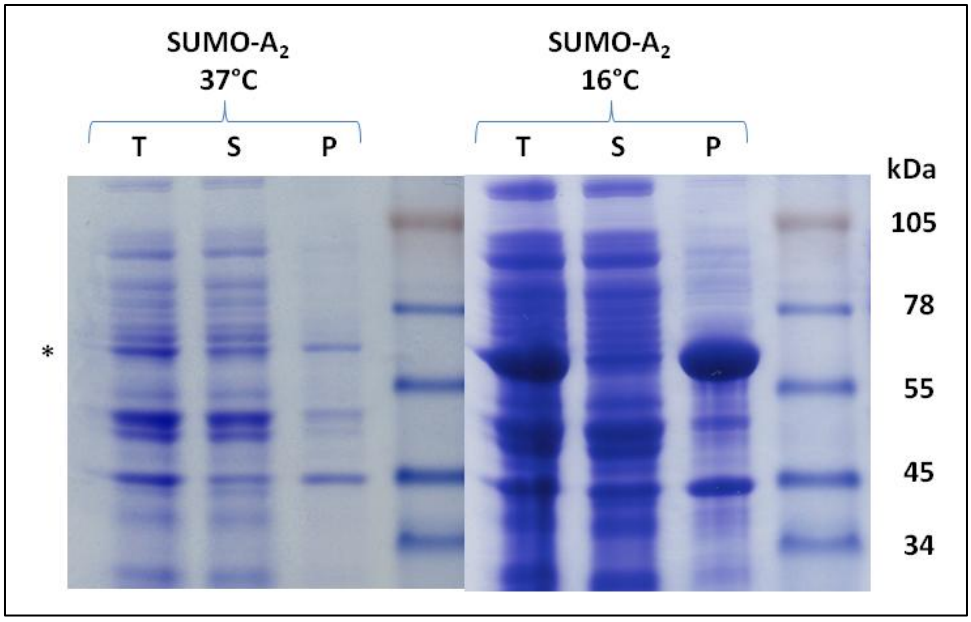

FIG. 25. SUMO-A_2 solubility at 37°C and 16°C expression. SUMO-A_2 (62 kDa) is labeled with an asterisk. (T) Total fraction, (S) supernatant after centrifugation, and (P) pellet after centrifugation

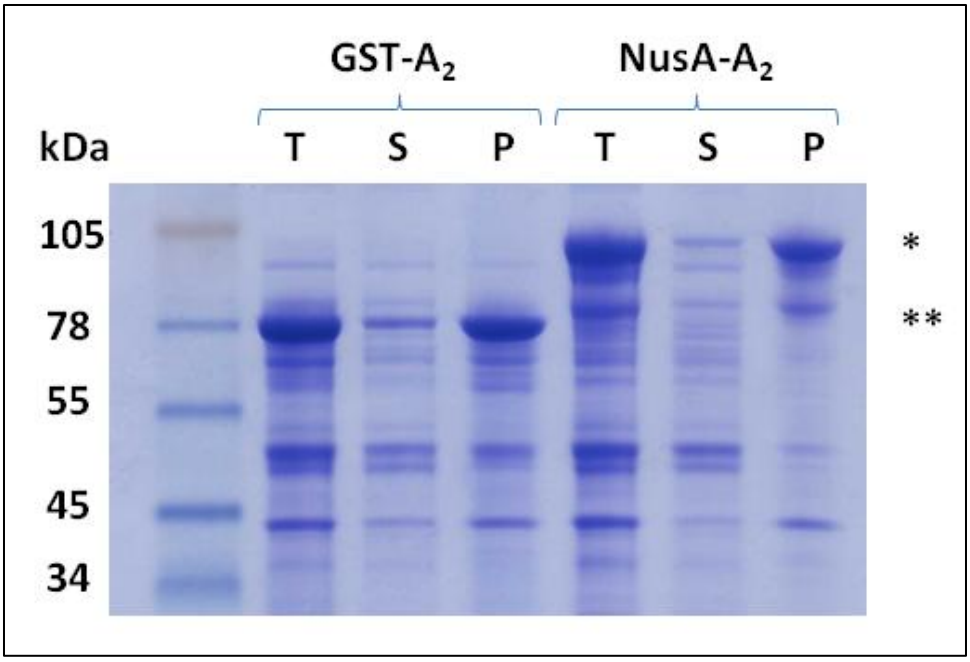

FIG. 26. GST-A_2 and NusA-A_2 solubility at 37°C expression. GST-A_2 (80 kDa) is labeled with double asterisks and NusA-A_2 (110 kDa) is labeled with a single asterisk. (T) Total fraction, (S) supernatant after centrifugation, and (P) pellet after centrifugation

GST-A_2

Total expression of GST-A_2 at 37°C was higher than for SUMO-A_2 (FIG. 26), but ~ 90% of the protein was found to be insoluble. Decreasing the temperature of expression increased the amount of soluble protein to ~ 70%, but there appeared to be an increase in a potential degradation product at ~ 60 kDa (FIG. 27). Since expression of the fusion protein at 16°C increased the yield of soluble protein, purification was

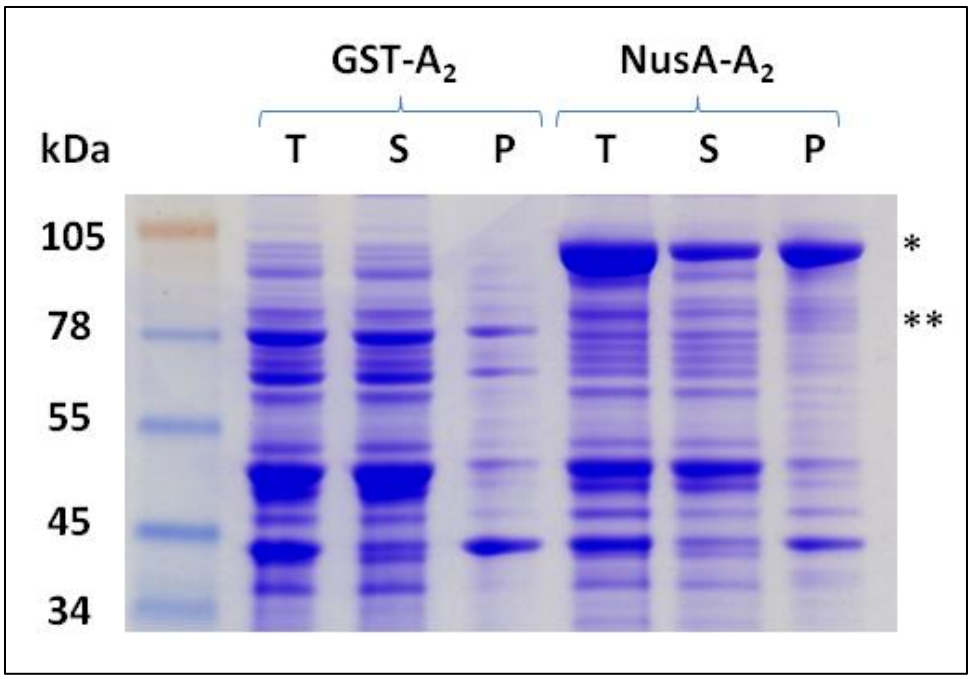

FIG. 27. GST-A_2 and NusA-A_2 solubility at 16°C expression. GST-A_2 (80 kDa) is labeled with double asterisks and NusA-A_2 (110 kDa) is labeled with a single asterisk. (T) Total fraction, (S) supernatant after centrifugation, and (P) pellet after centrifugation

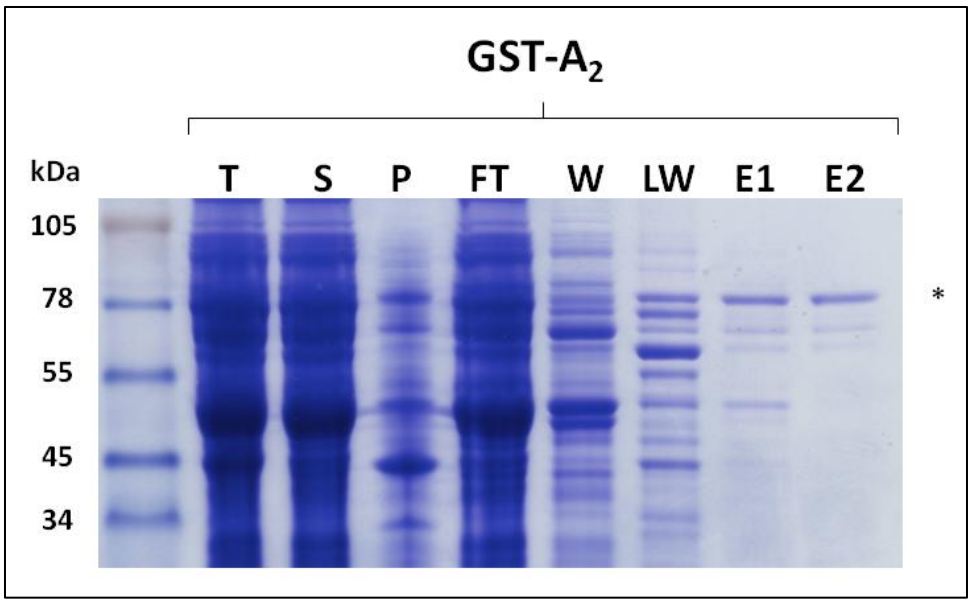

FIG. 28. GST-A_2 Talon resin purification. Purification fractions were run on an SDS-PAGE: Total lysate (T), lysate supernatant after centrifugation (S), lysate pellet after centrifugation (P), column flow through (FT), column wash (W), and eluate (E) from Talon resin. GST-A_2 (80 kDa) is labeled with an asterisk.

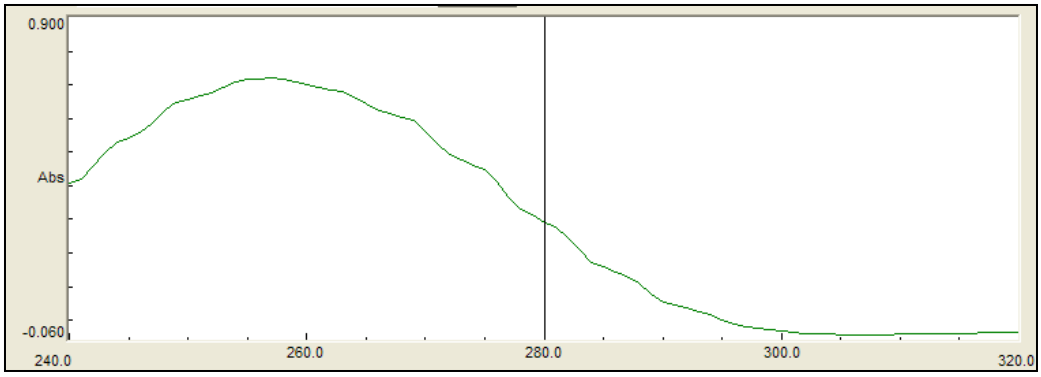

FIG. 29. GST-A_2 absorbance spectrum. GST-A_2 has maximal absorbance at 260 nm.

performed with the lower temperature expression conditions (FIG. 28). Eluates from the metal affinity purification contained species that co-eluted with GST-A_2 at apparent molecular masses of 65, 60 and 50 kDa, suggesting that the GST fusion does not protect A_2 from proteolytic degradation. Another possibility is that the degradation is from protease activity upon disruption of the cells and not due to *in vivo* activity during or after translation. There was also a considerable amount of protein contaminants that were removed in the low imidazole wash, which also partially removed the GST-A_2. The absorbance spectrum of the purified protein also revealed a shift in the maximum from 280 nm to 260 nm, suggesting a large amount of nucleic acid contamination (FIG. 29). A_2 is known to bind within its own coding mRNA; therefore, it is not surprising that RNA would co-purify with the protein. The yield of the purified GST-A_2 protein was 4.5 mg/L; however, this concentration may be an over-estimate, since the absorbance at 280 nm may reflect partial RNA absorbance.

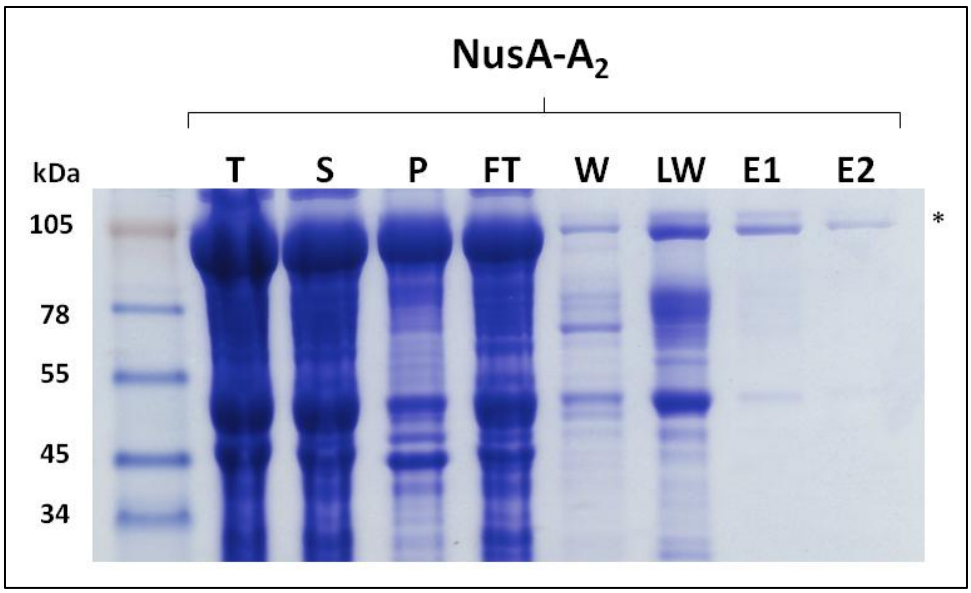

FIG. 30. NusA-A_2 Talon resin purification. Purification fractions were run on an SDS-PAGE: Total lysate (T), lysate supernatant after centrifugation (S), lysate pellet after centrifugation (P), column flow through (FT), column wash (W), and eluate (E) from Talon resin. NusA-A_2 (110 kDa) is labeled with an asterisk.

NusA-A_2

The NusA-A_2 fusion exhibited protein expression and insolubility characteristics similar to GST-A_2 for inductions and growth at 37°C (FIG. 26). An apparent degradation product ~ 80 kDa was detectable for expressions done at 37°C. Expression at 16°C increased the fusion protein solubility to about 40% (FIG. 27). The apparent 80 kDa degradation product was also reduced with expression under these conditions. A considerable amount of the fusion protein was observed in the flow-through fraction.

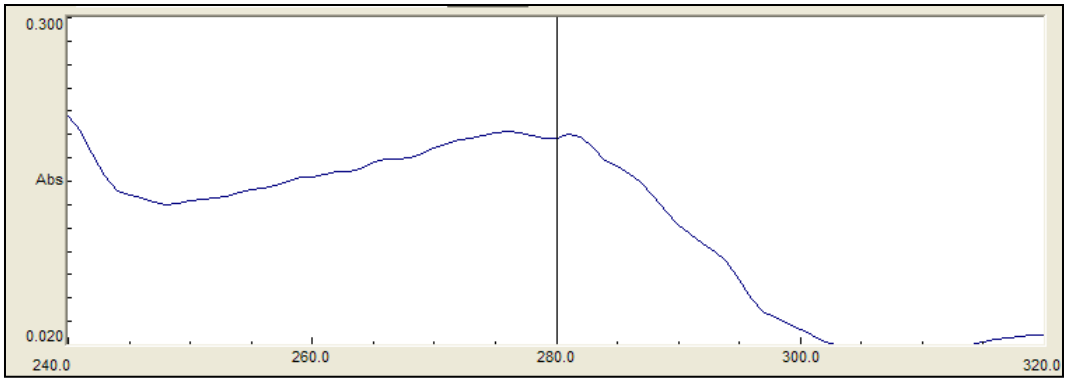

FIG. 31. NusA-A_2 absorbance spectrum. NusA-A_2 has maximal absorbance at 280 nm.

This could be from sequestering of the His-tag in the chimeric protein or saturation of binding capacity on the column. Three prominent protein species were eluted from the column in the low imidazole wash, which included a considerable amount of the full length fusion protein. Perhaps the two other species are degradation products since a band ~ 50 kDa was also observed for GST-A_2. Eluates from IMAC affinity purification of the fusion protein also contained the 50 kDa protein contaminant (FIG. 30); however, overall there appeared to be less proteolytic degradation with this fusion compared to the GST fusion. The absorbance of the protein had a maximum at 280 nm rather than 260 nm (FIG. 31), unlike GST-A_2 suggesting that there is not significant RNA contamination. The yield of the purified NusA-A_2 protein was 0.8 mg/L which was significantly less than GST-A_2.

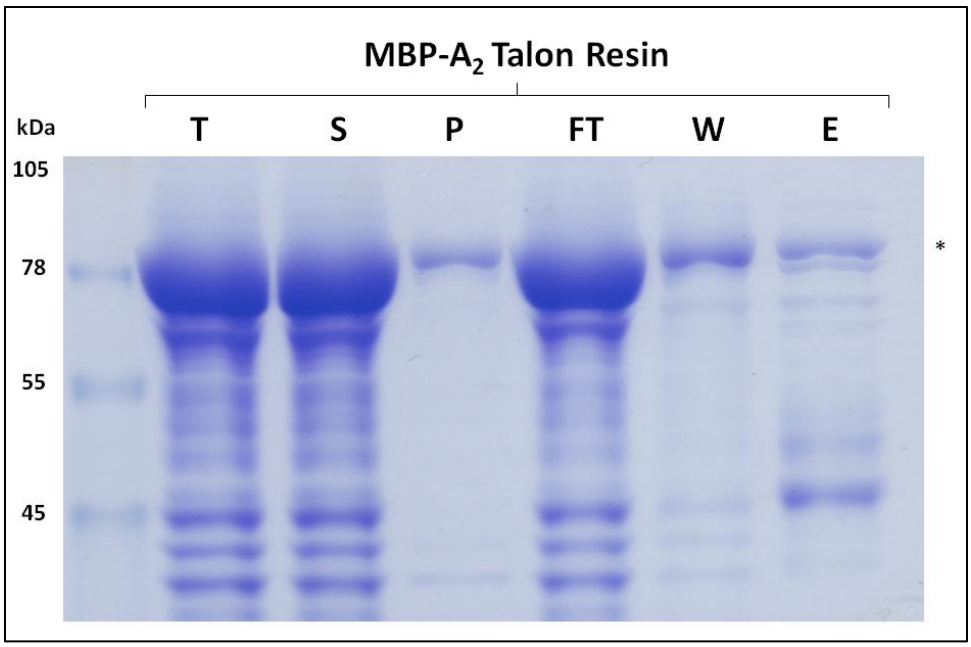

FIG. 32. MBP-A_2 purification with Talon resin. Purification fractions were run on an SDS-PAGE: Total lysate (T), lysate supernatant after centrifugation (S), lysate pellet after centrifugation (P), column flow through (FT), column wash (W), and eluate (E). MBP-A_2 (93 kDa) is labeled with an asterisk.

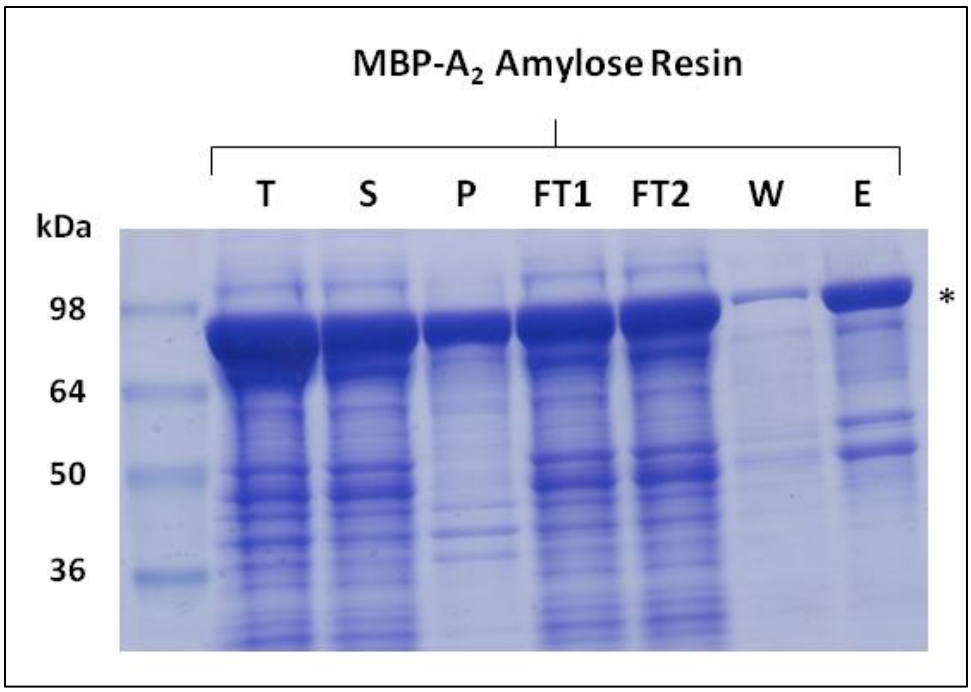

FIG. 33. MBP-A_2 purification with Amylose resin. Fractions from purification were run on an SDS-PAGE: Total lysate (T), lysate supernatant after centrifugation (S), lysate pellet after centrifugation (P), column flow through (FT), column wash (W), and eluate (E). MBP-A_2 (93 kDa) is labeled with an asterisk.

MBP-A_2

MBP-A_2 was expressed at 16°C and purification with both Talon and amylose resin was performed in collaboration with, V. Kuznetsov. With Talon resin chromatography, ~ 90% of the protein was found in the flow-through fraction of the column (FIG. 32), suggesting that the His-tag is sequestered in the chimeric protein; this was also observed with the NusA-A_2 construct (FIG. 30). With amylose resin

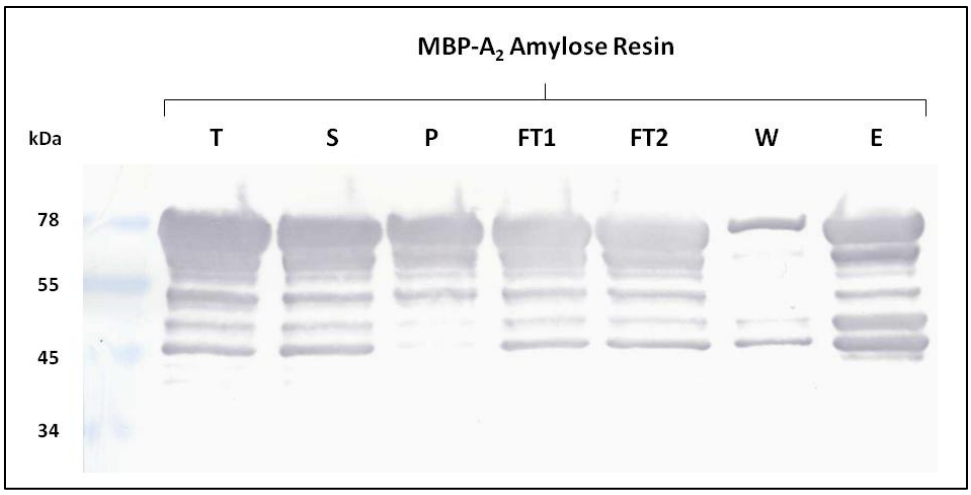

FIG. 34. Western blot of MBP-A_2 purification with Amylose resin. MBP-A_2 purification fractions were assessed by immune-blotting with the α-A_2 antibody. The antibody is specific for the first thirteen residues of A_2.

chromatography, the amount of protein bound to the resin was increased to ~ 40% (compare E fraction of Talon and amylose resin in FIG. 32 and FIG. 33). There was a significant amount of degradation at the C-terminus of the A_2 segment with this fusion construct, as judged by immune-blotting with an antibody specific for the extreme N-terminus of A_2 (FIG. 34). Addition of protease inhibitor in the purification buffer prior to cellular disruption significantly reduced the amount of degradation (FIG. 35). The MBP-A_2 fusion protein has a maximal absorbance at 270 nm (FIG. 36), which suggests there is a small amount of contaminating nucleic acid since purified MBP alone has a

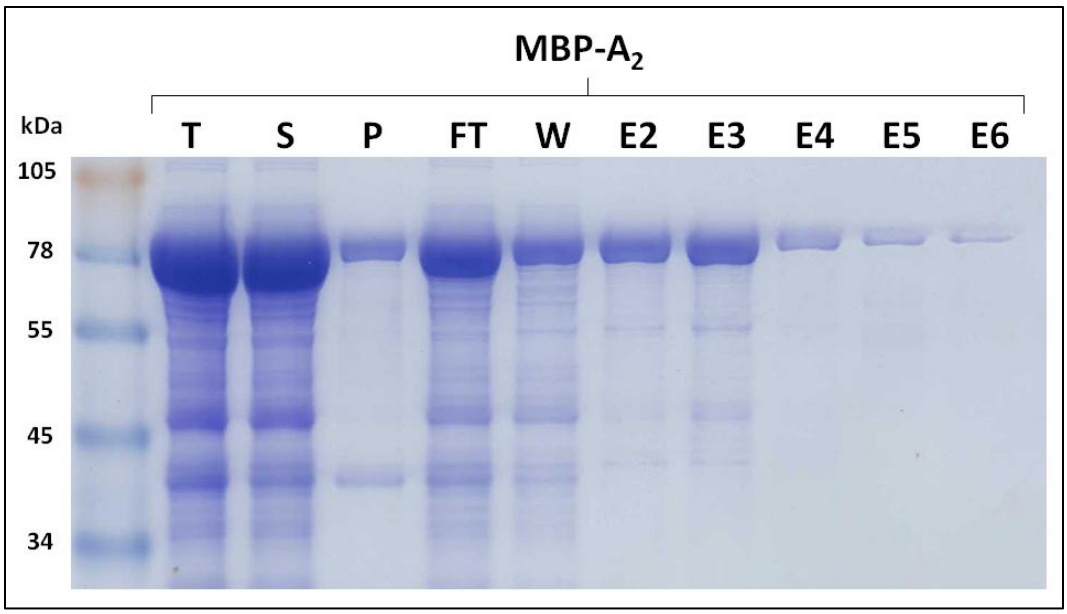

FIG. 35. MBP-A_2 purification with protease inhibitor cocktail. SDS-PAGE of MBP-A_2 (93 kDa) purification with protease inhibitors included in the lysis buffer: Total lysate (T), lysate supernatant after centrifugation (S), lysate pellet after centrifugation (P), column flow through (FT), column wash (W), and eluate fractions (E).

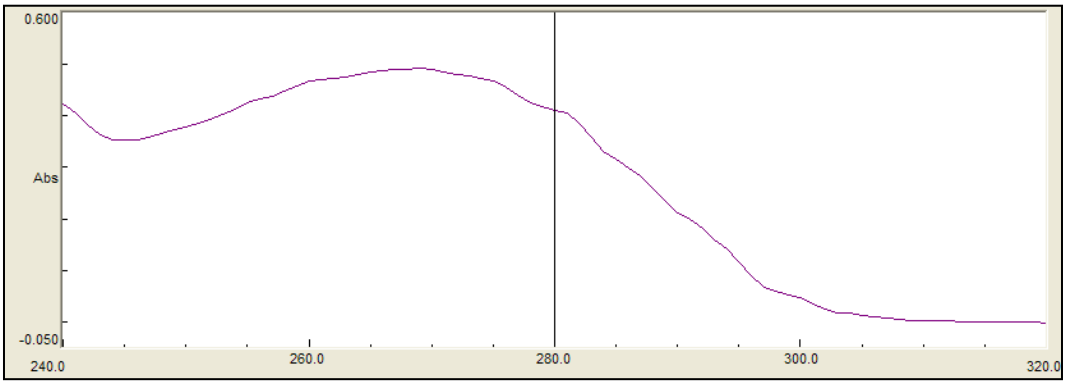

FIG. 36. MBP-A_2 absorbance spectrum. MBP-A_2 has maximal absorbance at 270 nm.

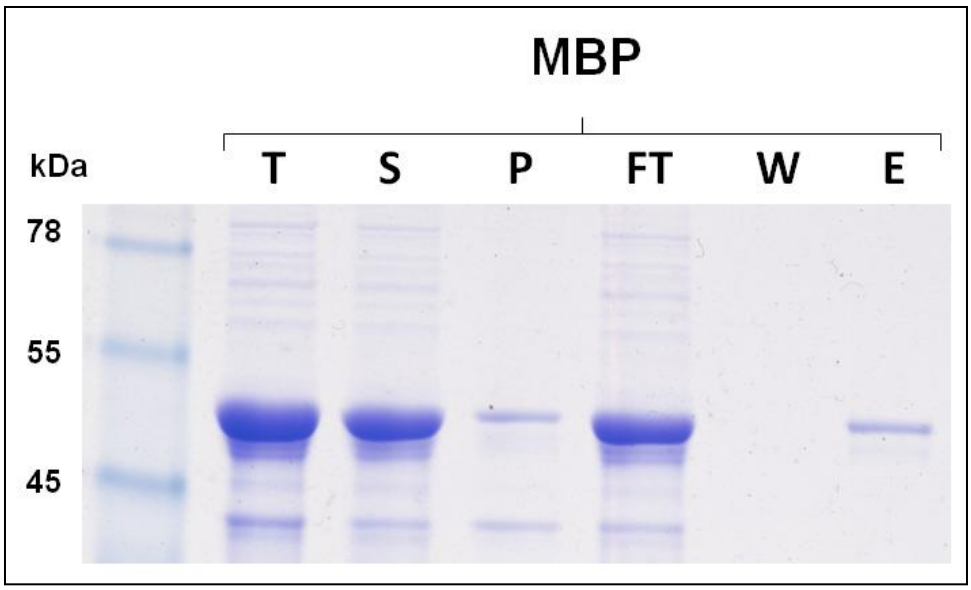

FIG. 37. MBP purification with amylose resin. MBP (48 kDa) purification fractions were run on an SDS-PAGE: Total lysate (T), lysate supernatant after centrifugation (S), lysate pellet after centrifugation (P), column flow through (FT), column wash (W), and eluate (E).

maximal absorbance at 280 nm (FIG. 37 and FIG. 38). The amount of nucleic acid contamination is significantly less than that of GST-A_2 which had a maximal absorbance at 260 nm (compare FIG. 36 and FIG. 29). Addition of RNase to the purification buffer for MBP-A_2 did not have an effect on the absorbance of the protein, suggesting that the RNA contamination it is limited to a small fragment protected from exogenous RNase by A_2. The yield of purified MBP-A_2 was 11 mg/L for amylose resin purification, which was the highest out of all the fusions tested.

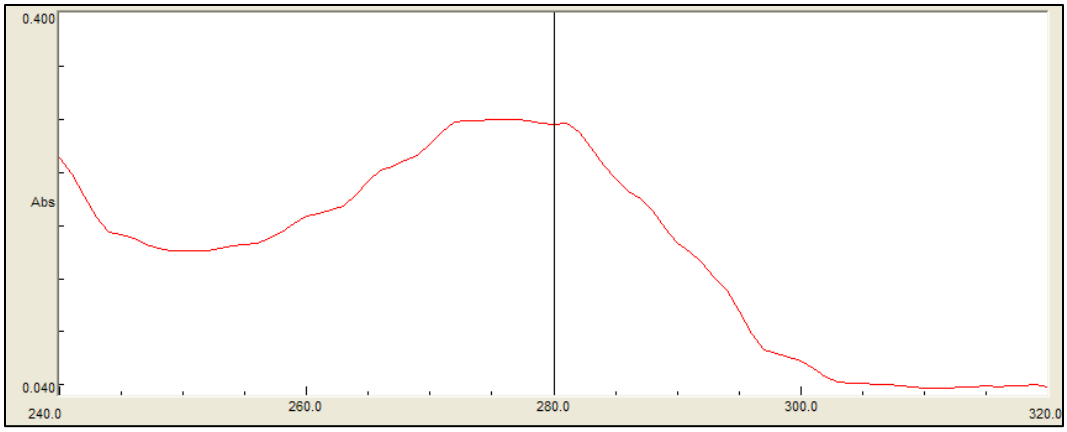

FIG. 38. MBP absorbance spectrum. MBP absorbs maximally around 280 nm.

Based on these criteria, the MBP-A_2 construct was chosen for further biochemical analysis in the following chapter. A parallel construct with the $A_2^{1\text{-}189}$ lytic truncation domain was also constructed.

Optimization of MBP-A_2 production

Small organic molecules that assist cells in offsetting damaging effects from osmotic stress are termed osmolytes. These molecules assist in stabilizing protein and preventing aggregation during protein folding (64). The effect of osmolyte inclusion in culture medium was also tested with MBP-A_2 expression at room temperature (FIG. 39). All osmolytes tested increased the amount of protein expressed. Benzyl alcohol had the most effect on protein expression, but the majority of the protein as in insoluble, ~ 70%.

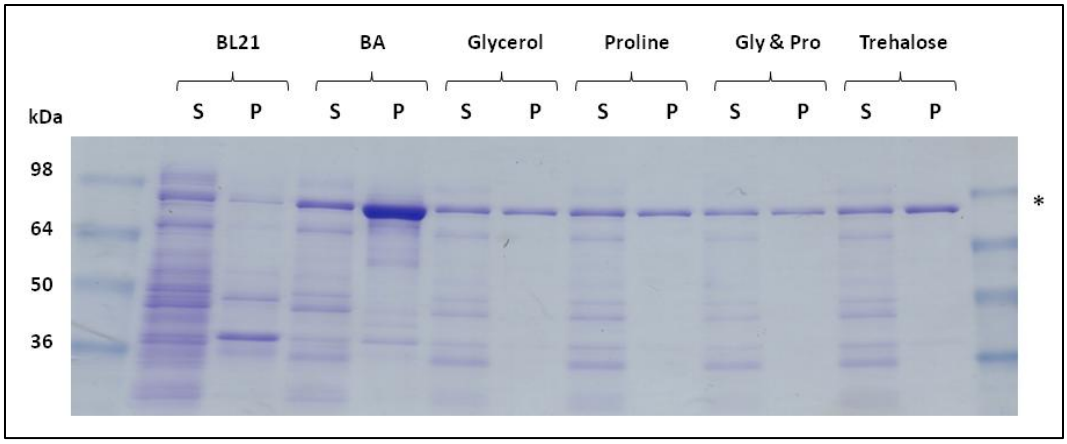

FIG. 39. MBP-A_2 osmolyte expression test. Solubility of fusion protein was tested under growth conditions (LB, 0.5M NaCl; expressed at room temperature) with different osmolytes: 0.1% v/v Benzyl alcohol (BA), 1% v/v glycerol, 1 mM proline, 1% v/v; 1 mM glycerol & proline (Gly & Pro), and 1 mM trehalose. MBP-A_2 (93 kDa) expression is labeled with an asterisk.

Addition of osmolytes also appeared to reduce the amount of proteolytic cleavage after cellular disruption since bands at approximately 45 and 40 kDa were not observed in 4 out of 5 of the osmolyte conditions tested (glycerol, proline, glycerol & proline, and trehalose); however, some potential degradation product was seen in the benzyl alcohol insoluble fraction. Alternatively, these lower molecular weight bands could be proteins in which expression is affected by inclusion of osmolytes in the medium since there are significantly more protein bands visible in the no osmolyte control. It would be interesting to see if addition of osmolytes to cultures with protein expression at 16°C would also reduce the amount of proteolytic degradation of A_2.

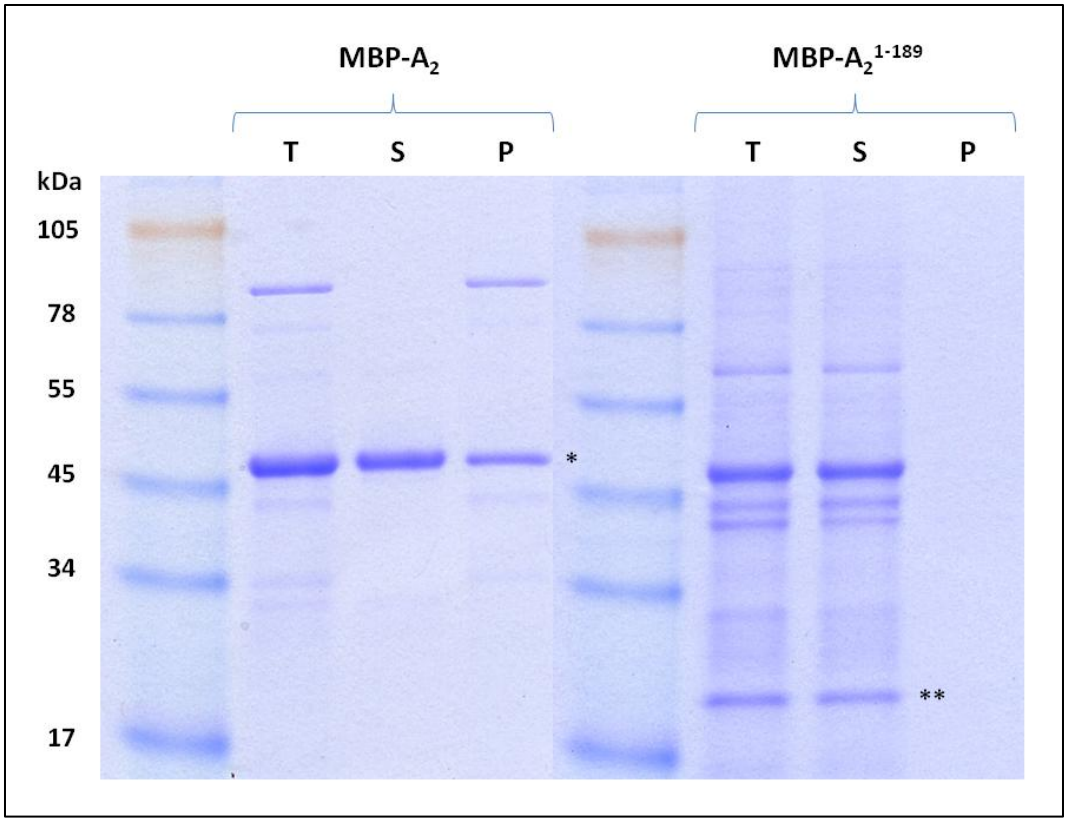

FIG. 40. MBP-A_2 and MBP-A_2^{1-189} fusion cleavage. SDS-PAGE analysis of MBP-A_2 and MBP-A_2^{1-189} cleavage products before centrifugation: Total (T) and after centrifugation: Supernatant (S) and Pellet (P). Cleaved: A_2 (*), A_2^{1-189} (**), and MBP (48 kDa); uncleaved MBP-A_2 (93 kDa), and MBP-A_2^{1-189} (66 kDa)

Cleavage of A_2 domains from MBP chimera

In an attempt to obtain soluble A_2 material, the purified fusion proteins were subjected to proteolytic cleavage using the TEV protease. TEV protease treatment of MBP-A_2 resulted in insoluble A_2 (pellet, FIG. 40); whereas, cleavage of MBP-$A_2^{1\text{-}189}$ produced soluble protein under the conditions assayed (supernatant, FIG. 40). However, even for MBP-$A_2^{1\text{-}189}$, scaling up at the level of the cleavage reaction or concentrating the cleaved protein resulted in insoluble protein. Concentration of MBP-A_2 also showed aggregation, as judged by cloudiness of the concentrated material; however, centrifugation at 18,000 xg for 15 minutes did not pellet the aggregates. A_2 appears to have hydrophobic characteristic since it aggregates when tethered to a large fusion protein. Dialysis of this solution in PBS reduced the amount of visible aggregation without significantly changing the concentration. Perhaps high concentrations of phosphate mimic RNA, a ligand of A_2, thereby causing the protein aggregate to dissociate.

Functional analysis of A_2 fusion protein in vitro

Inhibitory activity of the fusion proteins was assessed directly by measuring MurA activity. In these experiments, MurA activity was assayed by release of inorganic phosphate, a product of MurA catalysis (FIG. 6). This assay is laborious since it is an endpoint assay where samples are removed at various times from the reaction and individually processed. A MurA concentration was chosen in order to avoid excessive

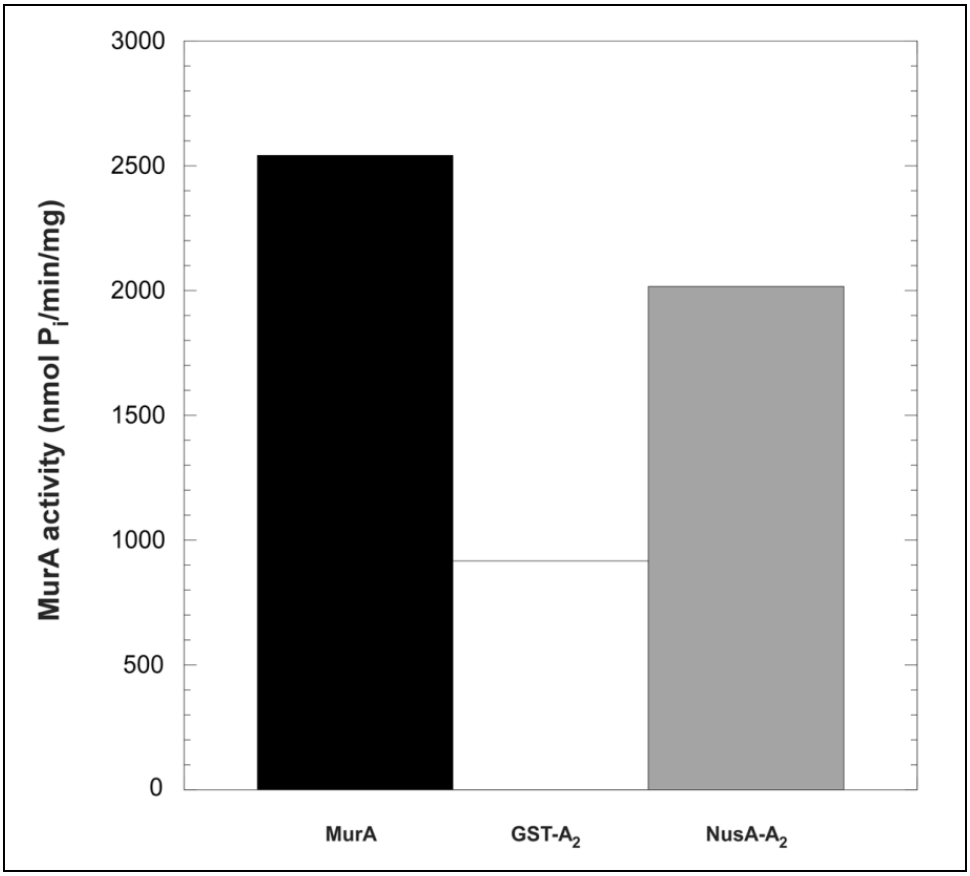

FIG. 41. GST-A_2 and NusA-A_2 inhibition of MurA. MurA (1 μM) specific activity alone or in the presence of GST-A_2 (30 μM) or NusA-A_2 (2 μM).

time in processing, but by doing so this reduced the ratio of fusion protein:MurA that could be tested because solubility limitations of the fusion proteins.

GST-A_2 (30 μM) reduced approximately 66% of MurA (1 μM) activity (FIG. 41). The samples of this reaction had a high background, probably due to the large amount of contaminating RNA. Alternatively, NusA-A_2 at a lower concentration (2 μM) was able to reduce MurA (1 μM) activity by 20% (FIG. 41). This fusion protein appears to be more efficient since only a 2-fold excess was able to reduce the activity of MurA by one-fifth compared to GST-A_2 with 15-fold more protein than MurA was able to reduce activity by two-thirds. NusA-A_2 also had significantly less background in the reactions than that of GST-A_2.

MBP-A_2 (1.8 μM) reduced the activity of MurA (0.2 μM) by about 20% when compared to a MBP (1.8 μM) control (FIG. 42). This is only a 9-fold molar excess of fusion protein to MurA. Surprisingly, the activity of $MurA^{L138Q}$ was increased by 25% compared to the MBP control (FIG. 42). Perhaps MBP-A_2 binds the L138Q mutant in such a manner that it does not inhibit the enzyme but rather stabilizes the protein in such a manner that the enzymatic activity is increased. Binding of A_2 to the mutant will be addressed in the following chapter.

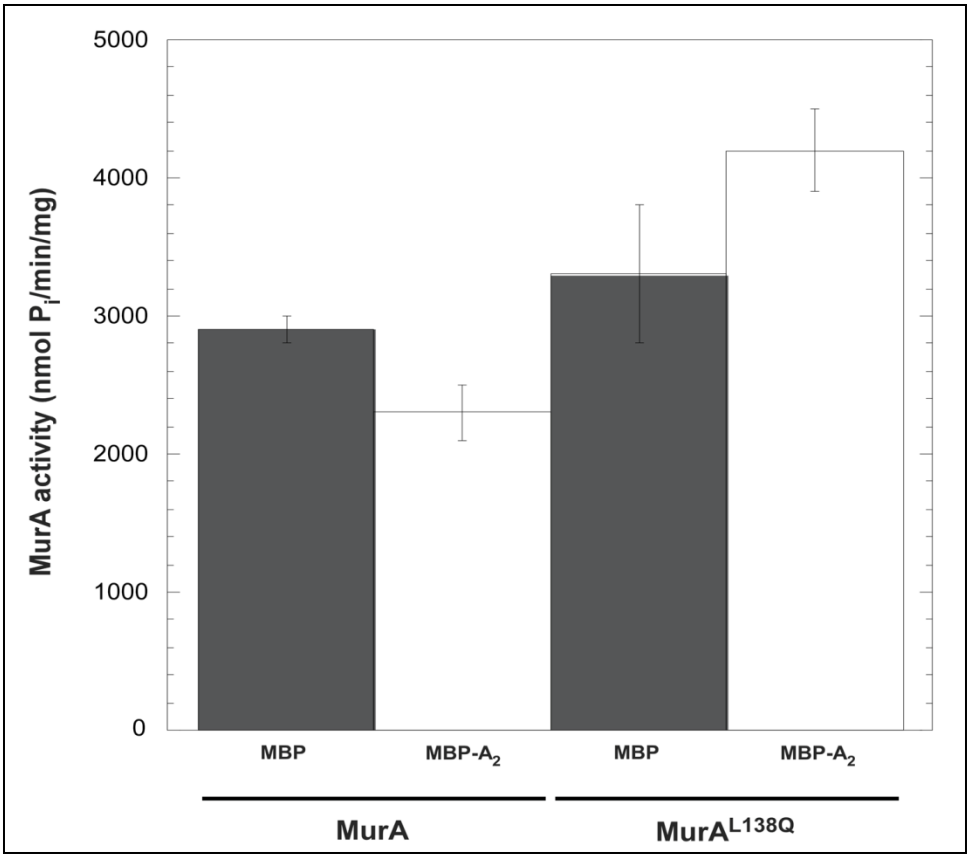

FIG. 42. MBP-A_2 inhibition of MurA. Specific activity of MurA and MurA^{L138Q} (0.2 μM) assayed in the presence of MBP (1.8 μM) or MBP-A_2 (1.8 μM). Reactions performed in triplicate.

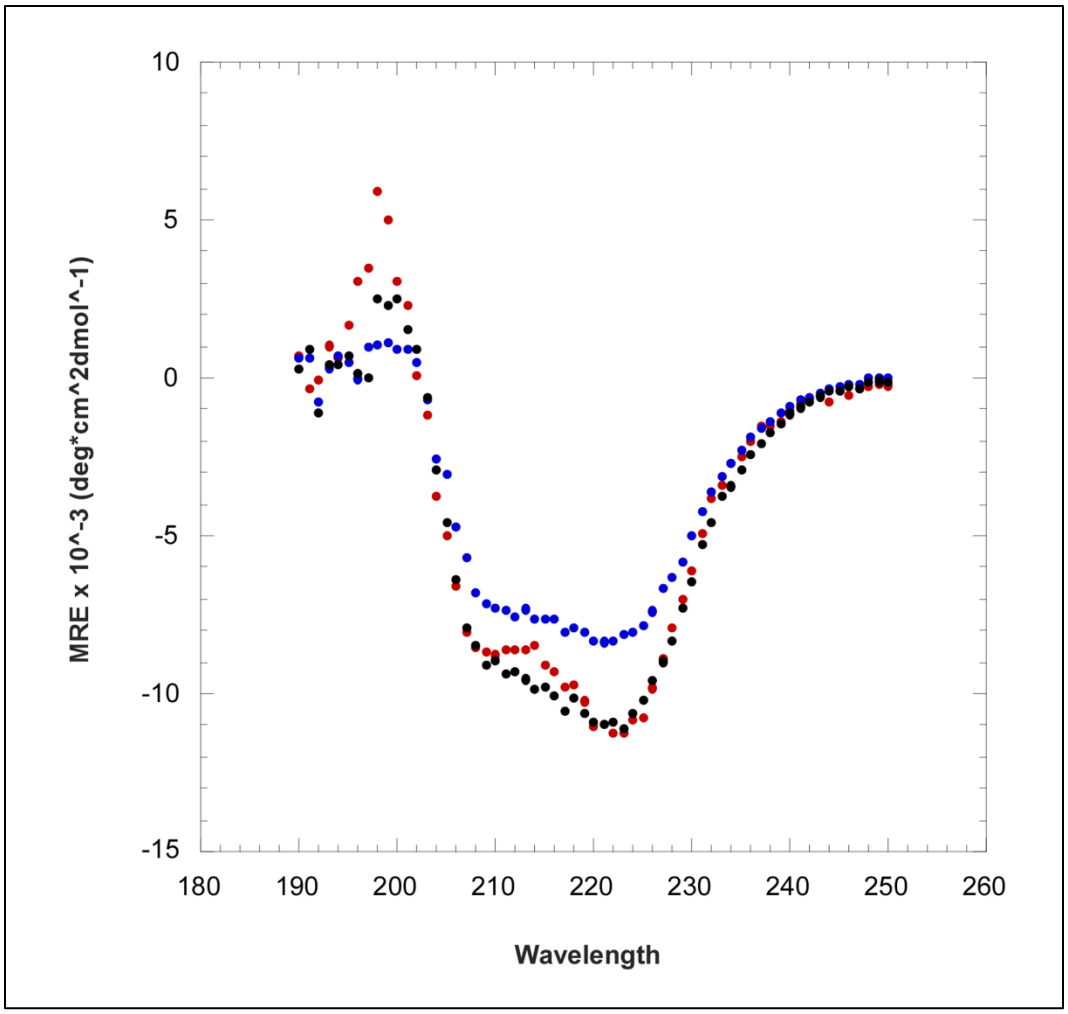

FIG. 43. Circular dichroism analysis of MBP-A_2 and MBP-$A_2^{1\text{-}189}$. CD spectrum of equivalent molar concentrations of: MBP (red circles) (4 μM), MBP-A_2 (blue circles) (4 μM), and MBP-$A_2^{1\text{-}189}$ (black circles) (4 μM).

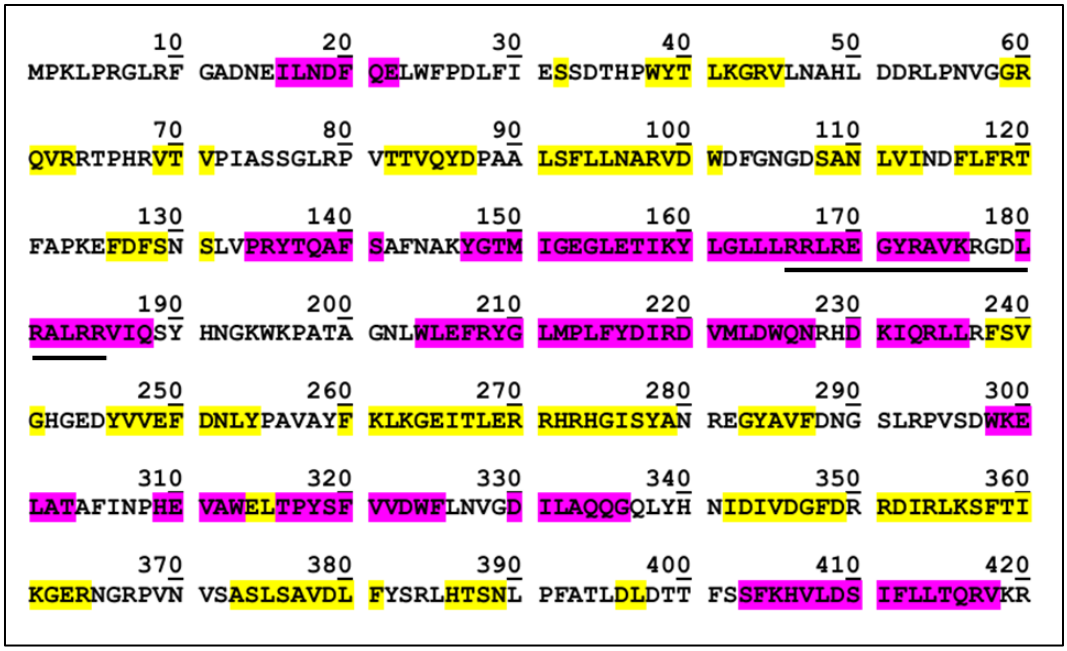

FIG. 44. Secondary structure prediction of A_2. Primary structure of A_2 shown with alpha helices labeled with purple and beta sheets with yellow. JPred3 was used for secondary structure prediction. Putative Arg rich motif (ARM domain) is labeled with a black bar. BindN was used for RNA binding motif predictions.

Characterization of the A_2 fusion structure

CD was used to characterize the secondary structure of the MBP-A_2 fusion protein, and the percent of contributing alpha helical content of A_2 was determined according to the equation listed in the Materials and Methods section. First, the experimental conditions and deconvolution program were validated with MBP by comparing the data to the published spectra (47), which indicated an alpha-helical content of 36%, and the crystal structure of MBP, in which ~ 40% of the residues are in

an alpha helix (144). Analysis of the MBP-A_2 fusion protein revealed an increase in the MRE magnitudes at 208 nm and 222 nm (FIG. 43), which are characteristic minima for alpha helices (75), suggesting a loss in the alpha helical content of the fusion. The contributing alpha helical percentage for A_2 was determined to be about 26%; whereas, the contributing percentage for a C-terminal truncation, A_2^{1-189} (FIG. 43), was 36% alpha-helical. The values correlate well with the secondary structure prediction analysis (Jpred3) (29) of both the full length A_2 and the A_2^{1-189} truncation in which approximately one-third of both proteins are predicted to be alpha helical (FIG. 44).

Probing the A_2 lytic domain

Previous work has shown that the lytic domain of A_2 is in the N-terminal 179 residues of A_2 (FIG. 45) (89). The structural elements of this segment were predicted to be alpha helix-6 beta sheets-3 alpha helices (FIG. 44). Although the N-terminal 1-179 truncation is fully lytic, the next largest fragment, 1-171, is not (FIG. 45). This truncation includes 5 residues of a predicted 30 aa long alpha helix that spans residues 147-176. This helix could be the functional domain of A_2, i.e., the major determinant for inhibitory binding of MurA and that by truncating the helix, lytic function is lost. This region also is predicted to bind RNA (BindN) (160) and contains a putative arginine-rich motif (ARM domain) (149) (FIG. 44), in that there are 8 Arg and 1 Lys residues, spaced every 3 to 4 residues between residues 166 and 185. Earlier, RNA binding was

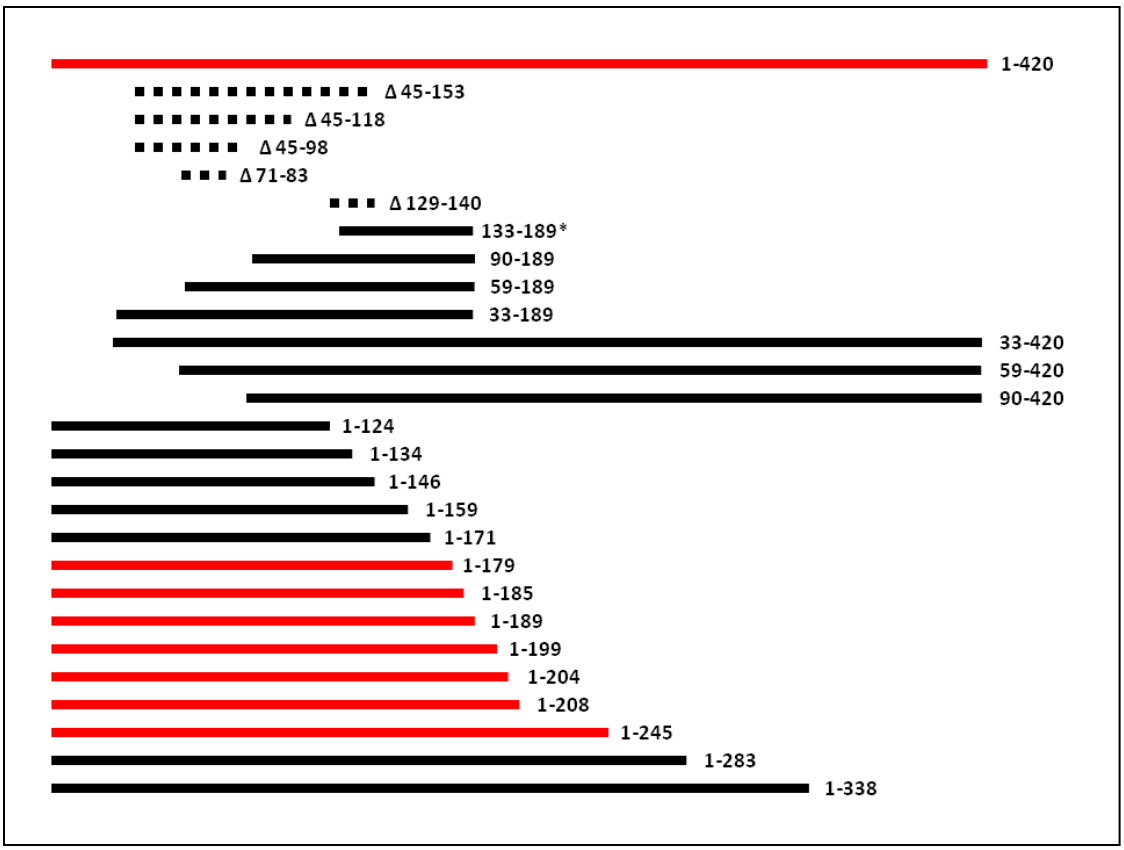

FIG. 45. A_2 Fragment analysis. Full length A_2 is 420 aa. Truncation data was reprinted with permission (89) for comparison. *Data obtained from collaborator, (R. Kongari). A_2 truncations depicted as solid bars. Internal deletions of the protein are shown as dashed lines. Functional (red) and non-functional (black)

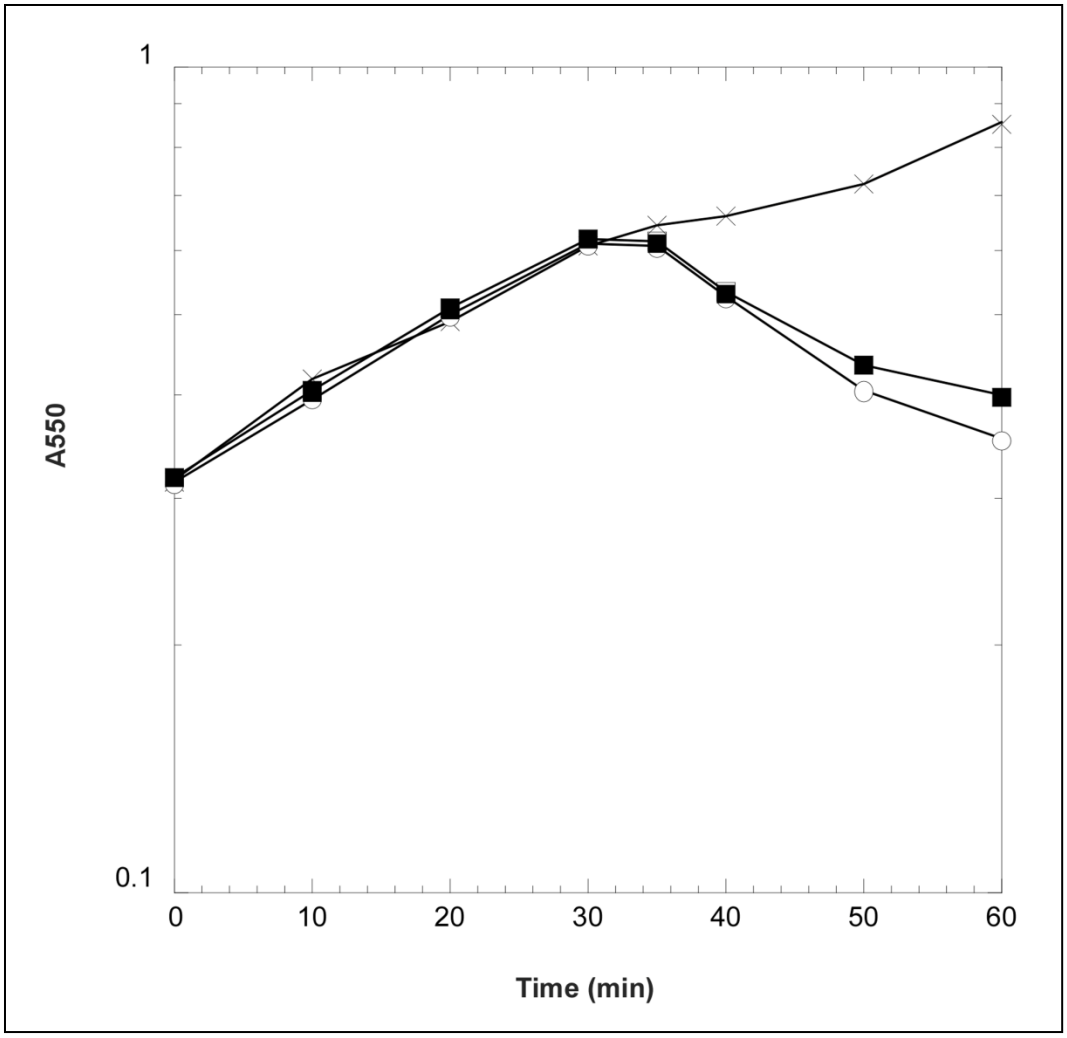

FIG. 46. A_2-A hybrid lysis phenotype. A_2-A hybrid lysis phenotype was compared to an A_2 control: A_2-A hybrid (white circles), A_2 (black squares), and uninduced control (X). HfrH *lacZ::*Tn*5* cells harboring either pZE12-A_2-*A* or pZE12-A_2 were induced with 100 μM IPTG (final) at Time = 0'.

proposed to be one mode by which A_2 is regulated (see Chapter II). This raises the attractive notion that the putative ARM domain could also be the lytic domain of A_2, and that RNA-dependent regulation of A_2 activity might simply reflect the occlusion of the MurA interaction surface. To test this possibility, an A_2-A hybrid was generated where residues 165-173 were replaced with the aligned residues 158-165 of MS2 A (FIG. 46); this replacement eliminates 4 of the 8 Arg residues. Analysis of the A_2-A hybrid revealed that the protein retained full lytic function (FIG. 45), which falsified our hypothesis. Moreover, an $A_2$133-189 fragment was also tested and found to be non-lytic (FIG. 45). Therefore, this predicted alpha helical domain does not appear to be the lytic domain of A_2 and is probably more important for stabilizing the tertiary structure of the protein by acting as a scaffold for beta sheet assembly.

Review of the A_2 truncation data showed that when the first 32 residues were removed from the N-terminus, the resultant protein lost lytic function. Perhaps the N-terminal helix as well plays an important role in maintaining the tertiary structure of the protein by functioning as a scaffold for the putative beta sheet domain. An alignment of the maturation proteins from Leviviruses and Allolevivirus revealed that the least conserved region between the lytic maturation proteins of the *Allolevivirus* and the non-lytic maturation proteins of the *Leviviridae* is a predicted beta-sheet domain in the N-terminal half of the protein (FIG. 44). All of the truncation data support the notion that the lytic domain is comprised of beta sheets that are supported by a series of 3 alpha helices; thus, by removing or deleting part of the alpha helices the protein is unable maintain the proper tertiary structure nor inhibit MurA.

CHAPTER IV

INHIBITORY MECHANISM OF THE Qβ LYSIS PROTEIN A_2*

Introduction

The Allolevivirus Qβ produces a single protein A_2 to effect bacterial lysis, in addition to serving as a structural component of the virion (FIG. 8). Unlike dsDNA phages that produce muralytic enzymes to degrade the cell wall, A_2 inhibits MurA, an enzyme that catalyzes the first committed step in cell wall synthesis (16). The key genetic result that led to this conclusion was the isolation of a dominant mutant resistant to Qβ lysis that mapped to the *murA* locus. This mutant, designated as *rat1* (resistant to A-two) was shown to be a Leu to Gln change at position 138 of MurA. In addition, Bernhardt and colleagues showed that MurA expression *in trans* protected cells from lysis during a Qβ phage infection. Moreover, purified Qβ particles were able to inhibit $MurA^{WT}$ activity, but not $MurA^{rat}$ activity, in a crude extract. Qβ mutants that were able to overcome the *rat* mutant lysis block were isolated and designated as *por* (plates on *rat*). These mutants were postulated to be compensatory for the L138Q mutation in the A_2-MurA interface (16). However, recent biochemical and genetic evidence has indicated that the suppressor phenotype of these mutants is due to translational up-

*Part of the data reported in this chapter is reprinted with permission from Understanding the lytic function of A_2: The maturation protein of ssRNA bacteriophage Qβ, C. Langlais, 2007, Texas A&M, College Station, TX. [2007]

regulation of A_2, deriving from disruption of regulatory RNA stem-loop structures (Chapter II).

To address the question of how lysis is regulated in a Qβ infection, a model was proposed in which A_2 lysis function was not fully realized until assembled into the capsid of the phage particle (54). However, previously we have shown that MurA actually inactivates Qβ particles, indicating that virions are not likely to be involved in lysis (Chapter II). Instead, quantitative analysis of the infection cycle indicated that free, unassembled A_2 is the inhibitory molecule of MurA. Characterization of the mechanism of MurA inhibition has been hindered due to the insolubility of A_2 apart from assembly into the virion capsid.

In this study we address the requirements for an A_2-MurA interaction. The results are discussed in terms of the molecular state of MurA when it is bound by A_2.

Materials and Methods

Bacterial strains and growth conditions

The following *E. coli* strains were used in this study: XL1-Blue (140) was used for all plasmid constructions, HfrH *lacZ::*Tn*5* served as lawns for bacteriophage plaque assays, and ER2738 was used for phage propagation and protein expression. Descriptions of these strains are listed in Chapter II. *E. coli* strains were grown with

aeration at 37°C in standard LB medium supplemented with 100 μg ml^{-1} ampicillin, 40 μg ml^{-1} kanamycin, or 10 μg ml^{-1} tetracycline when appropriate.

Plasmid construction

Several plasmids used in this study were described in the preceding chapters: pZE12-*murA*, pZA31-*murA*^{Bs}, and pET*MBP-A*$_2$. Alleles of *murA** used in the MurA bioassay were constructed by site-directed mutagenesis (140) into pZE12-*murA* with primers listed in TABLE 11. Construction of additional *murA** alleles is described elsewhere (6).

Protein expression and purification

Expression and purification of MurA and MBP-A_2 were described in previous chapters: Chapter II and Chapter III, respectively.

MurA activity assay

Qβ inhibition of MurA was performed as previously reported (16) but with 2 μg of purified MurA (0.4 μM) instead of cell lysate and 60 μl of Qβ (4 x 10^{13} physical particles) (~0.7 μM A_2) in a 100 μl reaction.

TABLE 11. Primers for construction of *murA** alleles.

Allele	Sequence
V87R	FOR:GCACCTTACGATCTGCGTAAAACCATGCGTGC
	REV:GCACGCATGGTTTTACGCAGATCGTAAGGTGC
K88E	FOR:CCTTACGATCTCGTTGAAACCATGCGTGCTTC
	REV:GAAGCACGCATGGTTTCAACGAGATCGTAAGG
T89R	FOR:GATCTGGTTAAACGCATGCGTGCTTC
	REV: GAAGCACGCATGCGTTTAACCAGATC
A154R	FOR:GGTCGTTTGAAAGGTCGTCATATCGTGATGG
	REV:CCATCACGATATGACGACCTTTCAAACGACC
H155R	FOR:CGTTTGAAAGGTGCACGTATCGTGATGGATAAAG
	REV:CTTTATCCATCACGATACGTGCACCTTTCAAACG
I156R	FOR:GTTTGAAAGGTGCACATCGTGTGATGGATAAAGTC
	REV:GACTTTATCCATCACACGATGTGCACCTTTCAAAC
V157R	FOR:GAAAGGTGCACATATCCGTATGGATAAAGTCAGC
	REV:GCTGACTTTATCCATACGGATATGTGCACCTTTC
T179R	FOR:CTGGCGGAAGGCCGTACGATTATTG
	REV:CAATAATCGTACGGCCTTCCGCCAG
I181R	FOR:GAAGGCACCACGCGTATTGAAAAC
	REV:GTTTTCAATACGCGTGGTGCCTTC
E183R	FOR:CCACGATTATTCGCAACGCAGCGCGTGAAC
	REV:GTTCACGCGCTGCGTTGCGAATAATCGTGG

Batch affinity fractionation experiments

Amylose magnetic beads were chosen for batch affinity fractionation experiments since the maltose binding protein (MBP) fusion binds specifically to amylose resin. An aliquot (40 μl, NEB) of beads was washed with of amylose buffer (Chapter III). A magnet was applied for 1 minute and supernatant was removed. MBP-A_2 (90 μl of 6 μM) was incubated for 30 minutes with rolling at 4°C. Beads were washed three times, as above, to remove unbound MBP-A_2, vortexing briefly before application of magnet and removal of supernatant. To assess MurA binding to A_2, beads with MBP-A_2 bound were resuspended in buffer containing 100 μl of 10 μM of MurA with the following substrate conditions: none, 1 mM PEP (Sigma), 1 mM UNAG (Sigma), and 1mM PEP/UNAG. Reactions were incubated at 4°C for 1 hour with rolling. Samples were washed three times and eluted by resuspending beads in 2X 40 μl of amylose elution buffer (Chapter III). Samples were analyzed by SDS-PAGE and immune-blotting as described previously (Chapter II). Unbound fractions (supernatant of first wash) were analyzed by SDS-PAGE and bound fractions were immune-blotted with the α-MurA antibody.

Fusion cleavage assay

Reactions containing 2.5 μM of MBP-A_2, 5 μM MurA under different substrate conditions: none, 1 mM PEP, 1 mM UNAG, 1mM PEP/UNAG, and 1 mM

UNAG/Fosfomycin (Sigma), and 10 μg of MBP-TEV protease, were processed as described in Chapter III. Fractions were analyzed with SDS-PAGE and immune-blotting, probed with the α-A_2 antibody.

MurA bioassay

Gradient induction of MurA in bacterial lawns of HfrH *lacZ::*Tn*5* harboring pZE12-*murA*, or various alleles (*murA**), was generated by plating 200 μl of a mid-log phase culture in a 0.7 % soft agar overlay supplemented with 2 mM $CaCl_2$ onto LB agar plates containing ampicillin and 0 μM, 12.5 μM, 25 μM, 50 μM, 100 μM or 1 mM of IPTG. An aliquot of cell-free Qβ lysate (~650 plaque forming units) was included in the overlay. Plates were incubated at 37ºC for 12-16 hrs prior to screening for plaque formation (FIG. 47).

Results and Discussion

Inhibition of purified MurA by Qβ

Bernhardt and colleagues (2001) had reported that virion-associated A_2 inhibits MurA in a crude lysate. To test whether this inhibition required any other host factor, the *in vitro* assay was repeated with purified MurA and Qβ particles. We chose a MurA concentration, 400 nM, which reflects the level of MurA in the host cell (Chapter II).

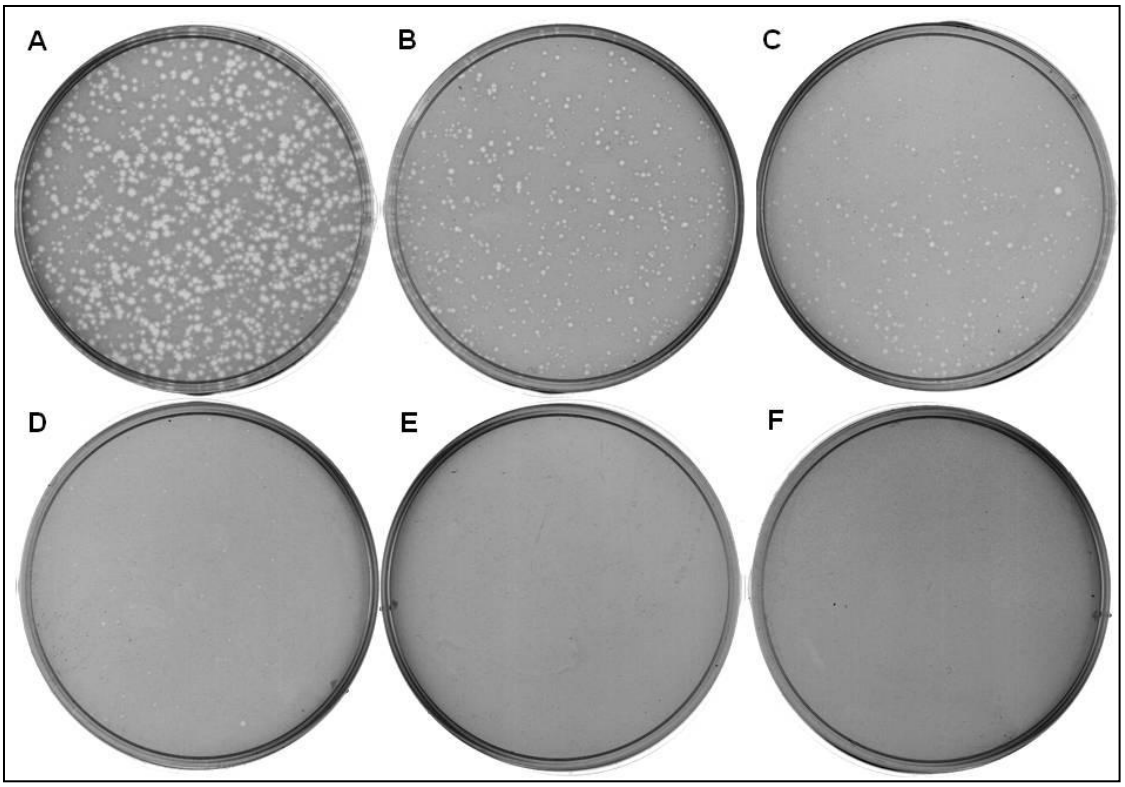

FIG. 47. MurA protection assay induction series. Protection from Qβ plating is observed on induction plates of 100 μM IPTG or greater. Qβ phage and bacteria are included in agar overlay on plates containing increasing amounts of IPTG (μM): (A) 0, (B) 12.5, (C) 25, (D) 50, (E) 100 and (F) 1000.

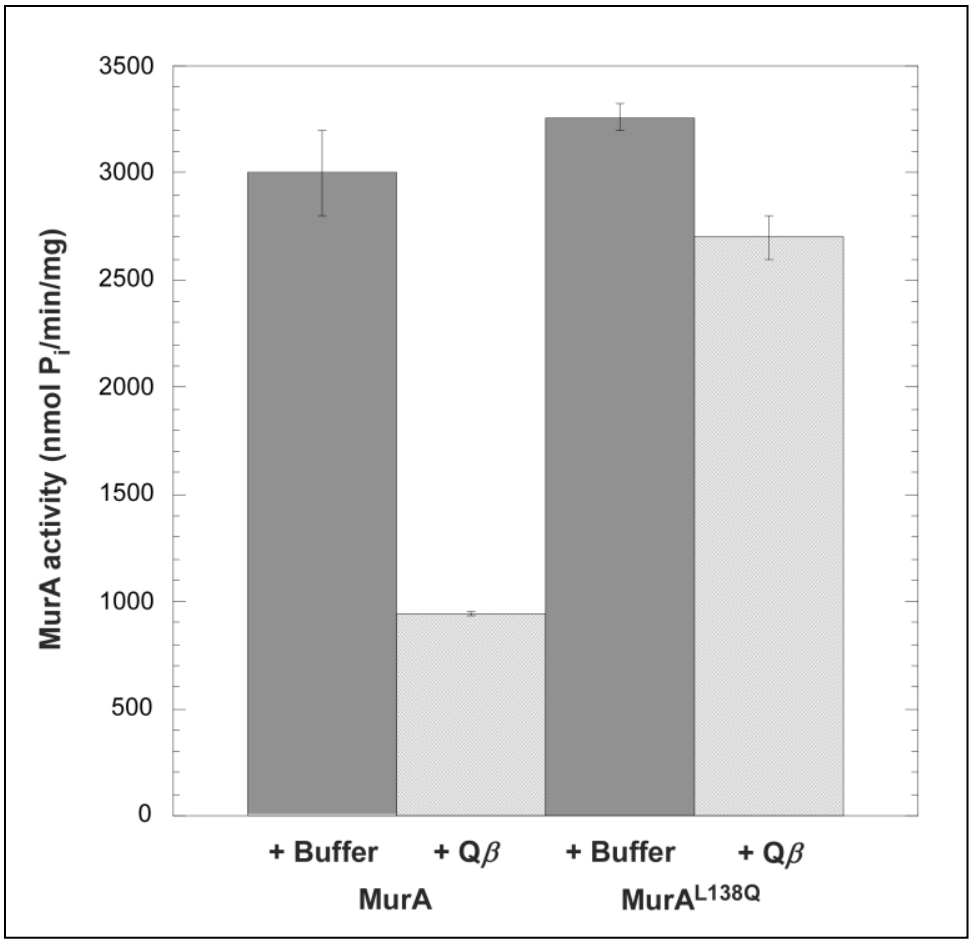

FIG. 48. Purified Qβ inhibits MurA *in vitro*. Activity of purified MurA was measured in the presence of buffer or purified Qβ particles. The *rat* mutant, MurA^{L138Q}, was tested in parallel. Values are averages of three samples.

The results showed that, under these conditions, at the highest possible concentration of virions (~700 nM) Qβ reduced the activity of MurA by 70% when compared to a reaction lacking phage particles (FIG. 48). Under the same conditions, A_2 caused only a marginal reduction in $MurA^{L138Q}$ activity (17%). These results rule out the need for other host components in the A_2 inhibition of MurA.

The A_2 interaction with MurA is conformation-dependent

Batch affinity fractionation experiments using a purified fusion protein, MBP-A_2, provide *in vitro* evidence for a direct interaction between A_2 and MurA (FIG. 49A-B). Information about the conformational state of MurA required for MBP-A_2 association was obtained by assaying binding in the presence of various substrates. MBP-A_2 preferentially bound to both the UNAG-liganded and the tetrahedral intermediate states of MurA but not the unliganded or PEP-bound states (FIG. 49A, lanes 2-5), suggesting that A_2 associates with MurA in a closed conformational state (FIG. 7). Binding of A_2 to $MurA^{L138Q}$ was not observed under these conditions (FIG. 49A, lanes 7-10), suggesting that the mutation reduces the affinity of A_2 for MurA.

Binding was also analyzed by another method in which cleavage of the fusion protein from A_2 was performed in the presence of various substrate-induced MurA conformations. A_2 cleaved from the MBP fusion protein was insoluble both in the absence and presence of unliganded MurA (FIG. 49C, lanes 4-9; FIG. 49D, lanes 2-7).

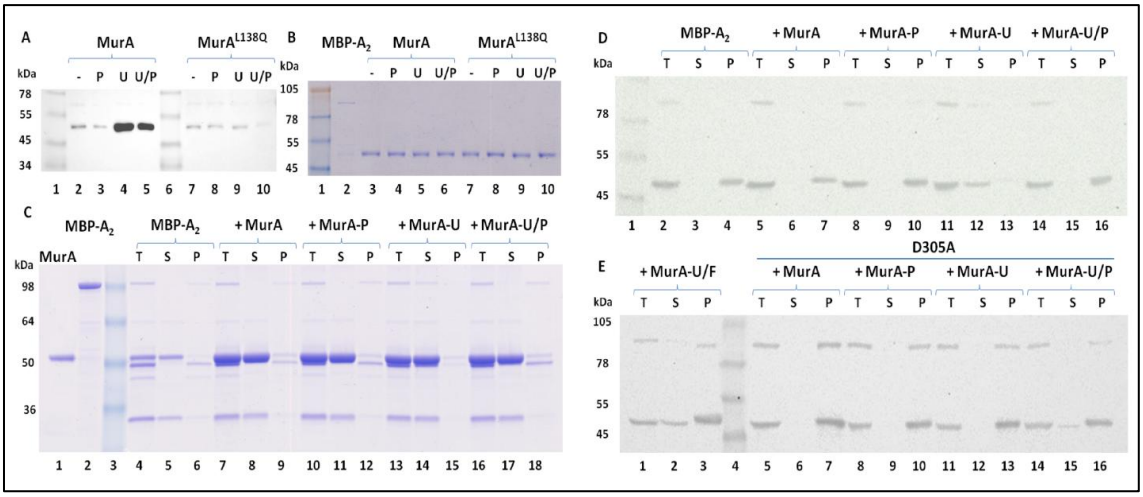

FIG. 49. A_2 binds MurA in a substrate-dependent manner. (A) MBP-A_2 associates with MurA in a closed conformational state. Eluates from amylose magnetic bead fractionation experiments were Western blotted and probed with the α-MurA antibody. MBP-A_2 was incubated with MurA under various substrate conditions: No substrate (-), PEP (P), UNAG (U), and both substrates (U/P). $MurA^{L138Q}$ *rat* mutant was tested in parallel. (B) Unbound fractions of panel (A) experiments. (C) Fusion cleavage analysis of A_2-MurA binding. MBP-A_2 was cleaved with TEV protease in the absence or presence of MurA under various substrate conditions (same as in panel A). Binding was assessed as A_2 solubility after centrifugation: Total fraction (T), supernatant after centrifugation (S), and pellet fraction (P). Samples were resolved on SDS-PAGE. MBP-A_2 has an apparent MW of 100 kDa. Cleaved A_2 runs at 50 kDa with the MBP running at the same apparent MW as MurA (~52 kDa). (D) A_2 binds MurA liganded to UNAG. Western blot analysis of fusion cleavage assays. Blots were probed with the α-A_2 antibody. Binding was tested with substrate conditions as in panel C. (E) A_2 does not bind the tetrahedral intermediate state of MurA. UNAG and Fosfomycin (U/F) liganded MurA and $MurA^{D305A}$ binding and immune-blotting was also performed in parallel as in

Addition of PEP to the reaction with MurA did not increase A_2 solubility (FIG. 49C, lanes 10-12; FIG. 49D, lanes 8-10), but when UNAG was included in the reaction, A_2 remained soluble (FIG. 49C, lanes 13-15; FIG. 49D, lanes 11-13), indicating the formation of an A_2-MurA complex. However, in the presence of both substrates, A_2 was insoluble (FIG. 49C, lanes 16-18; FIG. 49D, lanes 14-16), indicating a preference for binding to the UNAG liganded form and not the tetrahedral intermediate state. This result is contradictory to the batch affinity data in which MurA association was observed in the presence of both substrates (FIG. 49A, lane 5). Comparison of the two fractions revealed a reduction in the amount of MurA bound in the presence of both substrates suggesting that the fraction of MurA bound to A_2 could be in the UNAG liganded state, rather than tetrahedral intermediate state. Alternatively, the addition of fosfomycin with UNAG, which locks the enzyme into a closed conformational state (FIG. 7), reduced the amount of soluble A_2 but did not eliminate binding altogether (FIG. 49E, lanes 1-3).

Dynamics of the catalytic loop upon addition of both substrates might create unfavorable conditions for A_2 association. To address this possibility, $MurA^{D305A}$ was purified and fusion cleavage of MBP-A_2 was repeated. $MurA^{D305A}$ is unable to eliminate the product after substrate addition and locks MurA in the tetrahedral intermediate state (FIG. 50) (43, 130). Similarly to the fosfomycin with UNAG bound MurA, a portion of A_2 remained soluble in the presence of both UNAG and PEP; however, A_2 was insoluble with the addition of only UNAG (FIG. 49E, lanes 11-16). The purified D305A protein has an increase in absorbance at 260 nm, where UNAG absorbs, compared to WT (data not shown) suggesting that the substrates do co-purify with the protein. Therefore,

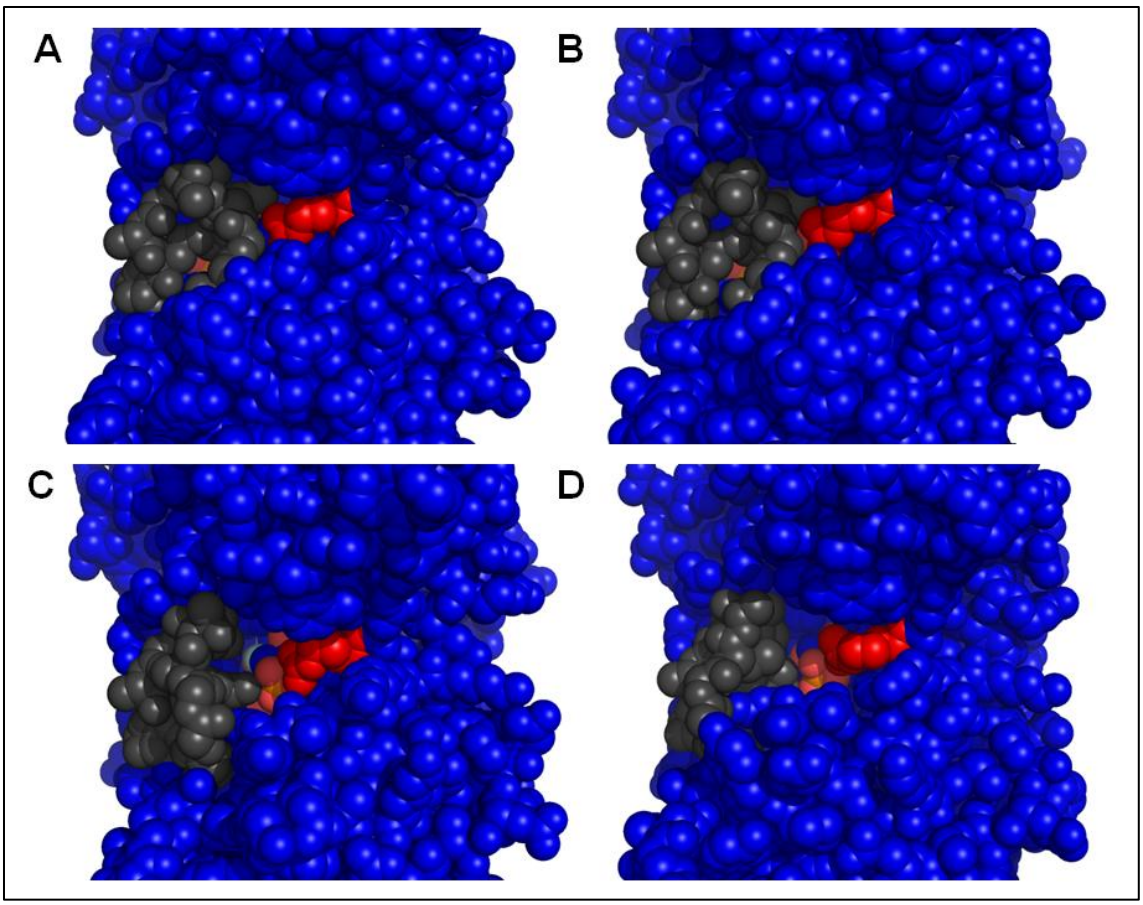

FIG. 50. Active site analyses of MurA substrate-dependent conformations. (A) MurA bound with UNAG (Han H., unpublished; PDB entry 3KQJ), (B) MurA bound with UNAG and Fosfomycin (PDB entry 1UAE) (138), (C) MurA tetrahedral intermediate with a fluorinated analog (PDB entry 1A2N) (137), and (D) MurA tetrahedral intermediate (D305A mutant, PDB entry 1Q3G) (43). Catalytic loop displayed as grey spheres, Arg 397 displayed as red spheres, and substrates shown as spheres and colored according to elements. Figures were generated using PyMOL (133).

addition of UNAG would have no effect on A_2 solubility since the protein already has both substrates bound and suggests that A_2 does not bind the tetrahedral intermediate state. The partial solubility of A_2 in the fraction that included both substrates (FIG. 49E, lane 15) was reproducible, possibly indicating that the mutant retains a low level of activity, such that A_2 is able to bind in the preferred UNAG-liganded state. When WT MurA is added to a reaction with both substrates without prior incubation on ice, a fraction of A_2 appears in the soluble fraction (data not shown) suggesting that A_2 is able to bind the UNAG state rather than the tetrahedral intermediate if the enzyme is not permitted to equilibrate with both substrates prior to the A_2 fusion addition.

When structures of the active sites and catalytic loop conformations of the various MurA-liganded states were viewed, no apparent conformational difference is seen between the UNAG and the UNAG/fosfomycin-liganded states (FIG. 50A-B); however, a difference between the conformations of the catalytic loop between the UNAG/fosfomycin and tetrahedral intermediate states is visible (FIG. 50B-D). The substrates appear to be more accessible to the solvent in the active site of the tetrahedral intermediate state than that of UNAG or UNAG/fosfomycin complexes. Perhaps this slight change in the conformation of the catalytic loop with the addition of another substrate besides UNAG can explain the differences in the solubility of A_2 above.

Interestingly, A_2 was soluble when cleaved from MBP in the presence of $MurA^{L138Q}$ liganded with UNAG (FIG. 51). This was surprising since the batch

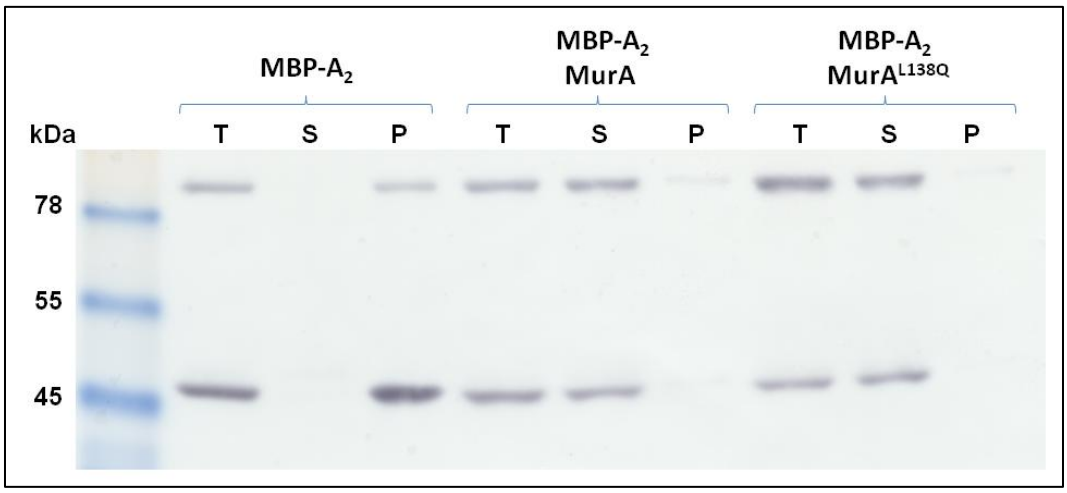

FIG. 51. A_2 binds $MurA^{L138Q}$. Fusion cleavage of MBP-A_2 was tested in the presence of UNAG bound MurA and $MurA^{L138Q}$. Solubility of A_2 after centrifugation: Total fraction (T), supernatant after centrifugation (S), and pellet fraction (P) was assessed by Western blot that was probed with the α-A_2 antibody.

affinity experiment in which MBP-A_2 did not bind $MurA^{L138Q}$ had higher concentrations of protein. MBP could be causing steric hindrance on A_2 association with MurA such that an addition of the L138Q substitution reduces the strength of the interaction. Alternatively, the bound fraction in the batch affinity experiment was washed three times prior to elution; these wash steps reduce the concentration of the protein in solution and could cause dissociation of the complex if the mutation has a reduced affinity for A_2. The notion that reduction in affinity between A_2 and the $MurA^{L138Q}$ mutant is supported by the yeast-two-hybrid data which had reduced growth compared to WT (FIG. 52) (89).

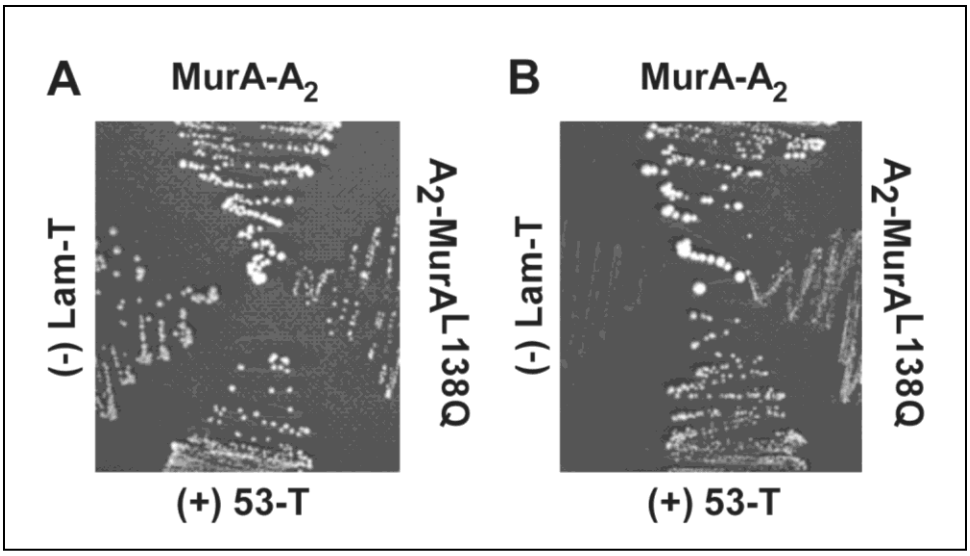

FIG. 52. Yeast-two-hybrid analysis of the A_2-MurA interaction. Data reprinted with permission (89). (A) Yeast strains harboring binding partners (A_2 and MurA/MurA^{L138Q}) on selection medium. (B) Yeast strains harboring binding partners on stringent medium conditions requiring protein association for growth. Negative control: Lam-T pair and positive control: 53-T pair

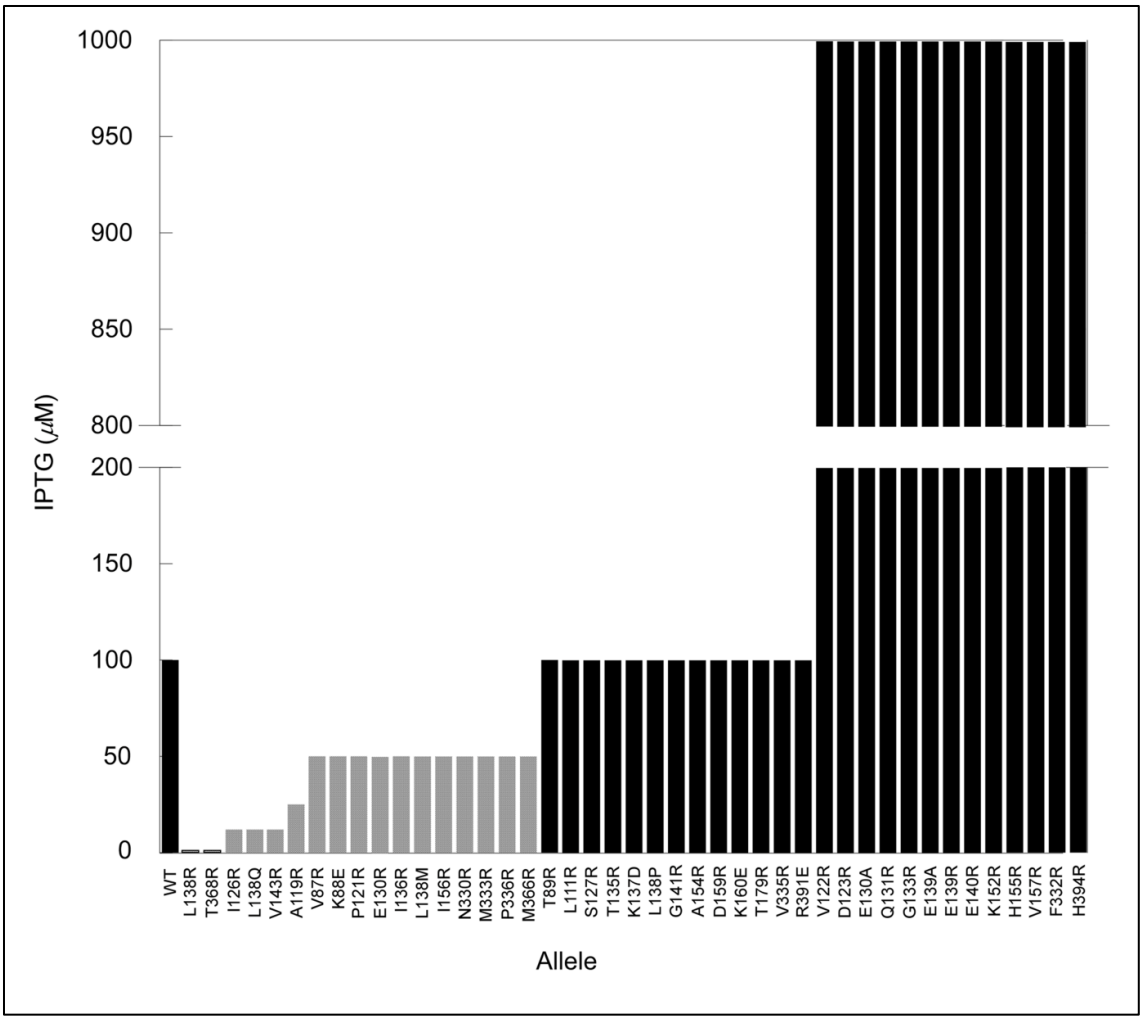

FIG. 53. MurA^{rat} alleles protect against A_2 at lower inducer concentrations. IPTG induction levels that afford cells expressing MurA* variants protection from Qβ infection are depicted by bars. *Rats* were considered any allele providing protection below the WT level of inducer concentration (100 μM) (grey bars). Alleles that protected at inducer concentration levels equivalent to or higher than WT are shown as black bars.

Identification of a MurA binding surface for A_2

To determine residues involved in the A_2 interaction with MurA, arginine-scanning mutagenesis of residues spatially surrounding the position of the original *rat* mutation, L138Q, was performed, with each allele assessed for its ability to confer resistance to Qβ. Each *murA** allele was expressed from a medium-copy plasmid over a range of inducer concentrations, and the level of inducer required to prevent Qβ plaque-formation was determined. Under these conditions, the WT *murA* allele provides protection at 100 μM IPTG (FIG. 53 and FIG. 47), whereas the L138Q *rat* allele required only 12.5 μM IPTG. Using these two benchmarks, the new Arg-substituted alleles, and a few alleles where parental Arg and Lys residues were changed to Glu or Asp, were assayed (FIG. 53).

The results showed that the mutant collection fell into several distinct classes. One class was indistinguishable from WT *murA*, in providing protection at 100 μM IPTG (FIG. 53) and were thus considered irrelevant to the A_2-MurA interaction. A second class required much higher levels of inducer than the parental allele. These variants accumulated normally *in vivo* (FIG. 54) but exhibited little to no enzymatic activity (data not shown), suggesting improper folding. A third group of alleles (Y84R, A134R, E337R and R340E) showed no protection at low inducer concentrations and were inviable when inducer was present at 1 mM IPTG (data not shown), presumably due to the accumulation of insoluble material to toxic levels.

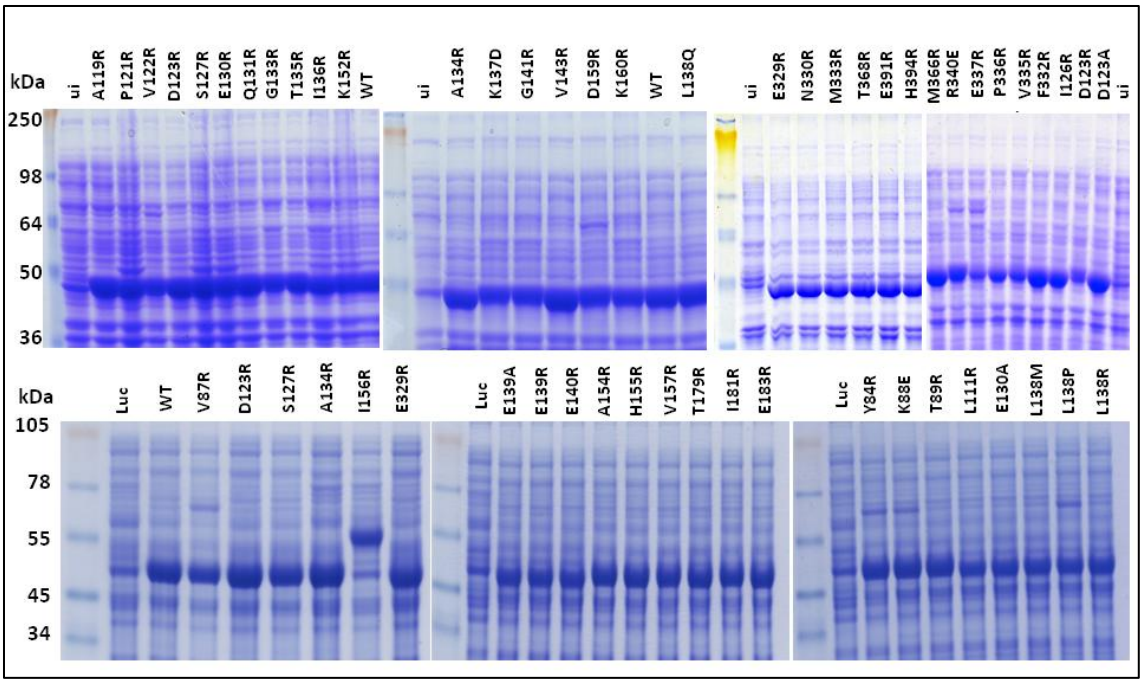

FIG. 54. MurA* variant expression test. TCA precipitated cells expressing MurA* variants were run on SDS-PAGE. Alleles are shown above lanes. Top panel reprinted with permission (89). Uninduced control (ui) and Luciferase control (Luc)

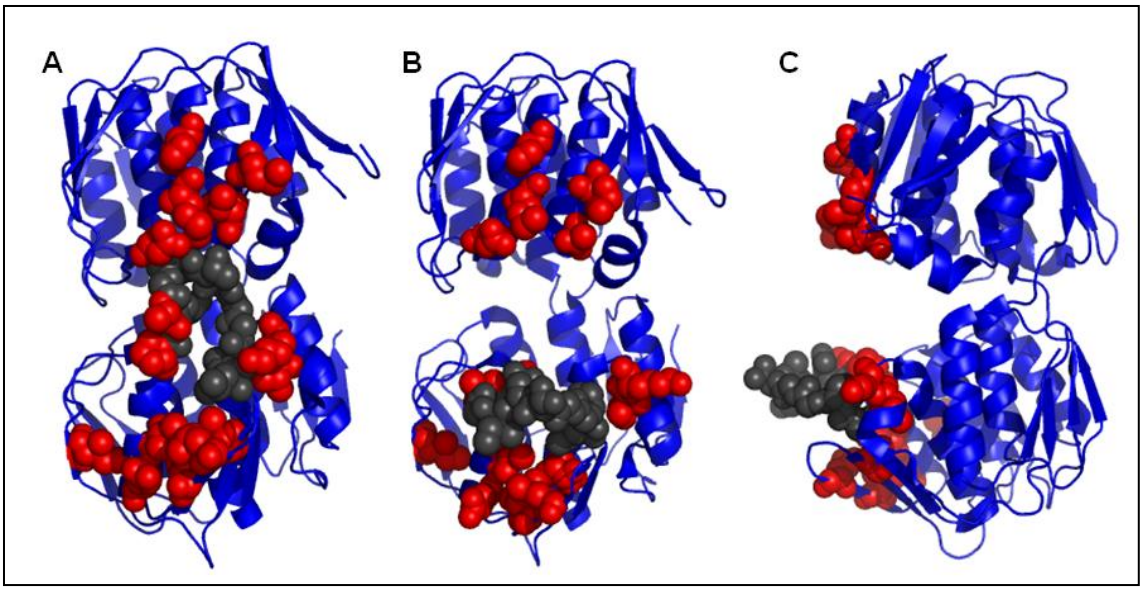

FIG. 55. Rat residues define a Qβ A_2 interaction surface important for inhibition of MurA. (A) Rat residues highlighted on the MurA UNAG-bound state (closed conformation, front view) (Han H., unpublished; PDB entry 3KQJ) defines a continuous surface for A_2 interaction. The structure of (B) MurA unliganded (front view) (131) and (C) MurA unliganded (side view) disrupts the A_2 interaction surface with the conformational change in the catalytic loop backbone. *Rat* residues depicted as red spheres. Residues of the catalytic loop are shown as grey spheres. Figures were generated using PyMOL (133).

A final class of variants were identified that provided resistance at inducer concentrations less than 100 μM were categorized as *rat* alleles; this class was comprised of 17 allelic substitutions at 15 codons (FIG. 53). When these mutations were mapped onto the UNAG-liganded MurA crystal structure, an apparent A_2-interaction surface could be visualized (FIG. 55 and FIG. 56). Residues important for A_2 inhibitory activity localize at sites surrounding the catalytic loop surface of the enzyme, including the catalytic domain, catalytic loop and C-terminal domain (FIG. 55A). Disruption of this interaction surface by conformational changes in backbone of the catalytic loop can be observed when the mutations are mapped on the unliganded MurA crystal structure (FIG. 55B-C). This genetic evidence supports the notion that a closed conformation of MurA is required for inhibition by A_2.

To determine whether the MurA* variants are not simply complementing the loss of the endogenous MurA activity, an additional D305A mutation was introduced to inactivate the enzyme (130). Under these conditions, protection from Qβ requires that each D305A variant titrates out the inhibitory A_2 produced during the infection cycle, thus sparing the endogenous parental MurA activity. However, if A_2 is unable to associate with the mutant protein because of disruption of the A_2-MurA binding interface, no protection should be observed. In this experiment, the D305A version of the parental MurA provides protection, whereas the D305A version of the canonical *rat*

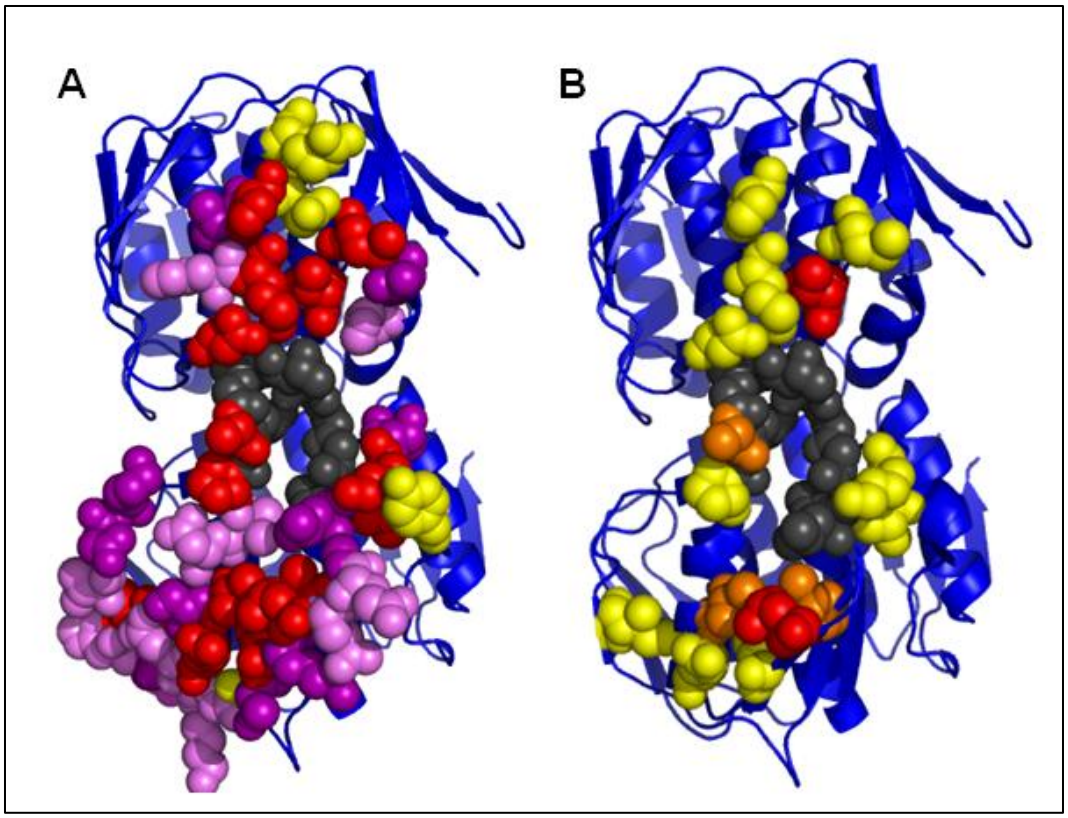

FIG. 56. MurA mutant surface maps. (A) MurA mutational data. Catalytic loop displayed as grey spheres. *Rats* are colored red. Residues providing protect ≥ WT are shown in purple (weaker WT induction phenotype is lighter purple). Residues that are non-functional are shown as yellow spheres. (B) Differentiation of *rat* residues. Basal level protection *rats* are displayed as red spheres. Medium protecting *rats* are colored orange. Low protecting *rats* are shown in yellow. All residues were mapped onto the MurA UNAG-bound state ("closed" conformation, front view) (Han H., unpublished; PDB entry 3KQJ). Figures were generated using PyMOL (133).

allele does not (TABLE 12). In this assay, all of the new *rat* alleles failed to provide protection against Qβ, supporting the notion that these alleles define an A_2 binding surface.

When the *rat* residues are differentiated based upon the level of inducer needed to provide protection, (FIG. 53 and FIG. 56) there appears to be a correlation with the position of the residue. The residues with the greatest effect are located at the base of the catalytic loop as well as the point where the loop contacts the C-terminal domain. This could suggest that dynamics of the catalytic loop play an important role in the inhibition process. However, when the catalytic activity of $MurA^{L138Q}$ was assayed, no difference was found between the mutant and WT (FIG. 48). From this perspective, it is more likely that these residues are important contacts for A_2 in preventing movement of the catalytic loop and blocking substrate accessibility once bound to MurA.

Discussion

A_2-MurA interaction: Model for inhibition

The combined results of the enzymatic assays with purified components, binding experiments using the MBP-A_2 fusion, and yeast-two-hybrid analysis demonstrate that the Qβ A_2 maturation protein inhibits MurA by forming a complex that requires no other host or viral protein. This finding is important for several reasons: (i) it demonstrates

TABLE 12. MurA*^{D305A} Qβ protection assay.

Protects	**Does not Protect**
No plaques	**Plaques**
WT (D305A)	L138Q
L111R	V87R
S127R	K88E
E130A	A119R
Q131R	P121R
G133R	V122R
T135R	I126R
K137D	E130R
L138P	I136R
E139A	L138M
E139R	L138R
E140R	V143R
G141R	I156R
K152R	N330R
H155R	F332R
V157R	M333R
D159R	P336R
K160R	M366R
V335R	T368R
R391R	H394R

that cellular lysis is not dependent on the participation of host components, (ii) it militates against the involvement of viral particles in lysis, and (iii) suggests that structural analysis of the A_2-MurA complex would be informative for identification of a potential peptide-based inhibitor of MurA.

Regarding the structure, the *in vivo* protection assays allowed us to characterize a potential A_2-MurA binding interface. These genetic results identified residues of importance that cover the catalytic loop/cleft and include residues that encompass both the catalytic and C-terminal domains of MurA. The fact that the surface spans the catalytic loop/cleft suggests that A_2 binds MurA in a closed conformation. This is supported by binding studies where we showed that A_2 preferentially associates with MurA in the UNAG singly-liganded state. Moreover, addition of a second substrate besides UNAG either severely reduces the ability of A_2 to complex with MurA or abrogates it altogether under the conditions assayed, suggesting that the catalytic cleft is in fact an important contact site for A_2. This binding interface of MurA is dominated by regions of negatively charged residues surrounding the rather hydrophobic catalytic loop (FIG. 57). A_2 seems to have hydrophobic character, based on its strong tendency to aggregate even when fused to highly soluble protein domains, and, in its role as the maturation protein, must be able to associate with the viral RNA. Thus the putative MurA binding surface we have described by genetic means has features consistent with binding properties of A_2. We hypothesize that the reason A_2 was able to acquire the role as lysis protein in the Qβ system, in addition to binding the F-pilus, protecting the viral

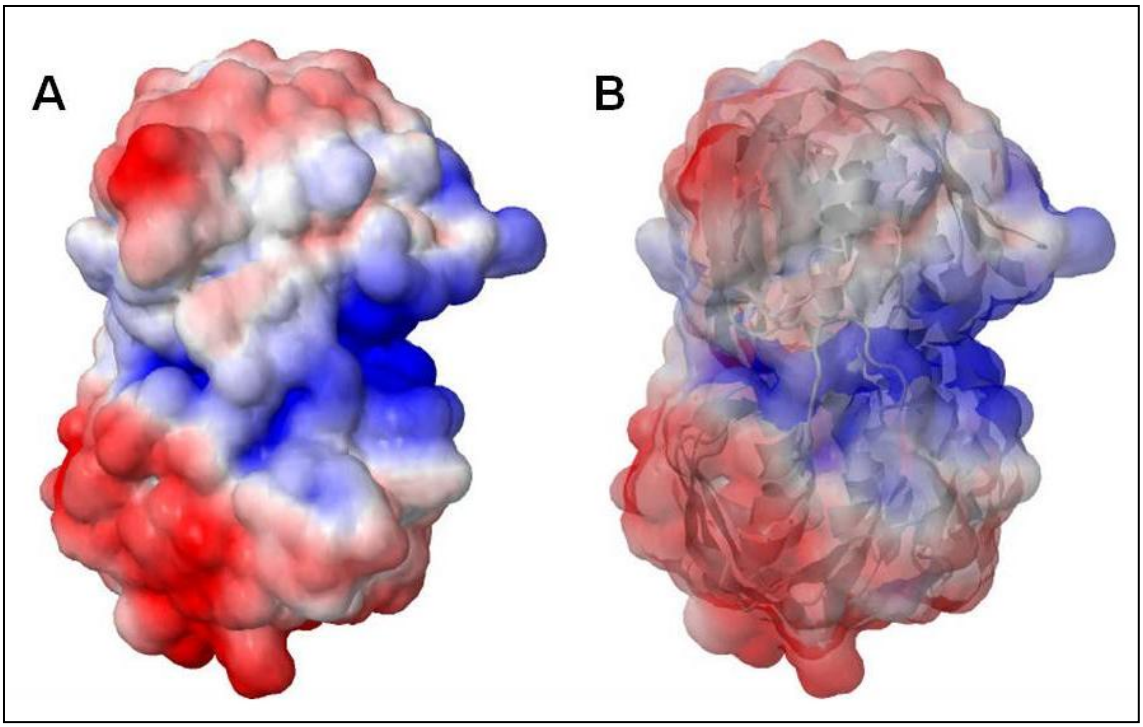

FIG. 57. The surface of MurA has negatively charged and hydrophobic characteristic. (Red) negatively charged residues, (blue) positively charged residues, and (white) hydrophobic residues. MurA tetrahedral intermediate (PDB entry 1A2N) (137) was used to generate figures with the online server: (http://kryptonite.nbcr.net/pdb2pqr/) (36). (A) surface view (B) transparent view

RNA, and assembly onto the virion capsid, was due to the hydrophobic and negatively charged nature of the MurA surface.

Proteins as inhibitors of enzymes

Protein inhibitors of enzymes involved in biosynthetic pathways are rare. One inhibitor, E, the lysis protein of ssDNA *Microviridae* phage ϕX174, targets MraY, an enzyme in the cell wall synthesis pathway (14). It was proposed that upon E binding to MraY a conformation change occurs in two transmembrane domains of MraY that in turn inactivates the enzyme irrespective of substrate binding (178). A second inhibitor, T7 Lysozyme, binds to the T7 RNA polymerase palm and finger sub-domains and locks the protein in a non-processive conformation (68, 176). This association is independent of substrate binding and does not occlude the active site thereby, inhibiting the protein indirectly by preventing a conformation change (176). A_2-MurA complex formation on the other hand, requires a conformational change of the catalytic loop produced from UNAG binding to MurA prior to A_2 association. The presence of an additional substrate molecule, such as PEP, prevents this A_2-MurA interaction (FIG. 49D, lanes 11-16). Therefore, A_2 must bind UNAG-liganded MurA over the catalytic loop/cleft and occlude PEP from the active site. Neither T7 lysozyme nor A_2 bind their targets directly in the active site. Perhaps evolving the ability to become a competitive inhibitor requires a protein to adopt a highly specific tertiary structure which limits the number of roles a

protein can fill. Thus, a form of mixed inhibition is better suited for these proteins to maintain additional functions apart from inhibition.

CHAPTER V

BACILLUS SUBTILIS MURAA STRUCTURE AND FUNCTION

Introduction

The Gram-negative bacterium *E. coli* contains only 1 UDP-*N*-acetylglucosamine 1-carboxyvinyltransferase, MurA, which is essential for catalysis of precursor subunits of peptidoglycan (97). In contrast, the Gram-positive bacterium *Bacillus subtilis* (*Bs*) has a homolog, MurAA, which shares 48% identity and 65% similarity to *E. coli* MurA (79). MurAA catalyzes the same step in the peptidoglycan synthesis pathway and complements an *E. coli murA* knockout (89). *Bs* also has paralog of MurAA, MurAB, which shares 50% identity and 70% similarity but is unable to complement the loss of MurAA. Perhaps MurAB serves to complement MurAA loss due to Clp-dependent proteolysis; the protein has a half-life for the protein of 55 minutes (79) and is degraded during stationary phase and MurAB assists in the transition into vegetative growth. Alternatively, the turn over number for MurAB catalysis could be too low to compensate for the cellular precursor subunit requirement.

Entry into stationary phase is regulated differently in *E. coli*. It was recently identified that the enzyme forms a dormant complex with UNAM (FIG. 6), the product of MurB, when the ratio of UNAM:UNAG is high (104). It is not until the intracellular concentration of UNAG increases and displaces the UNAM (179) that enzymatic is continued. The complex also forms a covalent adduct between the Cys in the catalytic loop and PEP, which may serve to prevent oxidation of the catalytic Cys.

It was previously determined that MurAA is able to complement the activity of *E. coli* MurA (89) and was used to aid in expression and purification of toxic A_2 (Chapter II). Even at low MurAA (plasmid with a pSC101* origin of replication) and high A_2 (T7 promoter) expression levels, cells were provided protection from lysis (FIG. 58). These data suggest that MurAA is a functional enzyme that can complement *E. coli* MurA activity but has intrinsic properties that afford it protection from A_2 inhibition. This chapter addresses whether an interaction between A_2 and MurAA occurs and characterizes the differences between MurAA and *E. coli* MurA that provides protection from A_2 inhibitory activity.

Material and Methods

Bacterial strains and growth conditions

The *Escherichia coli* strains used in this study: ER2738, HfrH, HfrH *lacZ::*Tn*5*, HfrH *murA::kan* pZE12-*murA*^{Bs}, and BL21(DE3) are previously described (Chapter II) (153). Standard molecular biology techniques were performed as described elsewhere (129). Bacterial growth conditions were described in Chapter II.

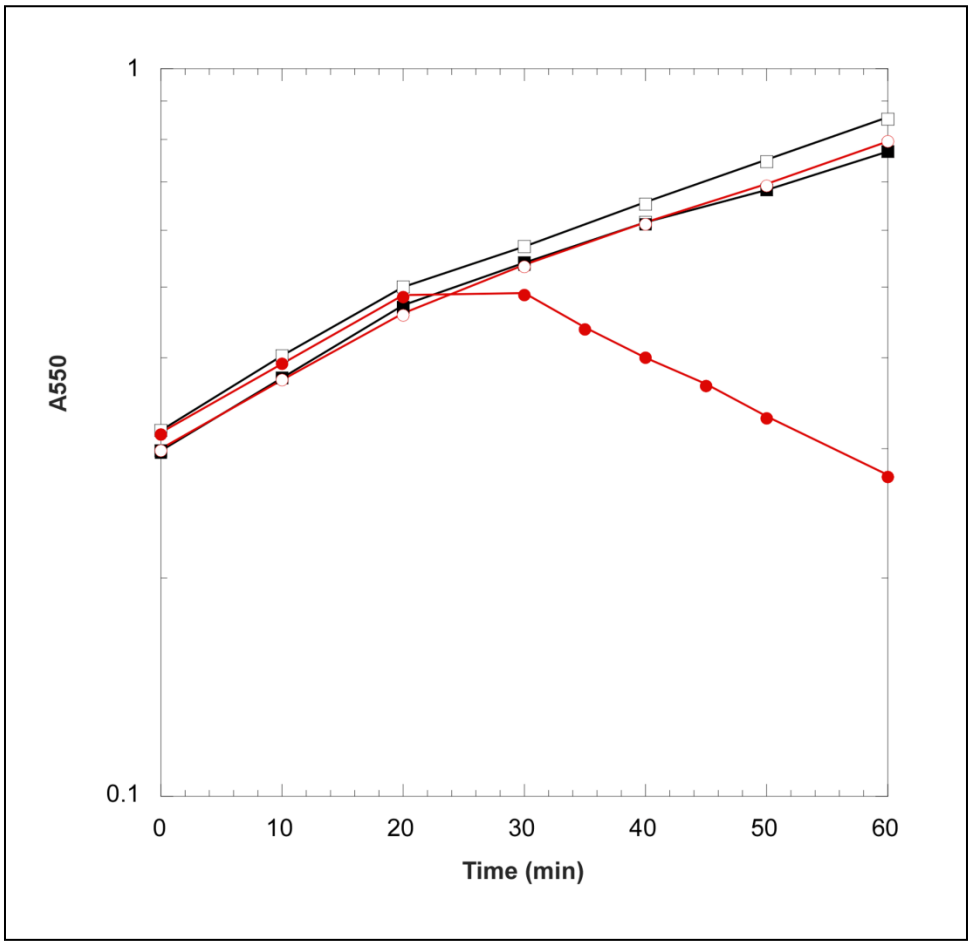

FIG. 58. The $A_2^{1\text{-}189}$ protein inhibits *Bs* MurAA. BL21(DE3) pLysS pZS*21-*murA*^{Bs} lysis was observed with: pET-*A*$_2$ (squares: uninduced, white; induced, black) or pET-*A*$_2$-*190* (circles: uninduced, white; induced, red). Samples were induced with 1 mM IPTG (final) at Time = 0'.

Plasmid construction

Plasmid construction for pZE12-*luc* was previously published (96). Construction of pZE12-A_2, pZE12-A_2*L28P*, pZE12-A_2*D52N*, pZE12-A_2*E125G*, pZE12-*murA*, and pZE12-$murA^{Bs}$ were described in Chapter II. pZE12-$murA^{Bs}$*D306A* was generated by site-directed mutagenesis with the following primers: BsMurA-D306A-For CCGGGCTTCCCGACTGCTATGCAGTCACAAATG and BsMurA-D306A-Rev CATTTGTGACTGCATAGCAGTCGGGAAGCCCGG. An oligo-histidine tag ($G_2H_6G_2$) was adjoined to the C-terminus of $murA^{Bs}$ by site-directed mutagenesis (V. Kuznetsov) for purification purposes. All *in vitro* analyses uses the oligo-histidine-tagged MurAA. pLysS and pET-11a were obtained from Novagen. pET-A_2 and pET-A_2-*190* were constructed previously (89). To generate pZS*21-$murA^{Bs}$, pZA31-$murA^{Bs}$ (89) was digested with AvrII and XhoI and ligated into pZS*24 (96), similarly digested. The pZS*21-$murA^{Bs}$ contains the $P_{Ltet0-1}$ promoter that is constitutively expressed in a $tetR^-$ background.

Protein expression and characterization

MurAA expression and purification were performed as described in Chapter II for *E. coli* MurA. MBP-A_2 was purified with amylose resin as described in Chapter III. Fusion cleavage and batch affinity fractionation experiments were performed as described previously (Chapter III and Chapter IV, respectively). SDS-PAGE and immune-blotting was performed as described (Chapter II) with the following

modifications: 1:3,000 dilution of α-His (Amersham) and 1;10,000 goat-anti-mouse 2° antibody (Pierce) were used for immune-blotting of MurAA.

To test activity of the MurAA, 2.5 X 10^8 cells were centrifuged at 18,000 xg for 5 min at 22°C. The cell pellet was resuspended in 1 ml LB with 0.5% toluene and incubated at 37°C for 5 minutes. Cells were pelleted as above, resuspended in 1 ml of buffer (0.1 M Tris-HCl [pH 8], 0.5% toluene) and incubated as stated above. Cells were pelleted a third time and resuspended in 100 μl of buffer (0.1 M Tris-HCl [pH 8]). Five μl of toluenized cells was assayed for MurA activity as described previously (97).

Phage purification and plating

Purification of cell-free phage lysate and plating methods were performed as previously described (Chapter II).

Results and Discussion

MurAA^{D306A} mutation does not protect in bioassay

An interaction between MurA and A_2 was previously demonstrated with plasmid induced *E. coli* MurA^{D305A} during a Qβ infection (see Chapter IV and FIG. 49D). The D305A mutant is catalytically inactive and affords the cell protection from lysis by binding and titrating A_2. To determine whether MurAA interacts with A_2 *in vivo*, the

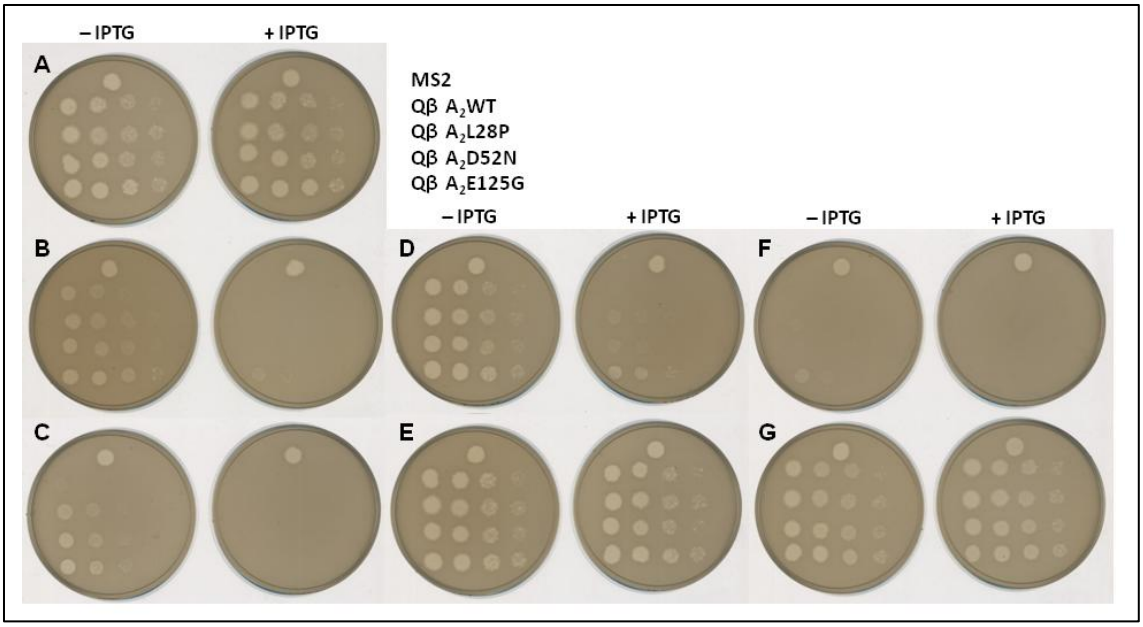

FIG. 59. *Bs* MurAA^{D306A} does not protect during a Qβ infection. Qβ phage was plated on HfrH *lacZ::*Tn*5* lawn harboring the following plasmids: (A) pZE12-*luc*, (B) pZE12-*murA*, (C) pZE12-*murA*^{L138Q}, (D) pZE12-*murA*^{D305A}, (E) pZE12-*murA*^{L138Q,D305A}, (F) pZE12-*murAA*, and (G) pZE12-*murAA*^{D306A}. Lawns were prepared with and without 1 mM of IPTG for protein expression.

equivalent to the D305A (D306A) change was incorporated into the sequence of MurAA and the Qβ plating bioassay was performed as in Chapter IV. The results were unambiguous. At uninduced, basal level of expression, the catalytically active MurAA, but not the catalytically inactive MurAA^{D306A}, provided protection from Qβ lysis (FIG. 59). Moreover, even induction of the mutant did not provide protect from Qβ plating (FIG. 59G). This plating phenotype is similar to that seen by *E. coli* MurA^{L138Q} (FIG. 59C & E) where incorporation of the D305A double mutation does not protect the

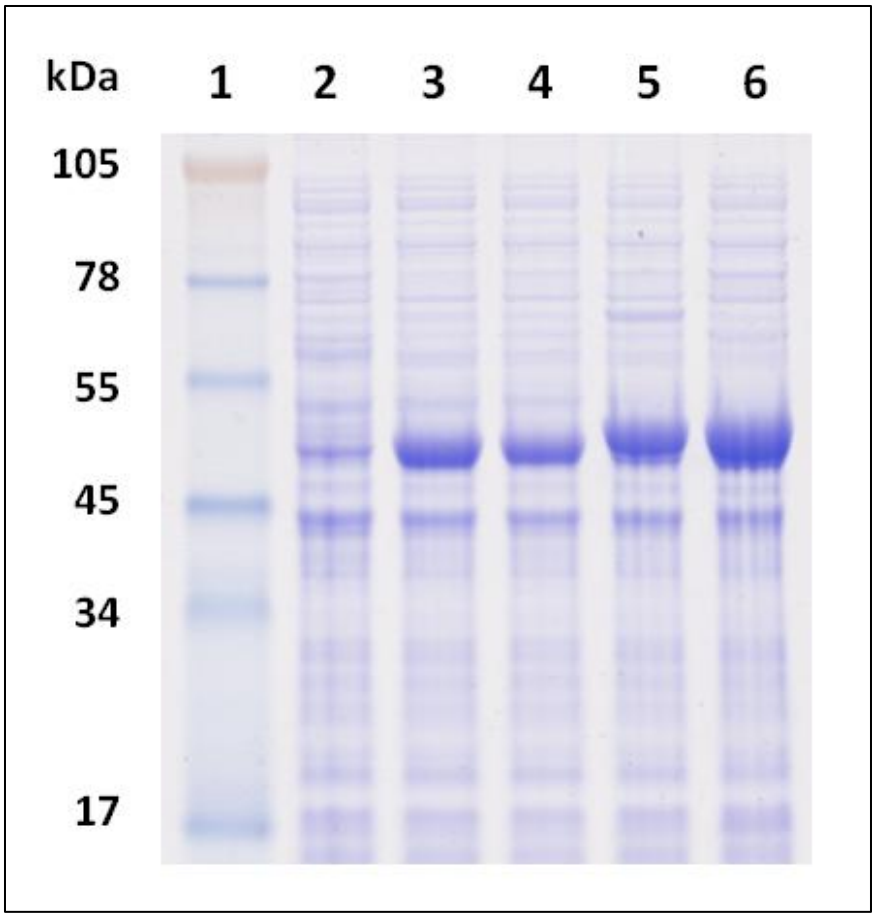

FIG. 60. *Bs* MurAA^{D306A} is expressed. Samples were resolved on SDS-PAGE. *E. coli* MurA has an apparent molecular mass of 50 kDa and MurAA, 52 kDa. Lanes: (1) Molecular mass standard, (2) Luciferase control, (3) *E. coli* MurA, (4) *E. coli* MurA^{D305A}, (5) MurAA, and (6) MurAA^{D306A}

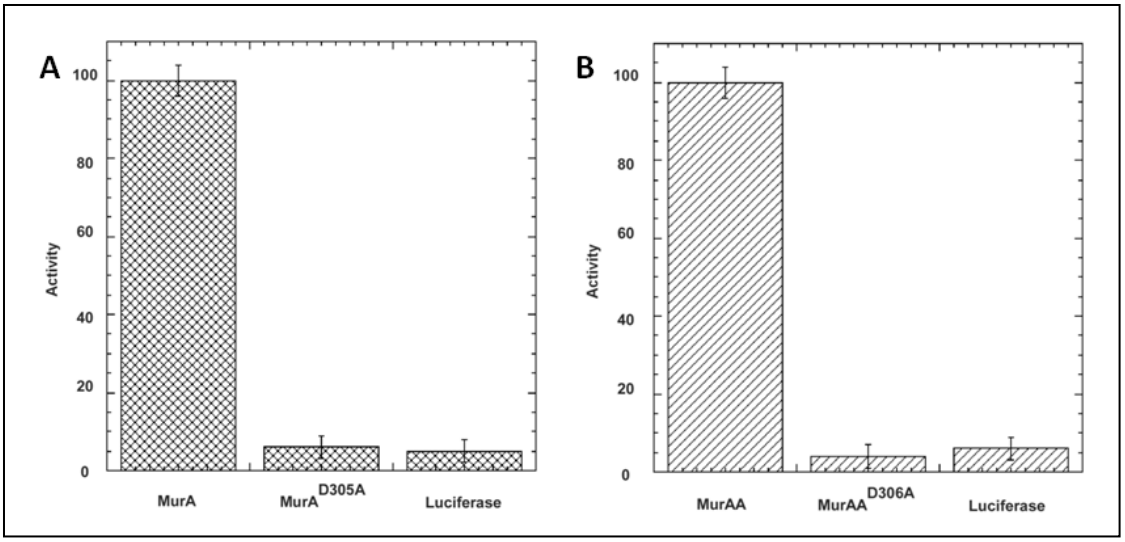

FIG. 61. *Bs* MurAA^{D306A} mutant is nonfunctional. *E. coli* toluenized cells expressing MurA^{D305A} have no activity compared to cells expressing MurA and the Luciferase control (panel A). Cells expressing MurAA^{D306A} similarly do not have any activity (panel B).

cells against a Qβ infection, suggesting that this mutation prevents A_2 from associating.

The phenotype could also be a result from expression of misfolded protein, such that A_2 binds the endogenous MurA and induces cellular lysis. To address this possibility, protein activity, accumulation, and solubility were assessed. Both the MurA^{D305A} and the MurAA^{D306A} mutants accumulated to similar levels as their prospective WT proteins (FIG. 60), and as expected, neither had detectable activity (FIG. 61). However, when the solubility of the proteins were analyzed the MurAA mutant showed substantial precipitation of the protein, with ~ 70% in the pellet fraction (FIG. 62); whereas, the *E. coli* mutant had about 50% in the pellet (130). Binding of

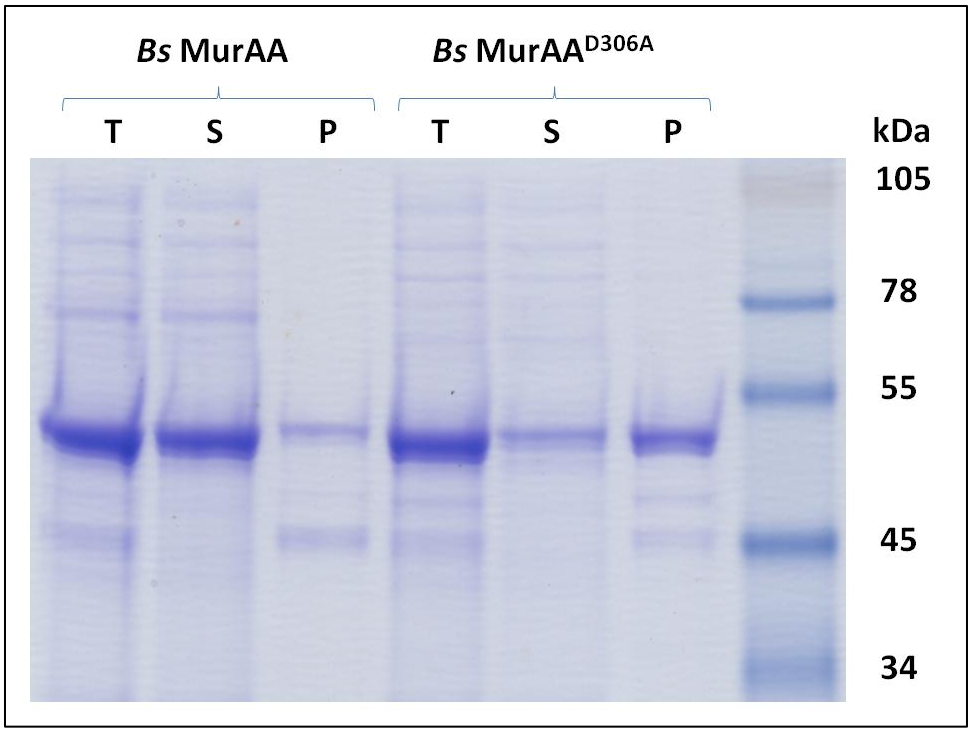

FIG. 62. *Bs* MurAA^{D306A} has reduced solubility. Cellular lysate prior to centrifugation, Total (T), and fractions after centrifugation, Supernatant (S) and Pellet (P), were resolved on SDS-PAGE. MurAA has an apparent molecular mass of 52 kDa.

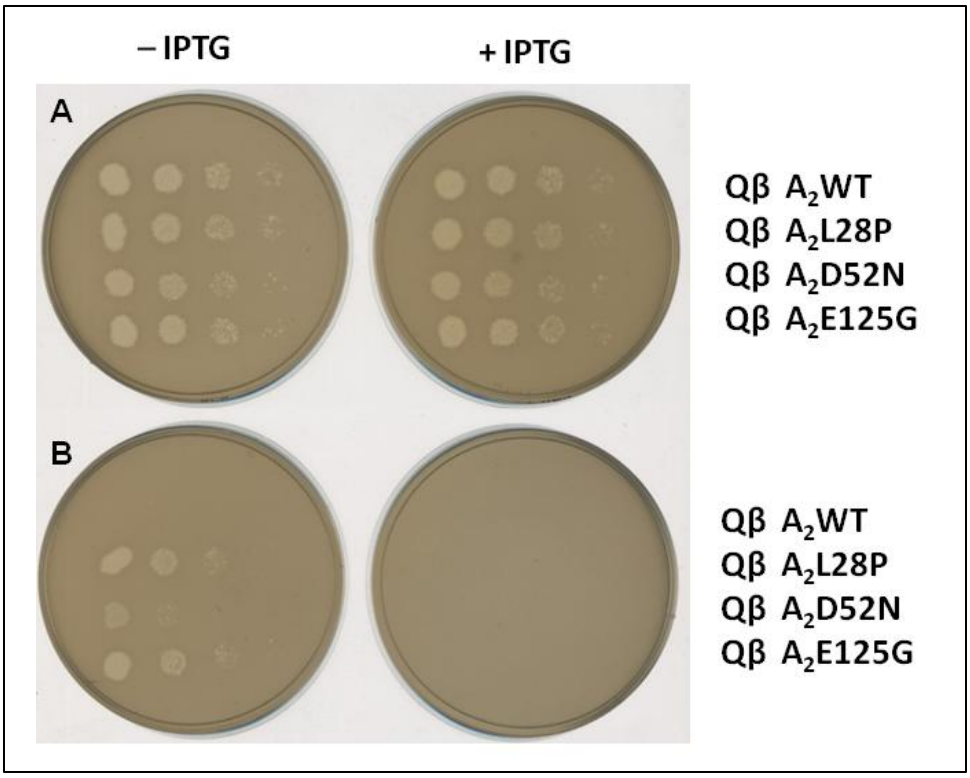

FIG. 63. MurAA protects during a Qβ infection. (A) HfrH overlays and (B) HfrH *murA::kan* pZE12-*murA*^{Bs} overlays: without (left) and with (right) 1 mM IPTG inducer, spotted with serial dilutions of phage, labeled above.

purified MurA^{D05A} to A_2 was previously demonstrated (Chapter IV) even though a high distribution of insoluble protein is obtained in the pellet fraction during purification. Therefore, the 30% of soluble protein could be properly folded, but the only measure for proper folding of the inactive enzyme is the ability to bind A_2. Since the ability of MurAA to bind A_2 is not known, we cannot determine from these experiments whether the mutant is misfolded and further characterization was abandoned.

MurAA is sensitive to Qβ A_2^{por} but not Qβ

To further address whether MurAA is able to bind A_2 *in vivo*, Q*β* was plated on a lawn of *E. coli* cells deleted for the chromosomal copy of the *murA* gene and carrying a complementing *murAA* gene on a plasmid. Even the basal level of MurAA was able to inhibit Q*β* plating (FIG. 63B) suggesting that A_2 does not inhibit MurAA. However, Q*β* A_2^{por} mutants exhibited low but detectable efficiencies of plating on these lawns (FIG. 63A). The *por* phenotype is due, at least in part, to an upregulation of A_2 expression during infection (Chapter II, FIG. 14). Thus, these plating results indicate that A_2 can bind and inhibit MurAA if expressed at enhanced levels. This interpretation is consistent with the ability of A_2^{por} alleles to support plaque formation on the *E. coli* ^{rat} mutants carrying the original L138Q change in MurA.

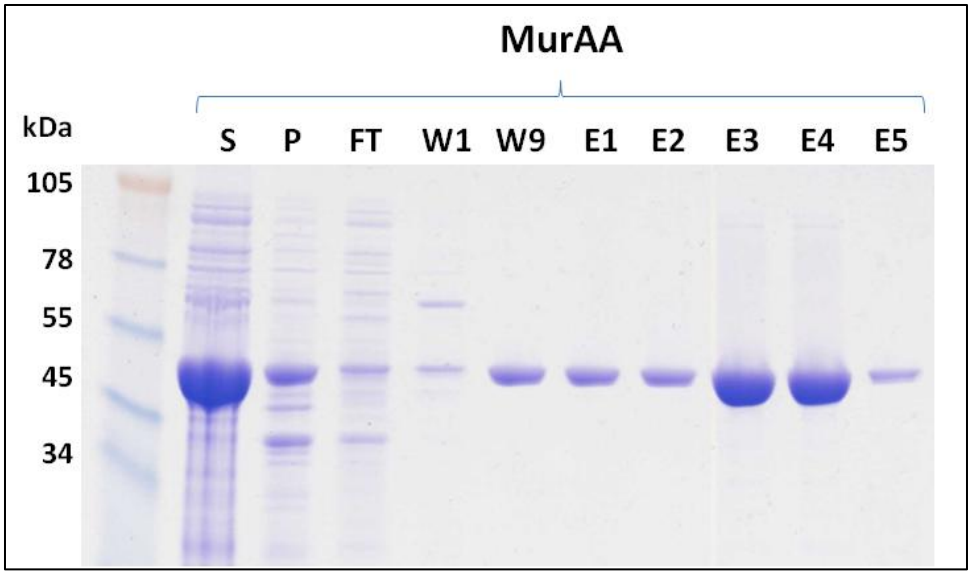

FIG. 64. Purification of MurAA. Purity of MurAA was verified by resolving on SDS-PAGE. Lanes: (S) Supernatant of clarified lysate, (P) Pellet of clarified lysate, (FT) Column flow-through, (W) Column washes, and (E) Eluate fractions

MurAA binding by A_2 cannot be detected in vitro

Binding and fusion-cleavage studies with a purified fusion of A_2, MBP-A_2, allowed characterization of the *E. coli* MurA-A_2 interaction (see Chapter IV). Therefore, these studies were repeated with MBP-A_2 and purified MurAA (FIG. 64). Batch affinity fractionation experiments revealed that MurAA did not bind to A_2 under any condition tested (FIG. 65); however, there is a high background from MBP-A_2 degradation products, at least in part because both MBP-A_2 and MurAA have a His-tag,

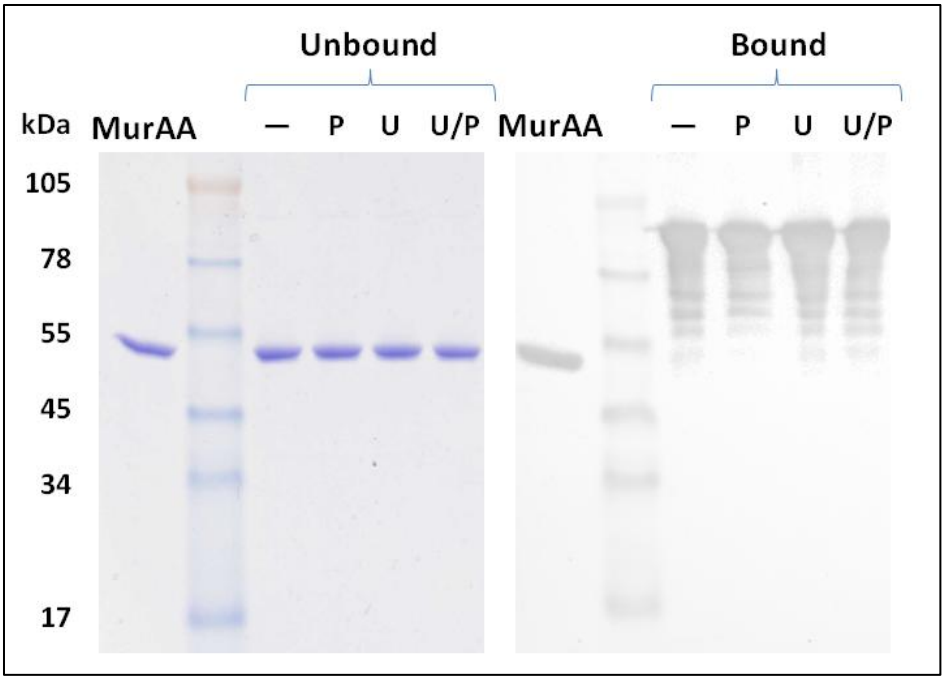

FIG. 65. Batch affinity fractionation of MBP-A_2 and MurAA. Unbound fractions were resolved on SDS-PAGE and Bound fractions were immune-blotted with an α-His antibody. MurAA runs at about 52 kDa and MBP-A_2 at approximately 98 kDa. Apparent protein laddering in Bound fractions is from MBP-A_2 degradation products.

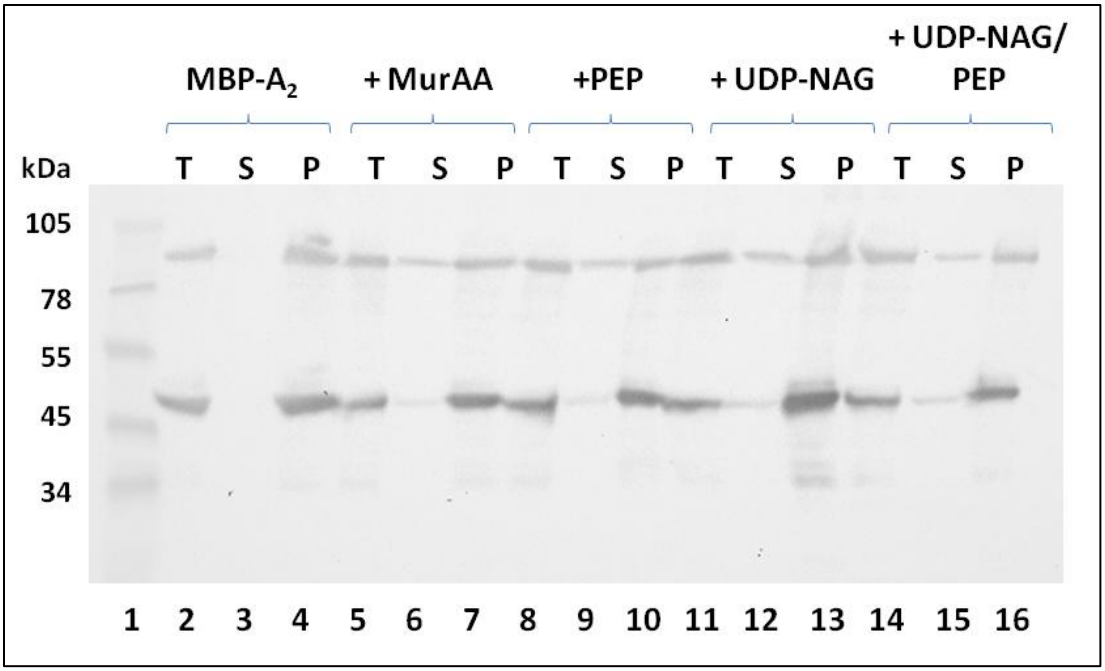

FIG. 66. Fusion cleavage analysis of MBP-A_2 with MurAA. Fractions of MBP-A_2 cleavage prior to centrifugation, Total (T), or after centrifugation, Supernatant (S) and Pellet (P), were immune-blotted with an α-A_2 antibody. Uncleaved MBP-A_2 has an apparent molecular mass of 98 kDa and cleaved A_2, ~ 50 kDa.

the epitope used for detection. Less ambiguous results were obtained with the fusion cleavage protocol. For all MurAA-liganded states tested, A_2 appears to be predominantly in the pellet fraction, with only a small fraction in the supernatant fraction (FIG. 66, lanes 5-16). This was not observed with the MBP-A_2-only control (FIG. 66, lane 2-4), which showed all of the A_2 protein in the insoluble fraction. The results were reminiscent of the results with the *E. coli* MurA-UNAG/fosfomycin- complex (FIG. 49) which exhibited reduced binding compared to the UNAG only state, presumably due to small differences in the loop structure (FIG. 50). One possibility to explain these results is that the protein was co-purified with UNAM and PEP bound, which induces a closed conformation of MurAA (87) (FIG. 67). A concentration of 1 mM UNAG can displace UNAM (179), and when included in the reactions there should be differential binding of A_2 in the 2 reactions that contained UNAG, as seen previously with *E. coli* MurA (see Chapter IV, FIG. 49); however, this was not observed for any of the samples. It is more likely that MurAA exhibits weak binding to A_2 that is not dependent on a conformational change for association.

A_2 truncation effects on MurAA inhibition

Previously it was demonstrated that expression of MurAA during a Qβ infection protects against cellular lysis (89). This protection was utilized for co-expression with A_2 fusion constructs to counteract the toxic effect of the lysis protein (Chapter III).

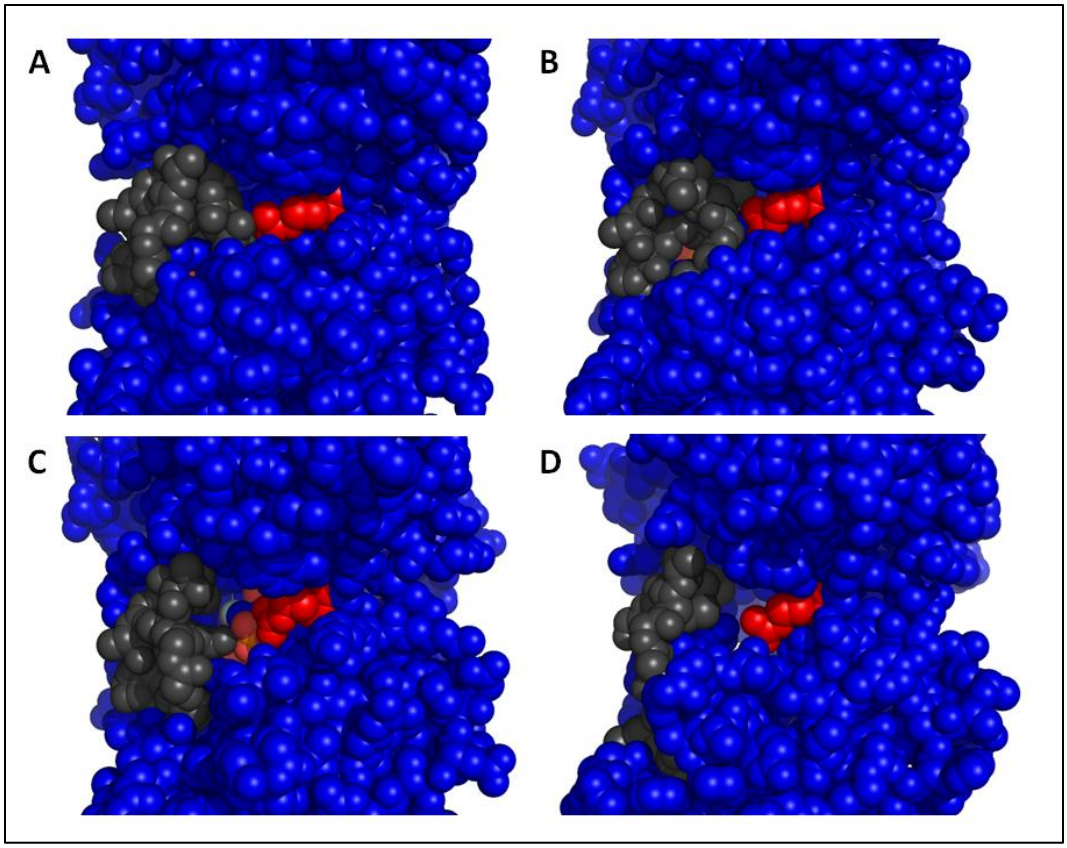

FIG. 67. Active site comparison of *E. coli* MurA and *Bs* MurAA. (A) *Enterobacter cloacae* MurA bound with UNAM and PEP (PDB entry 3SU9), (B) *E. coli* MurA bound with UNAG (PDB entry 3KQJ), (C) *E. coli* MurA tetrahedral intermediate (PDB entry 1A2N), and (D) MurAA bound with UNAM (V. Kuznetsov, unpublished). Catalytic loop displayed as grey spheres, Arg 397 (*E. coli*) and Arg 398 (*Bs*) displayed as red spheres, and substrates shown as spheres and colored according to elements (*E. coli* MurA, not displayed for MurAA).

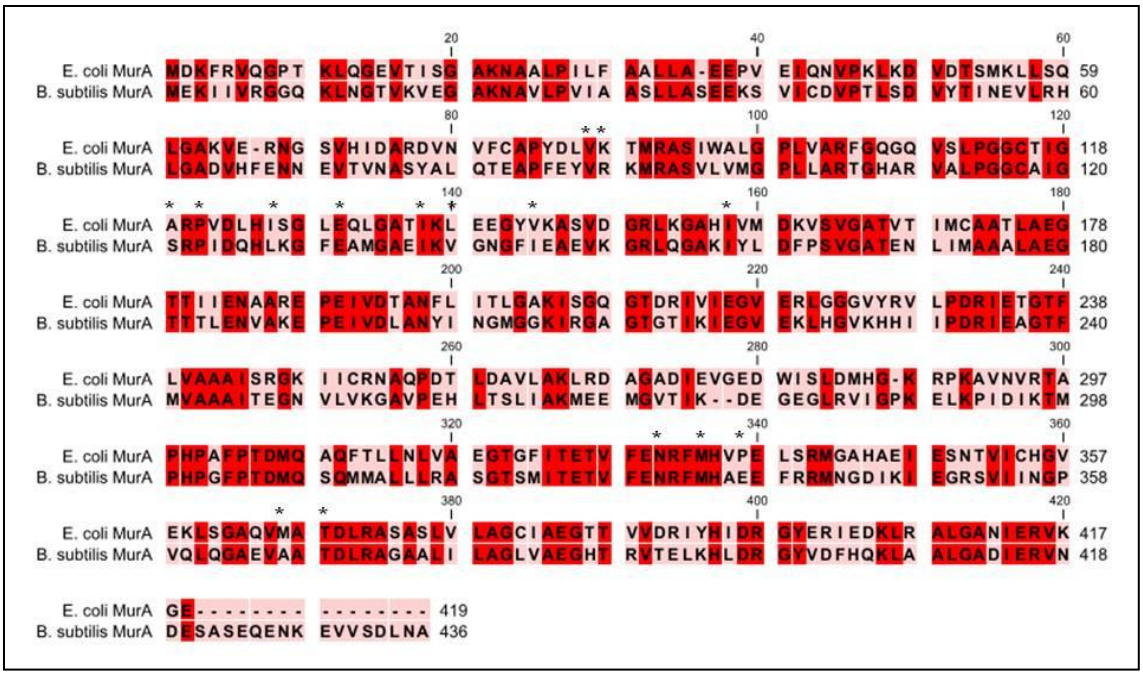

FIG. 68. *E. coli* MurA and *Bs* MurAA alignment. Residues important for an A_2 interaction are labeled with asterisks. Conserved residues (red) and non-conserved and semi-conserved residues (pink)

However, analysis of MurAA co-expression with the A_2^{1-189} truncation protein revealed that the protein is still lytic in cells that are expressing low levels of MurAA (FIG. 58). This lytic activity was not observed with the full length A_2. Perhaps the tertiary structure of the full length A_2 limits the ability of the protein to complex with MurAA. This notion is supported by the fact that two other truncation proteins, A_2^{1-338} and A_2^{1-283} (FIG. 45) are, although stable, soluble proteins *in vivo*, are both non-lytic, indicating that the C-terminal segment of A_2 contains a domain that can interfere with MurA binding.

Analysis of the MurAA surface

The *Alloleviviridae* exclusively infect Gram-negative hosts, so it is not surprising that A_2 is not able to bind and inhibit MurAA. An alignment of the MurAA and *E. coli* MurA primary structures showed 48% identity (FIG. 68). Comparison of the residues that were determined to be important in the *E. coli* MurA interaction with A_2 to those of MurAA revealed that 6 out of the 15 residues were not conserved; out of the 6, 3 were residues that were semi-conserved. The position of the non-conserved residues was at the base of the loop and at positions close to where the loop contacts the C-terminal domain (FIG. 69). These positions were determined to be important contacts for A_2 to associate with MurA and inhibit the activity of the enzyme (Chapter IV). Analysis of the residues positions revealed that 2 of the 3 (E337 and A367) that in positions on *E. coli* MurA (336 and 368) had the weakest protection phenotype against a Qβ infection (see Chapter IV FIG. 53). The third difference is a Ser substitution at position 121,

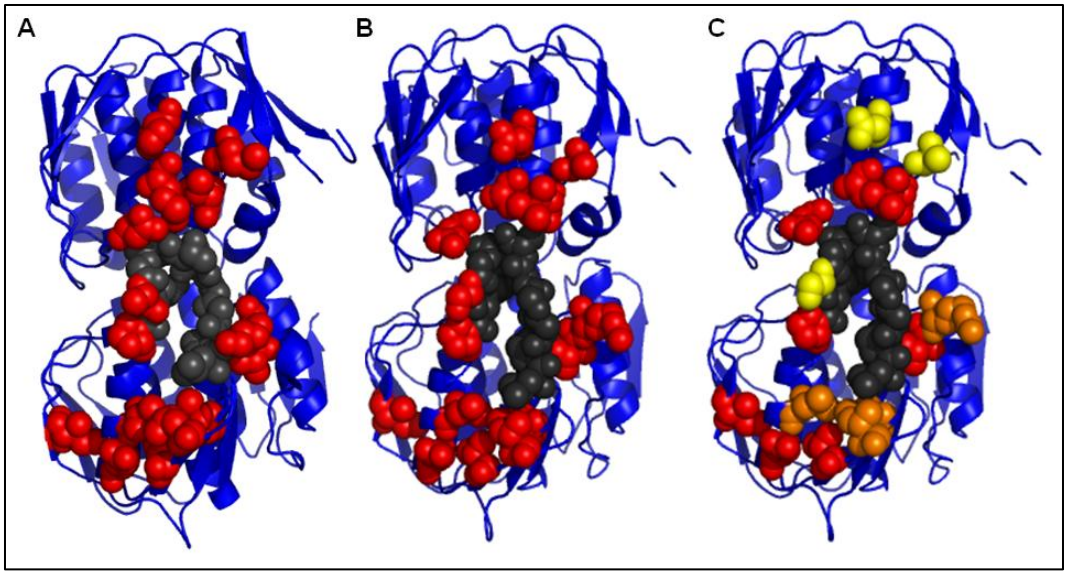

FIG. 69. Comparison of A_2 interaction surface between *E. coli* MurA and *Bs* MurAA. (A) *E. coli* MurA (PDB entry 3KQJ) and (B) MurAA (V. Kuznetsov, unpublished), and Residues of the A_2 interaction surface are depicted as red spheres. The catalytic loop is shown as grey spheres. (C) MurAA with differentiation of residues based on conservation: red (conserved), orange (semi-conserved), and yellow (non-conserved).

which aligns to *E. coli* MurA position 119; this position provided better protection against a Qβ infection than positions 336 and 368 of *E. coli* MurA. Any 3 of these substitutions would likely be sufficient to provide MurAA protection from A_2 inhibition. It would be interesting to see if conversion of these residues to the corresponding residues in *E. coli* MurA would confer some ability for A_2 to inhibit the enzyme. An additional non-conserved residue at position 118, an adjacent residue to the catalytic Cys within the loop, which was not subjected to extensive mutagenesis in *E. coli* MurA, could also potentially affect the ability of A_2 to bind MurAA (FIG. 68).

Another factor that influences the ability of A_2 to bind and inhibit MurA is the conformation of the catalytic loop. It was determined in the previous chapter that small conformational difference in the loop associated with differential substrate binding affected the degree of A_2 association with MurA. Comparison of the catalytic clefts/loops of UNAM-liganded MurAA and several MurA structures that are in a closed conformation revealed that UNAM-liganded MurAA has a more solvent-accessible active site, similar to the tetrahedral intermediate of *E. coli* MurA (FIG. 67). It was previously shown that A_2 binds the UNAG-liganded state of MurA and not the tetrahedral intermediate (Chapter IV, FIG. 49). Until structural data for other liganded states of MurAA is available, loop conformation cannot be considered as a major factor to explain why A_2 has a reduced affinity for MurAA.

Analysis of the electrostatic surface density of the two proteins revealed a large difference in the C-terminal domain just above the catalytic loop. MurAA had a

considerable region of negative charge in contrast to MurA, which had more hydrophobic characteristic (FIG. 70). The residues on the C-terminal domain contacted by the loop were determined to be important for A_2 inhibition of MurA (Chapter IV, FIG. 56B). Unfortunately, a more complete analysis of the A_2 interaction surface with *E. coli* MurA in this region could not be performed, because mutations in this region inactivate the enzyme. Therefore, interaction with A_2 in this domain cannot be excluded. Nevertheless, the striking difference in the charge density of this region in MurAA compared to *E. coli* MurA, must be considered as a dominant factor in the lack of the affinity of A_2 for MurAA.

Discussion

In vivo titration assays and *in vitro* binding studies have demonstrated that, despite the strong similarity between the crystal structures of MurA and MurAA, A_2 binding and/or inhibition of MurAA is severely compromised The defect in binding to MurAA could be due to several differences in the MurA residues shown to be important for A_2 binding, to differences in surface charge, or in the structure of the catalytic loop in this area Nevertheless, the Qβ A_2^{por} mutants can make plaques at a low but detectable efficiency on an *E. coli* host with *murAA* substituted for *murA*. It is unclear whether this is due to the increased level of A_2 in *por* infections or to the particular aa substitutions

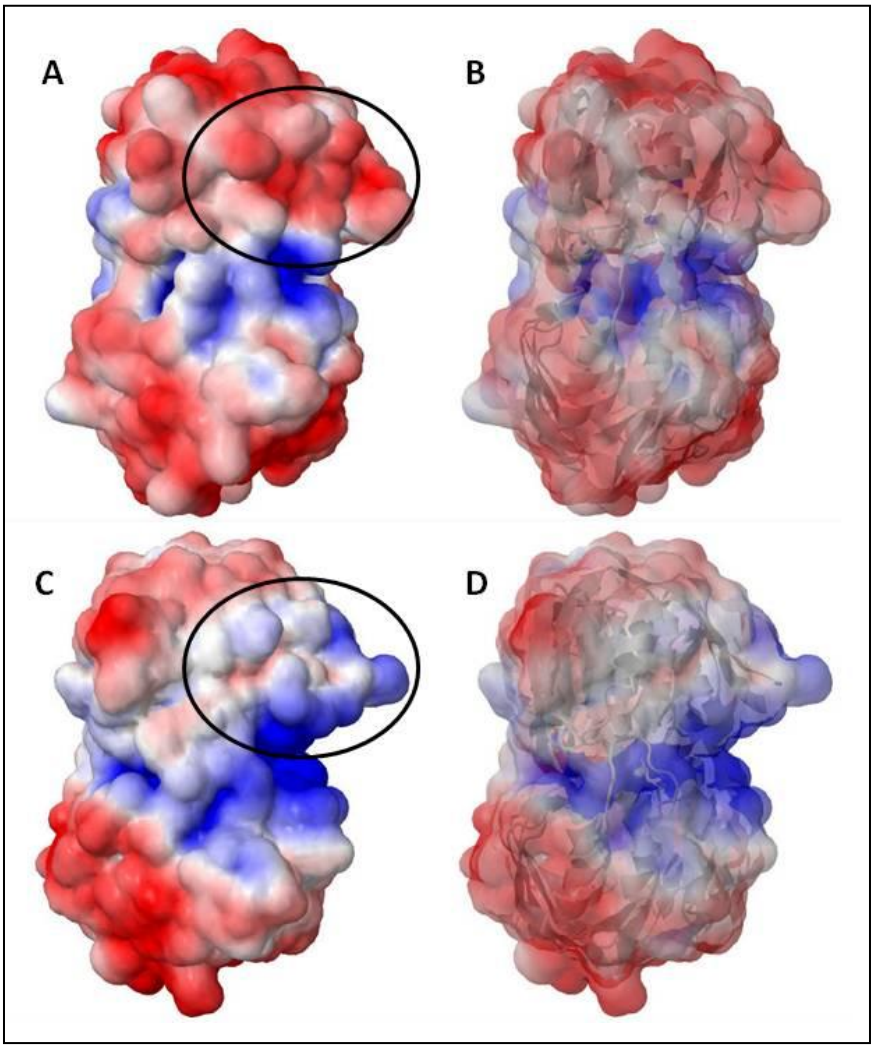

FIG. 70. Electrostatic density map comparison of *Bs* MurAA and *E. coli* MurA. Electrostatic density maps were generated for *Bs* MurAA liganded with UNAM (V. Kuznetsov, unpublished) (A-B) and *E. coli* MurA tetrahedral intermediate (PDB entry 1A2N) (C-D). Region of large charge difference on the C-terminal domain is highlighted by black oval. Figures generated with the online server: (http://kryptonite.nbcr.net/pdb2pqr/) (36).

in the *por* alleles, or both. A plasmid-based expression system for both A_2 and MurAA with the endogenous *E. coli murA* knocked out should be able to rule out the effects of A_2^{por} over-expression by normalizing the amount of protein expressed. Binding studies with A_2^{por} fusion proteins could also provide a way of determining the effect from the aa substitutions.

CHAPTER VI

SUMMARY AND FUTURE DIRECTIONS

Overview

Since the extensive studies on ssRNA phage replication and gene expression during the 1960s, the infection cycle of these paradigm phages has attracted little attention. In particular, since the identification of A_2 as the lysis protein in 1983 (72, 169), there has been nothing published regarding the lytic mechanism except the identification of MurA as the host protein targeted by A_2 (16). This dissertation has made advancements in this area by characterizing the regulation of A_2 expression an activity during an infection cycle and the mechanism of MurA inhibition through several biochemical and genetic studies.

Model for A_2 Regulation During a Qβ Infection

We have demonstrated that association of particle-mounted A_2 with MurA *in vitro* resulted in virion inactivation with a concomitant release of viral RNA from the particles (FIG. 9). This finding ruled out virion-associated A_2 as the inhibitory form of A_2. Moreover, titration experiments of plasmid-induced A_2 revealed that the amount of A_2 required to induce lysis is roughly equivalent to the cellular MurA levels (TABLE 6), which suggests that once the amount of A_2 accumulates to an equimolar amount the cell is committed to lysis. Quantitative analysis of the infection cycle showed that A_2 accumulates to equivalent levels of MurA by 30 minutes after infection (TABLE 7),

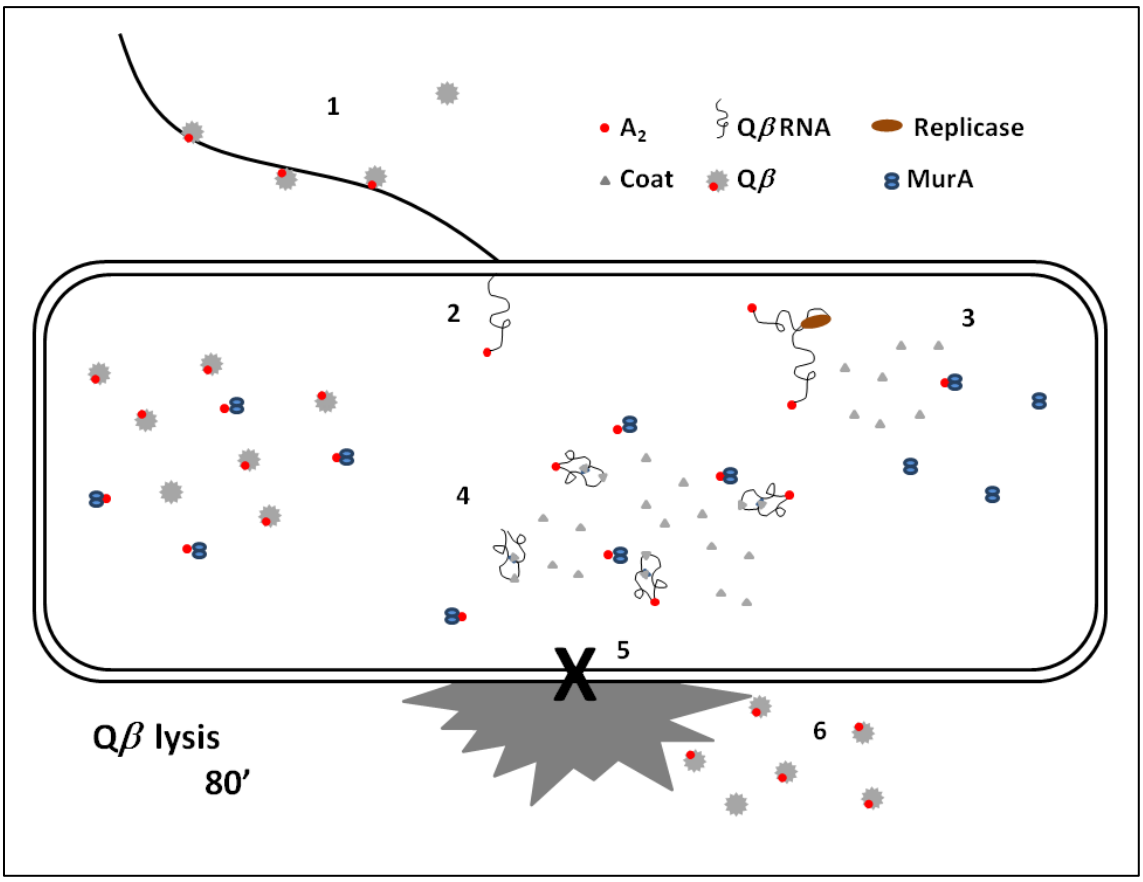

FIG. 71. Model for Qβ lysis. The Qβ infection cycle consists of several stages: (1) adsorption to the F-pilus, (2) injection of the A_2 and the viral RNA into the host cell, (3) synthesis of precursors for progeny virion particles, (4) morphogenesis of particles and inhibition of MurA by A_2, (5) cell wall synthesis inhibition ~60' after infection, and (6) release of particles at 80'.

but lysis is not observed for another 50 minutes (FIG. 14). The delay in lysis was considered to be provided by an unknown "buffer" for A_2, i.e., a component that binds A_2 and protects the endogenous MurA. Insight into this buffering capacity was obtained by analysis of $Q\beta^{por}$ mutant infections, which revealed an upregulation in the amount of A_2 earlier in infection, resulting in an earlier lysis phenotype (FIG. 14). These data are interpreted as showing the saturation of the A_2 buffering capacity of the system early in infection. Presumably the buffering agent is a viral component that accumulates simultaneously with A_2. A clue about the identity of the buffering agent was obtained from the observation that ejected RNA from virions protects particles from inactivation by MurA, which suggests that A_2 is occluded from MurA association by viral RNA.

We have proposed a model (FIG. 71) in which newly translated A_2 binds to the viral RNA and by doing so, is sequestered from association with MurA. Lysis timing in this model is linked to the level of free A_2 in the system. Accumulation of free A_2 would occur by one or both of two means: (i) displacement of the RNA-bound A_2 as viral RNA is packaged during morphogenesis or (ii) accumulation of free A_2 that exceeds the available binding sites of viral RNA during replication. We cannot distinguish rigorously between the two models with the techniques used in this work, but analysis of the $Q\beta^{por}$ data supports the latter model (FIG. 72). In $Q\beta^{por}$ infections the point at which MurA is inhibited is shortly after translation of A_2 begins, ~ 10-15 minutes after injection since there is a 20 minute delay from the point at which MurA is inhibited to

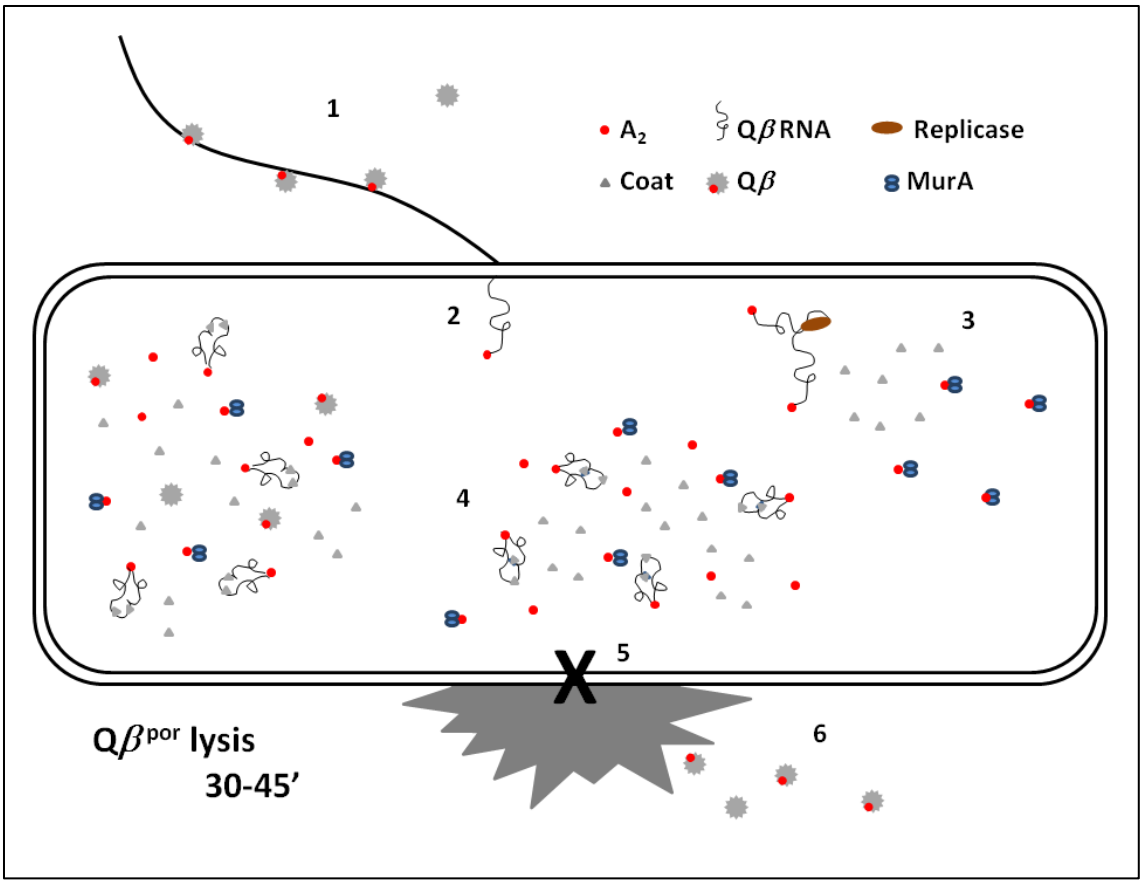

FIG. 72. Model for Qβ^{por} lysis. The Qβ^{por} infection cycle consists of several stages: (1) adsorption to the F-pilus, (2) injection of A_2 and the viral RNA into the host cell, (3) synthesis of precursors for progeny virion particles and inhibition of MurA by A_2, (4) morphogenesis of particles, (5) cell wall synthesis inhibition ~10-15' after infection, and (6) release of particles at 30-45'.

cellular lysis (16). This is when replication begins and is too early in the infection for sufficient particle accumulation to account for the hundreds of molecules needed for MurA inhibition. We have interpreted the early lysis phenotype of the *por* mutants as being due to over-production of A_2, due to disruption of inhibitory RNA structures that occlude the ribosome binding site of the A_2 gene. Nevertheless, it has to be noted that only non-synonymous mutations were obtained in the selection for the *por* mutants (TABLE 8). If upregulation in the translational rate of the A_2 gene was the only requirement for the plating of $Q\beta^{por}$ on the *rat* strain, then synonymous mutants that disrupt the secondary structures should also have been isolated. It is thus conceivable that the missense change associated with each *por* allele, and the consequent potential alteration of binding to MurA, also contributes to the *por* phenotype. It is also possible that the mutations, either at the RNA or aa level, reduce the ability of A_2 to bind the viral RNA, which would reduce the amount of A_2 assembled onto particles and increase the pool of free A_2. Alternatively, both the 5' and the 3'-ends of the viral RNA are identified as A_2 binding sites (136). Perhaps the *por* mutations, which cluster in the 5'-end, reduce the ability of A_2 to bind this region but not the 3'-end, so A_2 has a reduced number of binding sites on the RNA but can still assemble onto particles.

Characterization of A_2^{por} Mutants

Many questions have been raised about why *por* mutants produce an earlier lysis phenotype. *Por* mutant A_2 proteins need to be purified as soluble fusion proteins and

characterized with *in vitro* binding to MurA and *Bs* MurAA, in comparison to the WT A_2. RNA binding also needs to be tested with these mutants. This is more challenging because of two factors: (i) the fusion proteins appear to co-purify with RNA (Chapter III) and (ii) degradation of the protein occurs during the purification process (Chapter III). Use of a synthetic A_2 gene designed to have minimal RNA secondary structure could alleviate the problem with co-purification of RNA. Initial attempts to clone a synthetic *A_2* gene have resulted in frameshift mutations that produce inactive protein products (B.C. Bundy, unpublished data), which suggests that basal level of transcription during cloning is enough to produce sufficient A_2 to induce cellular lysis. A nonsense mutation could be engineered into the first part of the gene to correct the problem, so that construction of the synthetic clone could be done in a non-suppressing background where escape synthesis of the toxic A_2 protein could not occur. Expression of the protein *in vitro* could be also be a solution to the protease degradation issue (141).

Mechanism of MurA Inhibition

We have determined from *in vitro* binding studies with a soluble A_2 fusion hybrid that A_2 preferentially binds to the UNAG bound state of MurA. Under the conditions assayed, A_2 had a weakened affinity for the UNAG/fosfomycin complex, and did not display binding to the tetrahedral intermediate (FIG. 49). From crystal structure analyses, only minor differences in the loop are seen in the active site pocket (FIG. 50),

with the tetrahedral intermediate state exhibiting the largest difference suggesting that the loop conformation plays an important role in A_2 inhibition of MurA.

Characterization of A_2 binding to a dormant complex of MurA

A recent publication determined that MurA is bound to UNAM and PEP when the ratio of UNAM:UNAG is high in the cell (179). This dormant complex adopts a closed conformation very similar to the UNAG-liganded state; perhaps this is the state in which A_2 binds during an infection. Binding to the UNAM/PEP liganded state needs to be tested to determine whether A_2 associates with this dormant state of MurA. Purification of MurA excluding the ammonium sulfate precipitation step (Chapter II) will provide protein with UNAM and PEP bound.

Probing the A_2 Lytic Domain

Previous analysis of the lytic domain of A_2 revealed that the N-terminal 179 residues of A_2 still retain lytic function but the next largest fragment, 1-171, did not (FIG. 45) (89). Secondary structural analysis of A_2 predicted that this domain is comprised of several beta sheets that are sandwiched between alpha helices (FIG. 44). Deletion of the extreme N-terminal helix or truncation of 5 residues of a predicted helix that spans from residues 147-176 inactivates A_2 (FIG. 45). We concluded that perhaps

these helices act as a scaffold for beta sheet assembly and that this beta sheet domain is what comprises the lytic activity of A_2.

Characterization of the A_2 lytic domain

Truncation analyses of the first half of A_2 support the hypothesis that loss of lytic activity by several truncations is due to deletion of alpha helices that surround a beta sheet domain. Mutational analyses of conserved residues within the predicted beta sheets in the N-terminal half of A_2 need to be performed in an effort to identify the lytic domain.

Crystallization efforts with purified A_2 have not been possible up to this point, due to the poor solubility of the protein. A small fraction of the purified, full length fusion protein of A_2 has degradation of the C-terminal end. This domain is likely sequestered upon virion particle assembly, which is not normally exposed to cellular proteases. The use of lytic A_2 C-terminal truncations would alleviate this problem. The $A_2^{1\text{-}189}$ protein also has increased solubility compared to the full length protein (FIG. 40), although it still precipitated upon concentration. Future efforts may focus on using the truncation in complex with MurA. In addition, adding soluble N-terminal domains as extensions to the lytic truncation protein may also increase solubility. There are examples of protein fusion crystallization, especially if the linker between the two proteins is short (157).

Lysis Inhibition of Qβ (LIN)

We have shown that an infection of Qβ at high input MOI produces an LIN state (FIG. 22), defined as a state in which lysis protein expression does not result in lysis. The accumulation of the lysis protein was not perturbed between the different LIN-states; thereby, arguing against overall suppression of viral replication. This LIN state was previously noted by Ellis and colleagues for an MS2-like phage, R17 (42); however, no further characterization of this phenomenon has been reported. The fact that both Alloleviviruses and Leviviruses experience a similar LIN-induced state despite using completely different lysis mechanisms suggests that LIN is imposed by something that is common to the infection of both of these phages, when high MOI is used.

Several issues need to be addressed in order to characterize the LIN state of ssRNA phage. First, in the Levivirus system, the MS2 LIN state must be experimentally verified and it must be determined whether L accumulation is normal under LIN conditions. In view of the fact that L lysis does not require cell division, a division-independent model for the LIN state that is shared between the Alloleviviruses and Leviviruses must be proposed. In fact, it is not known why inhibition of cell wall synthesis by A_2 or by cell-wall specific antibiotics causes lysis. It is presumed that murein biosynthesis necessarily couples cell wall degradation with biosynthesis, to allow for incorporation of new polysaccharide strands; however, failure to incorporate the new NAM-NAG disaccharide subunits does not block the degradation process. Based on this operational analysis, one could speculate that the LIN process blocks the

degradation associated with murein biosynthesis. As noted above, it is not known how L causes cell wall degradation. However, the proteins responsible for degradation of murein when biosynthesis is inhibited might be the same as the muralytic proteins that appear to be activated by L. If so, then the LIN state might simply reflect the inhibition of these muralytic activities. There are a few candidates for the MOI-dependent LIN effector: the viral Coat, Replicase, or the RNA itself. Measurement of all viral components during an infection of under the LIN and non-LIN states will help clarify what is perturbing lysis. The *rat* strain could be used for quantification since this strain does not lyse when infected with Qβ WT. Alternatively, enrichment for phages that are able to overcome the LIN lysis block could provide insight into the mechanism of LIN regulation.

REFERENCES

1. **Adhin, M. R., and J. van Duin.** 1990. Scanning model for translational reinitiation in Eubacteria. J. Mol. Biol. **213:**811-818.

2. **Andrade, M. A., P. Chacon, J. J. Merelo, and F. Moran.** 1993. Evaluation of secondary structure of proteins from UV circular dichroism using an unsupervised neural network. Protein Eng. **6:**383-390.

3. **Atkins, J. F., J. A. Steitz, C. W. Anderson, and P. Model.** 1979. Binding of mammalian ribosomes to MS2 phage RNA reveals an overlapping gene encoding a lysis function. Cell **18:**247-256.

4. **Axelrod, V. D., E. Brown, C. Priano, and D. R. Mills.** 1991. Coliphage Qβ RNA replication: RNA catalytic for single-strand release. Virol. **184:**595-608.

5. **Barenboim, M., C. Y. Chang, F. dib Hajj, and R. Young.** 1999. Characterization of the dual start motif of a class II holin gene. Mol. Microbiol. **32:**715-727.

6. **Barrell, B. G., G. M. Air, and C. A. Hutchison.** 1976. Overlapping genes in bacteriophage ϕX174. Nature **264:**34-41.

7. **Beekwilder, J., R. Nieuwenhuizen, R. Poot, and J. van Duin.** 1996. Secondary structure model for the first three domains of Qβ RNA. Control of A-protein synthesis. J. Mol. Biol. **256:**8-19.

8. **Beremand, M. N., and T. Blumenthal.** 1979. Overlapping genes in RNA phage: a new protein implicated in lysis. Cell **18:**257-266.

9. **Berkhout, B., B. F. Schmidt, A. van Strien, J. van Boom, J. van Westrenen, and J. van Duin.** 1987. Lysis gene of bacteriophage MS2 is activated by translation termination at the overlapping coat gene. J. Mol. Biol. **195:**517-524.

10. **Bernardi, A., and P.-F. Spahr.** 1972. Nucleotide sequence at the binding site for coat protein on RNA of bacteriophage R17. Proc. Nat. Acad. Sci. U.S.A. **69:**3033-3037.

11. **Bernhardt, T. G.** 2001. Breaking free: small phages inhibit murein synthesis to lyse their host. Ph. D dissertation. Texas A&M University, College Station.

12. **Bernhardt, T. G., W. D. Roof, and R. Young.** 2002. The *Escherichia coli* FKBP-type PPIase SlyD is required for the stabilization of the E lysis protein of bacteriophage ϕX174. Mol. Microbiol. **45:**99-108.

13. **Bernhardt, T. G., W. D. Roof, and R. Young.** 2000. Genetic evidence that the bacteriophage ϕX174 lysis protein inhibits cell wall synthesis. Proc. Nat. Acad. Sci. U.S.A. **97:**4297-4302.

14. **Bernhardt, T. G., D. K. Struck, and R. Young.** 2001. The lysis protein E of ϕX174 is a specific inhibitor of the MraY-catalyzed step in peptidoglycan synthesis. J. Biol. Chem. **276:**6093-6097.

15. **Bernhardt, T. G., I. N. Wang, D. K. Struck, and R. Young.** 2002. Breaking free: "protein antibiotics" and phage lysis. Res. Microbiol. **153:**493-501.

16. **Bernhardt, T. G., I. N. Wang, D. K. Struck, and R. Young.** 2001. A protein antibiotic in the phage Qβ virion: diversity in lysis targets. Science **292:**2326-2329.

17. **Berry, J., E. J. Summer, D. K. Struck, and R. Young.** 2008. The final step in the phage infection cycle: the Rz and Rz1 lysis proteins link the inner and outer membranes. Mol. Microbiol. **70:**341-351.

18. **Black, L. W., J. A. Thomas, M. G. Rossmann, and V. B. Rao.** 2012. Condensed Genome Structure, p. 469-487. *In* M. G. Rossmann and V. B. Rao (ed.), Viral Molecular Machines, vol. 726. Springer US, New York.

19. **Bläsi, U., C. Y. Chang, M. T. Zagotta, K. Nam, and R. Young.** 1990. The lethal λ *S* gene encodes its own inhibitor. EMBO J. **9:**981-989.

20. **Blumenthal, T., and G. G. Carmichael.** 1979. RNA replication: function and structure of Qβ-replicase. Annu. Rev. Biochem. **48:**525-548.

21. **Blumenthal, T., T. A. Landers, and K. Weber.** 1972. Bacteriophage Qβ replicase contains the protein biosynthesis elongation factors EF Tu and EF Ts. Proc. Nat. Acad. Sci. U.S.A. **69:**1313-1317.

22. **Brinton, C. C. J.** 1965. The structure, function, synthesis and genetic control of bacterial pili and a molecular model for DNA and RNA transport in gram negative-bacteria. Trans. N.Y. Acad. Sci. **27:**1003-1054.

23. **Brown, E. D., E. I. Vivas, C. T. Walsh, and R. Kolter.** 1995. MurA (MurZ), the enzyme that catalyzes the first committed step in peptidoglycan biosynthesis, is essential in *Escherichia coli*. J. Bacteriol. **177:**4194-4197.

24. **Bull, J. J., D. W. Pfennig, and I. N. Wang.** 2004. Genetic details, optimization and phage life histories. Trends Ecol. Evol. **19:**76-82.

25. **Carmichael, G. G., K. Weber, A. Niveleau, and A. J. Wahba.** 1975. The host factor required for RNA phage Qβ RNA replication *in vitro*: intracellular location, quantitation, and purification by polyadenylate-cellulose chromatography. J. Biol. Chem. **250:**3607-3612.

26. **Caro, L. G., and M. Schnös.** 1966. The attachment of the male-specific bacteriophage f1 to sensitive strains of *Escherichia coli*. Proc. Nat. Acad. Sci. U.S.A. **56:**126-132.

27. **Caspar, D. L. D., and A. Klug.** 1962. Physical principles in the construction of regular viruses. Cold Spring Harb. Symp. Quant. Biol. **27:**1-24.

28. **Clarke, M., L. Maddera, R. L. Harris, and P. M. Silverman.** 2008. F-pili dynamics by live-cell imaging. Proc. Nat. Acad. Sci. U.S.A. **105:**17978-17981.

29. **Cole, C., J. D. Barber, and G. J. Barton.** 2008. The Jpred 3 secondary structure prediction server. Nucleic Acids Res. **36:**W197-W201.

30. **Cooper, S., and N. D. Zinder.** 1962. The growth of an RNA bacteriophage: the role of DNA synthesis. Virol. **18:**405-411.

31. **Curtiss, R.** 1969. Bacterial conjugation. Ann. Rev. Microbiol. **23:**69-136.

32. **Danziger, R. E., and W. Paranchych.** 1970. Stages in phage R17 infection: III. Energy requirements for the F-pili mediated eclipse of viral infectivity. Virol. **40:**554-564.

33. **Davis, J. E., and R. L. Sinsheimer.** 1963. The replication of bacteriophage MS2: 1. Transfer of parental nucleic acid to progeny phage. J. Mol. Biol. **6:**203-207.

34. **Dewey, J. S., C. G. Savva, R. L. White, S. Vitha, A. Holzenburg, and R. Young.** 2010. Micron-scale holes terminate the phage infection cycle. Proc. Nat. Acad. Sci. U.S.A. **107:**2219-2223.

35. **Doi, R. H., and S. Spiegelman.** 1962. Homology test between the nucleic acid of an RNA virus and the DNA in the host cell. Science **138:**1270-1272.

36. **Dolinsky TJ, N. J., McCammon JA, Baker NA.** 2004. PDB2PQR: an automated pipeline for the setup, execution, and analysis of Poisson-Boltzmann electrostatics calculations. Nucleic Acids Res. **32:**W665-W667.

37. **Domingo, E., and J. J. Holland.** 1997. RNA virus mutations and fitness for survival Annu. Rev. Microbiol. **51:**151-178.

38. **Domingo, E., D. Sabo, T. Taniguchi, and C. Weissmann.** 1978. Nucleotide sequence heterogeneity of an RNA phage population. Cell **13:**735-744.

39. **Drake, J. W.** 1993. Rates of spontaneous mutation among RNA viruses. Proc. Nat. Acad. Sci. U S A **90:**4171-4175.

40. **Dykeman, E. C., N. E. Grayson, K. Toropova, N. A. Ranson, P. G. Stockley, and R. Twarock.** 2011. Simple rules for efficient assembly predict the layout of a packaged viral RNA. J. Mol. Biol. **408:**399-407.

41. **Ellis, D. B., and W. Paranchych.** 1963. Synthesis of ribonucleic acid and protein in bacteria infected with an RNA bacteriophage. J. Cell. Physiol. **62:**207-213.

42. **Engelberg-Kulka, H., L. Dekel, and M. Israeli-Reches.** 1977. Streptomycin-resistant *Escherichia coli* mutant temperature sensitive for the production of Qβ-infective particles. J. Virol. **21:**1-6.

43. **Eschenburg, S., W. Kabsch, M. L. Healy, and E. Schönbrunn.** 2003. A new view of the mechanisms of UDP-N-acetylglucosamine enolpyruvyl transferase (MurA) and 5-enolpyruvylshikimate-3-phosphate synthase (AroA) derived from X-ray structures of their tetrahedral reaction intermediate states. J. Biol. Chem. **278:**49215-49222.

44. **Eschenburg, S., M. Priestman, and E. Schönbrunn.** 2005. Evidence that the fosfomycin target Cys-115 in UDP-*N*-actetylglucosamine enolpyruvyltransferase (MurA) is essential for product release. J. Biol. Chem. **280:**3757-3763.

45. **Franze de Fernandez, M. T., L. Eoyang, and J. T. August.** 1968. Factor fraction required for the synthesis of bacteriophage Qβ-RNA. Nature **219:**588-590.

46. **Frost, L. S., B. B. Finlay, A. Opgenorth, W. Paranchych, and J. S. Lee.** 1985. Characterization and sequence analysis of pilin from F-like plasmids. J. Bacteriol. **164:**1238-1247.

47. **Ganesh, C., A. N. Shah, C. P. Swaminathan, A. Surolia, and R. Varadarajan.** 1997. Thermodynamic characterization of the reversible, two-state unfolding of maltose binding protein, a large two-domain protein. Biochemistry **36:**5020-5028.

48. **Godson, G. N., and R. L. Sinsheimer.** 1967. The replication of bacteriophage MS2: VI. Interaction between bacteriophage RNA and cellular components in MS2-infected *Escherichia coli*. J. Mol. Biol. **23:**495-521.

49. **Greenfield, N. J.** 2006. Using circular dichroism collected as a function of temperature to determine the thermodynamics of protein unfolding and binding interactions. Nat. Protoc. **1:**2527-2535.

50. **Groeneveld, H., K. Thimon, and J. van Duin.** 1995. Translational control of maturation-protein synthesis in phage MS2: a role for the kinetics of RNA folding? RNA **1:**79-88.

51. **Gründling, A., U. Bläsi, and R. Young.** 2000. Biochemical and genetic evidence for three transmembrane domains in the class I holin, λ S. J. Biol. Chem. **275:**769-776.

52. **Gunetileke, K. G., and R. A. Anwar.** 1968. Biosynthesis of Uridine Diphospho-N-acetylmuramic acid. J. Biol. Chem. **243:**5770-5778.

53. **Haruna, I., K. Nozu, Y. Ohtaka, and S. Spiegelman.** 1963. An RNA "replicase" induced by and selective for a viral RNA: isolation and properties. Proc. Nat. Acad. Sci. U.S.A. **50:**905-911.

54. **Hatfull, G. F.** 2001. The great escape. Science **292:**2263-2264.

55. **Haywood, A. M., and R. L. Sinsheimer.** 1963. Inhibition of protein synthesis in *E. coli* protoplasts by actinomycin-D. J. Mol. Biol. **6:**247-249.

56. **Hindley, J., D. H. Staples, M. A. Billeter, and C. Weissmann.** 1970. Location of the coat cistron on the RNA of phage Qβ. Proc. Nat. Acad. Sci. U.S.A. **67:**1180-1187.

57. **Hofstetter, H., H. J. Monstein, and C. Weissmann.** 1974. The readthrough protein A_1 is essential for the formation of viable Qβ particles. Biochim. Biophys. Acta. **374:**238-251.

58. **Holtje, J. V., W. Fielder, H. Rotering, B. Walderich, and J. van Duin.** 1988. Lysis induction of *Escherichia coli* by the cloned lysis protein of the phage MS2 depends on the presence of osmoregulatory membrane-derived oligosaccharides. J. Biol. Chem. **263:**3539-3541.

59. **Horiuchi, K., and S. Matsuhashi.** 1970. Three cistrons in bacteriophage Qβ. Virol. **42:**49-60.

60. **Hotham-Iglewski, B., and R. M. Franklin.** 1967. Replication of bacteriophage ribonucleic acid: Alterations in polyribosome patterns and association of double-stranded RNA with polyribosomes in *Escherichia coli* infected with bacteriophage R17. Proc. Nat. Acad. Sci. U.S.A. **58:**743-749.

61. **Hotham-Iglewski, B., L. A. Phillips, and R. M. Franklin.** 1968. Viral RNA transcription-translation complex in *Escherichia coli* infected with bacteriophage R17. Nature **219:**700-703.

62. **Hung, P. P., E. M. Hale, and L. R. Overby.** 1969. Comparative antigenicities of Qβ phage, its structural components and reconstituted particles. Virol. **38:**703-706.

63. **Hung, P. P., C. M. Ling, and L. R. Overby.** 1969. Self-assembly of Qβ and MS2 phage particles: possible function of initiation complexes. Science **166:**1638-1640.

64. **Ignatova, Z., L. M. Gierasch, H. u. Dieter, and S. Helmut.** 2007. Effects of osmolytes on protein folding and aggregation in cells, p. 355-372. *In* D. Häussinger and H. Sies (ed.), Methods Enzymol., vol. 428. Academic Press, Waltham, MA.

65. **Ishihama, Y., T. Schmidt, J. Rappsilber, M. Mann, F. U. Hartl, M. Kerner, and D. Frishman.** 2008. Protein abundance profiling of the *Escherichia coli* cytosol. BMC Genomics **9:**102.

66. **Jayant, L., C. Priano, and D. R. Mills.** 2010. In polycistronic Qβ RNA, single-strandedness at one ribosome binding site directly affects translational initiations at a distal upstream cistron. Nucleic Acids Res. **38:**7199-7210.

67. **Jeppesen, P. G., J. A. Steitz, R. F. Gesteland, and P. F. Spahr.** 1970. Gene order in the bacteriophage R17 RNA: 5'-a protein-coat protein-synthetase-3'. Nature **226:**230-237.

68. **Jeruzalmi, D., and T. A. Steitz.** 1998. Structure of T7 RNA polymerase complexed to the transcriptional inhibitor T7 lysozyme. EMBO J. **17:**4101-4113.

69. **Kahan, F. M., J. S. Kahan, P. J. Cassidy, and H. Kropp.** 1974. The mechanism of action of fosfomycin (phosphonomycin). Ann. N.Y. Acad. Sci. **235:**364-386.

70. **Kamen, R.** 1970. Characterization of the subunits of Qβ replicase. Nature **228:**527-533.

71. **Kamen, R. I.** 1975. Structure and function of the Qβ RNA replicase, p. 203-234. *In* N. D. Zinder (ed.), RNA Phages. Cold Spring Harbor Laboratory, Cold Spring Harbor, NY.

72. **Karnik, S., and M. Billeter.** 1983. The lysis function of RNA bacteriophage Qβ is mediated by the maturation (A_2) protein. EMBO J. **2:**1521-1526.

73. **Karring, H., S. G. J. Mathu, J. van Duin, B. F. C. Clark, B. Kraal, and C. R. Knudsen.** 2004. Qβ-phage resistance by deletion of the coiled-coil motif in elongation factor Ts. J. Biol. Chem. **279:**1878-1884.

74. **Kastelein, R. A., E. Remaut, W. Fiers, and J. van Duin.** 1982. Lysis gene expression of RNA phage MS2 depends on a frameshift during translation of the overlapping coat protein gene. Nature **295:**35-41.

75. **Kelly, S. M., T. J. Jess, and N. C. Price.** 2005. How to study proteins by circular dichroism. Biochim. Biophys. Acta. **1751:**119-139.

76. **Kim, D. H., W. J. Lees, K. E. Kempsell, W. S. Lane, K. Duncan, and C. T. Walsh.** 1996. Characterization of a Cys115 to Asp substitution in the *Escherichia coli* cell wall biosynthetic enzyme UDP-GlcNAc enolpyruvyl transferase (MurA) that confers resistance to inactivation by the antibiotic fosfomycin. Biochemistry **35:**4923-4928.

77. **Klovins, J., N. A. Tsareva, M. H. de Smit, V. Berzins, and J. van Duin.** 1997. Rapid evolution of translational control mechanisms in RNA genomes. J. Mol. Biol. **265:**372-384.

78. **Knolle, P., and T. Hohn.** 1975. Morphogenesis of RNA phages, p. 147-201. *In* N. D. Zinder (ed.), RNA Phages. Cold Spring Harbor Laboratory, Cold Spring Harbor, NY.

79. **Kock, H., U. Gerth, and M. Hecker.** 2004. MurAA, catalysing the first committed step in peptidoglycan biosynthesis, is a target of Clp-dependent proteolysis in *Bacillus subtilis*. Mol. Microbiol. **51:**1087-1102.

80. **Kolakofsky, D., M. A. Billeter, H. Weber, and C. Weissmann.** 1973. Resynchronization of RNA synthesis by coliphage Qβ replicase at an internal site of the RNA template. J. Mol. Biol. **76:**271-284.

81. **Kolakofsky, D., and C. Weissmann.** 1971. Possible mechanism for transition of viral RNA from polysome to replication complex. Nat. New Biol. **231:**42-46.

82. **Kolakofsky, D., and C. Weissmann.** 1971. Qβ replicase as repressor of Qβ RNA-directed protein synthesis. Biochim. Biophys. Acta. **246:**596-599.

83. **Kozak, M., and D. Nathans.** 1971. Fate of maturation protein during infection by coliphage MS2. Nat. New Biol. **234:**209-211.

84. **Kozlovska, T. M., I. Cielens, D. Dreilinna, A. Dislers, V. Baumanis, V. Ose, and P. Pumpens.** 1993. Recombinant RNA phage Qβ capsid particles synthesized and self-assembled in *Escherichia coli*. Gene **137:**133-137.

85. **Krahn, P. M., R. J. O'Callaghan, and W. Paranchych.** 1972. Stages in phage R17 infection VI. Injection of A protein and RNA into the host cell. Virol. **47:**628-637.

86. **Krahn, P. M., and W. Paranchych.** 1971. Heterogeneous distribution of A protein in R17 phage preparations. Virol. **43:**533-535.

87. **Kuznetsov, V.** 2011. Structural studies of phage lysis proteins and their targets. Texas A&M University, College Station.

88. **Landers, T. A., T. Blumenthal, and K. Weber.** 1974. Function and structure in ribonucleic acid phage Qβ ribonucleic acid replicase. J. Biol. Chem. **249:**5801-5808.

89. **Langlais, C.** 2007. Understanding the lytic function of A_2: the maturation protein of ssRNA bacteriophage Qβ. Texas A&M, College Station.

90. **Lease, R. A., and S. A. Woodson.** 2004. Cycling of the Sm-like protein Hfq on the DsrA small regulatory RNA. J. Mol. Biol. **344:**1211-1223.

91. **Ling, C. M., P. P. Hung, and L. R. Overby.** 1970. Independent assembly of Qβ and MS2 phages in doubly infected *Escherichia coli*. Virol. **40:**920-929.

92. **Lodish, H. F.** 1968. Bacteriophage f2 RNA: control of translation and gene order. Nature **220:**345-350.

93. **Lodish, H. F., K. Horiuchi, and N. D. Zinder.** 1965. Mutants of the bacteriophage f2: V. On the production of noninfectious phage particles. Virol. **27:**139-155.

94. **Lodish, H. F., and N. D. Zinder.** 1966. Mutants of the bacteriophage f2: VIII. Control mechanisms for phage-specific syntheses. J. Mol. Biol. **19:**333-348.

95. **Loeb, T., and N. D. Zinder.** 1961. A bacteriophage containing RNA. Proc. Nat. Acad. Sci. U.S.A. **47:**282-289.

96. **Lutz, R., and H. Bujard.** 1997. Independent and tight regulation of transcriptional units in *Escherichia coli* via the LacR/O, the TetR/O and AraC/I1-I2 regulatory elements. Nucleic Acids Res. **25:**1203-1210.

97. **Marquardt, J. L., D. A. Siegele, R. Kolter, and C. T. Walsh.** 1992. Cloning and sequencing of *Escherichia coli murZ* and purification of its product, a UDP-N-acetylglucosamine enolpyruvyl transferase. J. Bacteriol. **174:**5748-5752.

98. **Marvin, D. A., and B. Hohn.** 1969. Filamentous bacterial viruses. Bact. Rev. **33:**172-209.

99. **Mengin-Lecreulx, D., B. Flouret, and J. van Heijenoort.** 1982. Cytoplasmic steps of peptidoglycan synthesis in *Escherichia coli*. J. Bacteriol. **151:**1109-1117.

100. **Mengin-Lecreulx, D., B. Flouret, and J. van Heijenoort.** 1983. Pool levels of UDP N-acetylglucosamine and UDP N-acetylglucosamine-enolpyruvate in *Escherichia coli* and correlation with peptidoglycan synthesis. J. Bacteriol. **154:**1284-1290.

101. **Miller, J. H.** 1972. Experiments in molecular genetics. Cold Spring Harbor Laboratory, Cold Spring Harbor, NY.

102. **Mills, D. R., C. Priano, P. A. Merz, and B. D. Binderow.** 1990. Qβ RNA bacteriophage: Mapping *cis*-acting elements within an RNA genome. J. Virol. **64:**3872-3881.

103. **Miranda, G., D. Schuppli, I. Barrera, C. Hausherr, J. M. Sogo, and H. Weber.** 1997. Recognition of bacteriophage Qβ plus strand RNA as a template by Qβ replicase: role of RNA interactions mediated by ribosomal proteins S1 and host factor. J. Mol. Biol. **267:**1089-1103.

104. **Mizyed, S., A. Oddone, B. Byczynski, D. W. Hughes, and P. J. Berti.** 2005. UDP-N-acetylmuramic acid (UDP-MurNAc) is a potent inhibitor of MurA (enolpyruvyl-UDP-GlcNAc synthase). Biochemistry **44:**4011-4017.

105. **Model, P., R. E. Webster, and N. D. Zinder.** 1979. Characterization of Op3, a lysis-defective mutant of bacteriophage f2. Cell **18:**235-244.

106. **Morton, V. L., E. C. Dykeman, N. J. Stonehouse, A. E. Ashcroft, R. Twarock, and P. G. Stockley.** The impact of viral RNA on assembly pathway selection. J. Mol. Biol. **401:**298-308.

107. **Moussa, S. H., V. Kuznetsov, T. A. T. Tran, J. C. Sacchettini, and R. Young.** Protein determinants of phage T4 lysis inhibition. Protein Sci. **21:**571-582.

108. **Nallamsetty, S., and D. S. Waugh.** 2006. Solubility-enhancing proteins MBP and NusA play a passive role in the folding of their fusion partners. Protein Expr. Purif. **45:**175-182.

109. **Nelson, D. L., and M. M. Cox.** 2005. Lehninger: Principles of Biochemistry, fourth ed. W. H. Freeman and Company, New York.

110. **Ni, C., R. Syed, R. Kodandapani, J. Wickersham, D. S. Peabody, and K. R. Ely.** 1995. Crystal structure of the MS2 coat protein dimer: implications for RNA binding and virus assembly. Structure **3:**255-263.

111. **Ou, J. T., and T. F. Anderson.** 1970. Role of pili in bacterial conjugation. J. Bacteriol. **102:**648-654.

112. **Ozaki, K., and R. C. Valentine.** 1973. Inhibition of bacterial cell wall mucopeptide synthesis: a new function of RNA bacteriophage Qβ. Biochim. Biophys. Acta. **304:**707-714.

113. **Palmer, I., and P. T. Wingfield.** 2001. Preparation and extraction of insoluble (inclusion-body) proteins from *Escherichia coli*, p. 6.3.1-6.3.15. *In* Current Protocols in Protein Science. John Wiley & Sons, Inc.

114. **Pang, T., C. G. Savva, K. G. Fleming, D. K. Struck, and R. Young.** 2009. Structure of the lethal phage pinhole. Proc. Nat. Acad. Sci. U.S.A. **106:**18966-18971.

115. **Paranchych, W.** 1966. Stages in phage R17 infection: the role of divalent cations. Virol. **28:**90-99.

116. **Paranchych, W., S. K. Ainsworth, A. J. Dick, and P. M. Krahn.** 1971. Stages in phage R17 infection: V. Phage eclipse and the role of F pili. Virol. **45:**615-628.

117. **Paranchych, W., and A. F. Graham.** 1962. Isolation and properties of an RNA-containing bacteriophage. J. Cell. Comp. Physiol. **60:**199-208.

118. **Paranchych, W., P. M. Krahn, and R. D. Bradley.** 1970. Stages in phage R17 infection. Virol. **41:**465-473.

119. **Paranchych, W., and N. D. Zinder.** 1975. Attachment, ejection, and penetration stages of the RNA phage infectious process, p. 85-111. *In* N. D. Zinder (ed.), RNA phages. Cold Spring Harbor Laboratory, Cold Spring Harbor, NY.

120. **Park, T., D. K. Struck, C. A. Dankenbring, and R. Young.** 2007. The pinholin of lambdoid phage 21: control of lysis by membrane depolarization. J. Bacteriol. **189:**9135-9139.

121. **Polissi, A., L. Goffin, and C. Georgopoulos.** 1995. The *Escherichia coli* heat shock response and bacteriophage λ development. FEMS Microbiol. Rev. **17:**159-169.

122. **Poot, R. A., N. V. Tsareva, I. V. Boni, and J. Van Duin.** 1997. RNA folding kinetics regulates translation of phage MS2 maturation gene. Proc. Nat. Acad. Sci. U.S.A. **94:**10110-10115.

123. **Raab, R., G. Neal, C. Sohaskey, J. Smith, and R. Young.** 1988. Dominance in lambda *S* mutations and evidence for translational control. J. Mol. Biol. **199:**95-105.

124. **Riley-Lovingshimer, M. R., and G. D. Reinhart.** 2001. Equilibrium binding studies of a Tryptophan-shifted mutant of Phosphofructokinase from *Bacillus stearothermophilus*. Biochemistry **40:**3002-3008.

125. **Roberts, J. W., and J. E. Steitz.** 1967. The reconstitution of infective bacteriophage R17. Proc. Nat. Acad. Sci. U.S.A. **58:**1416-1421.

126. **Robertson, H. D.** 1975. Functions of replicating RNA in cells infected by RNA bacteriophages, p. 113-145. *In* N. D. Zinder (ed.), RNA Phages. Cold Spring Harbor Laboratory, Cold Spring Harbor, NY.

127. **Robertson, H. D., and H. F. Lodish.** 1970. Messenger characteristics of nascent bacteriophage RNA. Proc. Nat. Acad. Sci. U.S.A. **67:**710-716.

128. **Robertson, H. D., and N. D. Zinder.** 1969. Purification and properties of nascent f2 phage ribonucleic acid. J. Biol. Chem. **244:**5790-5800.

129. **Sambrook, J., E. F. Fritsch, and T. Maniatis.** 1989. Molecular cloning: a laboratory manual. Cold Spring Harbor Laboratory Press, Cold Spring Harbor,NY.

130. **Samland, A. K., T. Etezady-Esfarjani, N. Amrhein, and P. Macheroux.** 2001. Asparagine 23 and aspartate 305 are essential residues in the active site of UDP-N-acetylglucosamine enolpyruvyl transferase from *Enterobacter cloacae*. Biochemistry **40:**1550-1559.

131. **Schönbrunn, E., S. Eschenburg, F. Krekel, K. Luger, and N. Amrhein.** 2000. Role of the loop containing residue 115 in the induced-fit mechanism of the bacterial cell wall biosynthetic enzyme MurA. Biochemistry **39:**2164-2173.

132. **Schönbrunn, E., Svergun, D. I., Amrhein, N. and Koch, M. H. J.** 1998. Studies on the conformational changes in the bacterial cell wall biosynthetic enzyme UDP-N-acetylglucosamine enolpyruvyltransferase (MurA). Eur. J. Biochem. **253:**406-412.

133. **Schrödinger, LLC.** 2010. The PyMOL Molecular Graphics System, Version 0.99.

134. **Schuppli, D., G. Miranda, H.-C. T. Tsui, M. E. Winkler, J. M. Sogo, and H. Weber.** 1997. Altered 3'-terminal RNA structure in phage Qβ adapted to host factor-less *Escherichia coli*. Proc. Nat. Acad. Sci. U.S.A. **94:**10239-10242.

135. **Shiba, T., and T. Miyake.** 1975. New type of infectious complex of *E. coli* RNA phage. Nature **254:**157-158.

136. **Shiba, T., and Y. Suzuki.** 1981. Localization of A protein in the RNA-A protein complex of RNA phage MS2. Biochim. Biophys. Acta **654:**249-255.

137. **Skarzynski, T., D. H. Kim, W. Lees, C. T. Walsh, and K. Duncan.** 1998. Stereochemical course of enzymatic enolpyruvyl transfer and catalytic conformation of the active site revealed by the crystal structure of the fluorinated analogue of the reaction tetrahedral intermediated bound to the active site of the C115A mutant of MurA. Biochemistry **37:**2572-2577.

138. **Skarzynski, T., A. Mistry, A. Wonacott, S. E. Hutchinson, V. A. Kelly, and K. Duncan.** 1996. Structure of UDP-N-acetylglucosamine enolpyruvyl transferase, an enzyme essential for the synthesis of bacterial peptidoglycan, complexed with substrate UDP-N-acetylglucosamine and the drug fosfomycin. Structure **4:**1465-1474.

139. **Skripkin, E. A., and A. B. Jacobson.** 1993. A Two-dimensional model at the nucleotide level for the central hairpin of coliphage Qβ RNA. J. Mol. Biol. **233:**245-260.

140. **Smith, D. L., D. K. Struck, J. M. Scholtz, and R. Young.** 1998. Purification and biochemical characterization of the lambda holin. J. Bacteriol. **180:**2531-40.

141. **Smith, M. T., C. T. Varner, D. B. Bush, and B. C. Bundy.** 2012. The incorporation of the A2 protein to produce novel Qβ virus-like particles using cell-free protein synthesis. Biotechnol. Prog. **28:**549-555.

142. **Spiegelman, S., and M. Hayashi.** 1963. The present status of the transfer of genetic information and its control. Cold Spring Harbor Symp. Quant. Biol. **28:**161.

143. **Spiegelman, S., N. R. Pace, D. R. Mills, R. Levisohn, T. S. Eikhom, M. M. Taylor, R. L. Peterson, and D. H. L. Bishop.** 1968. The mechanism of RNA replication. Cold Spring Harbor Symp. Quant. Biol. **33:**101.

144. **Spurlino, J. C., G. Lu, and Q. F.A.** 1991. The 2.3-Å resolution structure of the maltose- or maltodextrin-binding protein, a primary receptor of bacterial active transport and chemotaxis. J. Biol. Chem. **266:**5202-5219.

145. **Staples, D. H., J. Hindley, M. A. Billeter, and C. Weissmann.** 1971. Localization of Qβ maturation cistron ribosome binding site. Nat. New Biol. **234:**202-204.

146. **Strauss, J. H., and R. L. Sinsheimer.** 1963. Purification and properties of bacteriophage MS2 and of its ribonucleic acid. J. Mol. Biol. **7:**43-54.

147. **Sugiyama, T., R. R. Hebert, and K. A. Hartman.** 1967. Ribonucleoprotein complexes formed between bacteriophage MS2 RNA and MS2 protein *in vitro*. J. Mol. Biol. **25:**455-463.

148. **Sugiyama, T., and D. Nakada.** 1967. Control of translation of MS2 RNA cistrons by MS2 coat protein. Proc. Nat. Acad. Sci. U.S.A. **57:**1744-1750.

149. **Tian, B., C. Bevilacqua, A. Diegelman-Parente, and M. B. Mathews.** 2004. The double-stranded-RNA-binding motif: interference and much more. Mol. Cell Biol. **5:**1013-1023.

150. **Tomasz, A.** 1979. The mechanism of the irreversible antimicrobial effects of penicillins: how the beta-lactam antibiotics kill and lyse bacteria. Annu. Rev. Microbiol. **33:**113-137.

151. **Toropova, K., P. G. Stockley, and N. A. Ranson.** 2011. Visualising a viral RNA genome poised for release from its receptor complex. J. Mol. Biol. **408:**408-419.

152. **Tran, T. A., D. K. Struck, and R. Young.** 2007. The T4 RI antiholin has an N-terminal signal anchor release domain that targets it for degradation by DegP. J. Bacteriol. **189:**7618-7625.

153. **Tran, T. A. T., D. K. Struck, and R. Young.** 2005. Periplasmic domains define holin-antiholin interactions in T4 lysis inhibition. J. Bacteriol. **187:**6631-6640.

154. **Tsukada, K., M. Okazaki, H. Kita, Y. Inokuchi, I. Urabe, and T. Yomo.** 2009. Quantitative analysis of the bacteriophage Qβ infection cycle. Biochim. Biophys. Acta, Gen. Subj. **1790:**65-70.

155. **Valentine, R. C., and M. Strand.** 1965. Complexes of F-pili and RNA bacteriophage. Science **148:**511-513.

156. **van Duin, J., and Tsareva, N. .** 2006. Single-stranded RNA phages, p. 175-196. *In* R. Calendar (ed.), The Bacteriophages, 2nd ed. Oxford University Press, Oxford.

157. **Walls, D., and S. T. Loughran.** 2011. Tagging recombinant proteins to enhance solubility and aid purification, p. 151-175. *In* J. M. Walker (ed.), Methods in Molecular Biology, vol. 681. Humana Press, New York, NY.

158. **Wang, I. N.** 2006. Lysis timing and bacteriophage fitness. Genetics **172:**17-26.

159. **Wang, I. N., J. Deaton, and R. Young.** 2003. Sizing the holin lesion with an endolysin-beta-galactosidase fusion. J. Bacteriol. **185:**779-787.

160. **Wang, L., and S. J. Brown.** 2006. BindN: A web-based tool for efficient prediction of DNA and RNA binding sites in amino acid sequences. Nucleic Acids Res. **34:**W243-W248.

161. **Wang, Y. A., X. Yu, P. M. Silverman, R. L. Harris, and E. H. Egelman.** 2009. The structure of F-pili. J. Mol. Biol. **385:**22-29.

162. **Watanabe, I.** 1964. Persistent infection with an RNA bacteriophage. Nihon Rinsho **22:**243-251.

163. **Weber, H., M. A. Billeter, S. Kahane, and C. Weissmann.** 1972. Molecular basis for repressor activity of Qβ replicase. Nat. New Biol. **237:**166-170.

164. **Weber, K., W. Konigsberg, and N. D. Zinder.** 1975. Proteins of the RNA phages, p. 51-84. *In* N. D. Zinder (ed.), RNA phages. Cold Spring Harbor Laboratory, Cold Spring Harbor, NY.

165. **Weiner, A. M., and K. Weber.** 1973. A single UGA codon functions as a natural termination signal in the coliphage Qβ coat protein cistron. J. Mol. Biol. **80:**837-855.

166. **Weissbach, H., D. Lee Miller, and J. Hachmann.** 1970. Studies on the role of factor Ts in polypeptide synthesis. Arch. Biochem. Biophys. **137:**262-269.

167. **Weissmann, C., G. Feix, and H. Slor.** 1968. In vitro synthesis of phage RNA: The nature of the intermediates. Cold Spring Harbor Symp. Quant. Biol. **33:**83-100.

168. **Weissmann, C., L. Simon, and S. Ochoa.** 1963. Induction by an RNA phage of an enzyme catalyzing incorporation of ribonucleotides into ribonucleic acid. Proc. Nat. Acad. Sci. U.S.A. **49:**407-414.

169. **Winter, R. B., and L. Gold.** 1983. Overproduction of bacteriophage Qβ maturation (A_2) protein leads to cell lysis. Cell **33:**877-885.

170. **Wong, K., and W. Paranchych.** 1976. The polarity of penetration of phage R17 RNA. Virol. **73:**489-497.

171. **Wong, K., and W. Paranchych.** 1976. The preservation of the secondary structure of R17 RNA during penetration into host bacteria. Virol. **73:**476-488.

172. **Xu, M., D. K. Struck, J. Deaton, I. N. Wang, and R. Young.** 2004. The signal arrest-release (SAR) sequence mediates export and control of the phage P1 endolysin. Proc. Nat. Acad. Sci. U.S.A. **101:**6415-6420.

173. **Young, R.** 1992. Bacteriophage lysis: mechanism and regulation. Microbiol. Rev. **56:**430-481.

174. **Young, R., and I. N. Wang.** 2006. Phage lysis, p. 104-126. *In* R. Calendar (ed.), The Bacteriophages, 2nd ed. Oxford University Press, Oxford.

175. **Zagotta, M. T., and D. B. Wilson.** 1990. Oligomerization of the bacteriophage lambda S protein in the inner membrane of *Escherichia coli*. J. Bacteriol. **172:**912-921.

176. **Zhang, X., and F. W. Studier.** 1997. Mechanism of inhibition of bacteriophage T7 RNA polymerase by T7 lysozyme. J. Mol. Biol. **269:**10-27.

177. **Zheng, Y., D. K. Struck, C. A. Dankenbring, and R. Young.** 2008. Evolutionary dominance of holin lysis systems derives from superior genetic malleability. Microbiol. **154:**1710-1718.

178. **Zheng, Y., D. K. Struck, and R. Young.** 2009. Purification and functional characterization of ϕX174 lysis protein E. Biochemistry **48:**4999-5006.

179. **Zhu, J.-Y., Y. Yang, H. Han, S. Betzi, S. H. Olesen, F. Marsilio, and E. Schönbrunn.** 2012. Functional consequence of covalent reaction of phosphoenolpyruvate with UDP-N-acetylglucosamine 1-carboxyvinyltransferase (MurA). J. Biol. Chem. **287:**12657-12667.

180. **Zinder, N. D., and S. Cooper.** 1964. Host-dependent mutants of the bacteriophage f2: I. Isolation and preliminary classification. Virol. **23:**152-158.

181. **Zinder, N. D., and L. B. Lyons.** 1968. Cell lysis: another function of the coat protein of the bacteriophage f2. Science **159:**84-86.

VITA

Catrina Anne Reed received her Bachelor of Science degree in biochemistry from McMurry University in 2007. She entered the Biochemistry and Biophysics Department at Texas A&M University in August 2007 and joined the laboratory of Dr. Ry Young in April of 2008. She received her Doctor of Philosophy degree in August 2012. Her research focuses on characterization of the ssRNA phage Qβ lysis protein A_2.

Dr. Reed may be reached at Texas A&M University, TAMU 2128, BIO/BIO 311, College Station, TX 77843. Her email is reed_catrina@tamu.edu.